Investigating the Role of the Dorsal Filament in Weakly Electric Fish

Hugo Paradis

A thesis submitted to the University of Ottawa in partial fulfillment of the requirements for the Master of Science degree in Biology

Ottawa-Carleton Institute of Biology
Department of Biology
Faculty of Science
University of Ottawa

Acknowledgments

Before anything else, I would like to thank Dr. John Lewis for giving me the immense opportunity of taking me on as a master's student. I sincerely thank you for taking me on even if you knew that I didn't have any research experience prior to my arrival in the lab. Thank you for all the guidance and especially for the continuous feedback on all aspects of my research project. A high-quality product such as this thesis would not have been possible without you.

I would like to thank all my lab mates over the years, especially my fellow graduate lab mates Mary Upshall and Parisa Nazemi that worked with me for the whole duration of my master's program. Thank you both for all the support and constructive feedback you have given me over the years. I learned so much from both of you and my experience in the lab would not have been the same without you.

I would also like to thank Dr. Emily Standen and Dr. Tuan Bui for accepting to be part of my Thesis Advisory Committee and for agreeing to review and evaluate this thesis for me. Thanks for the great feedback during the committee meetings and continued interest in my research project.

Finalement, un merci tout spécial à ma famille, Suzanne, André et Yan. Je vous remercie de m'avoir laissé la liberté de poursuivre mes études universitaires et de m'avoir supporté tout au long de mon parcours. Mom, merci pour tous les devoirs corrigés, les repas préparés, et les heures de divertissements avec tes événements communautaires. Papa, merci pour tout ce qu'on fait et construit ensemble les week-ends, pour les longues heures passées au téléphone et discussions qu'on a eu au fil des années. Yan, merci pour toutes les rides jusqu'en résidence durant ma première année, merci d'être mon consultant privé en mécanique et assistant occasionnel en construction, mais surtout, merci d'être le meilleur frère sur la terre.

Résumé

Les humains et les animaux utilisent des récepteurs sensoriels spécialisés pour encoder des informations sur leur environnement. La densité de ces récepteurs peut avoir un impact significatif sur l'acuité sensorielle et la qualité de l'information obtenue. Par exemple, la fovéa de la rétine humaine présente la région de la rétine ayant la densité de photorécepteurs la plus élevée, ce qui améliore l'acuité visuelle.

Le poisson faiblement électrique *Apteronotus albifrons* habite les eaux néotropicales. Il est réputé pour sa capacité remarquable à naviguer et à capturer des proies dans l'obscurité sans se fier à des repères visuels. Tout comme d'autres poissons faiblement électriques du type ondulatoire, cette espèce génère un champ électrique de faible intensité dans les eaux environnantes. La production de ce champ électrique est continue, et varie dans le temps. Tout objet à proximité du poisson et ayant des propriétés électriques différentes comparativement aux eaux environnantes provoque des perturbations dans ce champ électrique. Ces perturbations sont détectées par des milliers d'électrorécepteurs qui sont situés partout sur la peau du poisson.

Chez l'*Apteronotus albifrons*, la densité d'électrorécepteurs n'est pas uniforme. Les deux régions ayant la plus haute densité de récepteurs sont la tête et le filament dorsal, une structure située sur la surface dorsale du poisson. La tête contient d'autres systèmes sensoriels tels que la vision, tandis que le filament dorsal ne contient que des électrorécepteurs. Cela suggère qu'il pourrait servir principalement d'organe électrorécepteurs. Bien qu'il y eût des indications d'un biais dorsal lors de la capture de proies, le rôle précis du filament dorsal dans le système électrosensoriel reste incertain.

Dans cette thèse, des mesures quantitatives du comportement des poissons sont utilisées pour analyser la façon dont ceux-ci répondent à des stimuli électrosensoriel positionnés à divers endroits autour de leurs corps. Après l'initiation du stimulus, le poisson se rapproche de l'endroit d'où provient stimulus. Dans certains cas, il y a aussi un léger mouvement de roulis vers le stimulus. De plus, la fréquence de détection des stimuli provenant d'au-dessus du filament dorsal est plus élevée que lorsqu'elle provient d'autres endroits autour de la même région du tronc. Collectivement, ces observations proposent que le filament dorsal produit une image électrique supérieure comparativement au reste du tronc.

Abstract

Animals use specialized sensory receptors to encode information about their environment. The density of these receptors can significantly impact sensory acuity and the quality of the information they provide. For instance, the fovea in the human retina has the highest photoreceptor density, which enhances visual acuity.

Apteronotus albifrons, a weakly electric fish that inhabits neotropical waters, is renowned for its remarkable ability to navigate and capture prey in the dark, without relying on visual cues. Like other wave-type weakly electric fishes, this species generates a time-varying electric field in the water surrounding its body. Any nearby object with distinct electrical properties compared to the surrounding waters will cause perturbations in this electric field. These perturbations are detected by thousands of electroreceptors located on the fish's skin.

Electroreceptor density on the fish's skin isn't uniform. The two highest density regions are the head and the dorsal filament, a distinct structure situated on the dorsal edge of the trunk. The head includes other sensory systems like vision, but, the dorsal filament appears to be innervated solely by afferents originating from electroreceptors. This suggests that it primarily serves as an electroreceptive organ. While there is some evidence indicating a dorsal bias during prey capture behavior, the precise role of the dorsal filament in electric sensing is uncertain.

Here, quantitative measurements of fish behavior were used to evaluate sensitivity to electrosensory stimuli positioned at various locations. Upon stimulus onset, fish approached the stimulus location, orienting with small changes in roll angle in some cases. In addition, the fish showed a higher detection frequency for stimuli located over the dorsal filament, compared to the rest of the trunk. These observations collectively suggest that the dorsal filament provides a superior electric image compared to the rest of the trunk.

Table of Contents

This thesis contains underlined hyperlinks. Clicking on those links will bring the reader to the appropriate section of the thesis. *Writing Tools* from Apple Intelligence (iPad OS 18) was used as an editing tool for some sections of this document.

List of Figures

List of Figures - Appendix

List of Tables

List of Tables - Appendix

Introduction

Acquiring information about the environment is the primary objective of every sensory system. However, this complex task varies among sensory systems. Why is it so challenging? Simple physical aspects of the stimulus significantly influence how the sensory system reacts to it. For instance, a weak signal in a noisy environment could be difficult to detect. Moreover, the nature of the stimulus itself plays a crucial role in determining the requirements in terms of receptor type and related structures. Every single stimulus type requires its own specialized receptor. The location of the sensory organ and the receptor density are also important factors that dictate how the organism can utilize the sensory system. A region with a high receptor density might provide better quality information about a stimulus, and the structure on which these receptors are located allows for optimal sensing.

The electrosensory system in weakly electric fish is an intriguing sensory system that humans don't have. To fully comprehend how these fish utilize this sensory system, all previously explained factors are essential. The electrosensory system itself relies on specialized electroreceptors to detect electrical stimuli and is organized in a unique manner in weakly electric fish (Carr et al., 1982; Scheich et al., 1993). This omnidirectional sensory system exhibits varying densities of electroreceptors on the fish's skin (Carr et al., 1982; Franchina & Hopkins, 1996). A distinctive structure with a high electroreceptor density, known as the dorsal filament, is found in certain species (Franchina & Hopkins, 1996). Electrical stimuli can vary in intensity, have low electrical contrast relative to their surroundings, originate from multiple locations, and be noisy. Could this dorsal filament assist in overcoming these challenges? The primary goal of this thesis is to investigate the role of this structure in electrosensing by thoroughly exploring two hypotheses. The first hypothesis is that the dorsal filament enables enhanced sensitivity to weaker signals compared to the corresponding ventral areas. The second hypothesis is that the dorsal filament provides superior quality information compared to the rest of the trunk by repositioning and orienting the dorsal edge towards an electrosensory stimulus.

Sensitivity & Acuity in Sensory Systems

Every sensory system has their own characteristics. But what they all share in common is being composed of sensory cells physically located in specific body regions, and, innervated by afferents that transmit the information to the central nervous system. While the nature of the receptors and the destination in the central nervous system varies among these systems, certain principles apply in all of them, such as acuity and sensitivity. However, the meaning of these terms can differ depending on the sensory system. For instance, in vision, spatial acuity refers to the ability to discern fine details in space, while sensitivity denotes the ability to detect low-contrast objects irrespective of their size (Zimmerman et al., 2011). In contrast, in hearing, acuity measures the sensitivity to sounds, which is the intensity required for a sound to be audible (Alhazmi, 2020). Similarly, in tasting, acuity is also a measure of sensitivity (McDaid et al., 2007). In smelling, olfactory acuity describes thresholds and discrimination, also known as olfactory sensitivity (Stafford & Welbeck, 2011). Regarding tactile sensing, acuity and sensitivity returns to separate definitions. Sensitivity refers to the threshold of detecting a tactile stimulus, while acuity characterizes the ability to discriminate between a stimulus being present at a single location or more (Zingaretti et al., 2019). In electrosensing, we consider the quality of sensory input as spacial and temporal acuity (Babineau et al., 2007), as well as the sensitivity, which is the intensity required for an electrical stimulus to be detectable. Obviously, sensitivity and acuity are related to the location of the sensory organ itself, which contains the sensory cells.

Although sensory receptors can be found on occasion on non-sensory organ locations (Dalesio et al., 2018), they are typically found on specific and specialized organs to optimize sensing. For example, photoreceptors are found on the retina in the eye, taste cells in the mouth, olfactory cells in the nose, hearing cells in the ear, and tactile cells distributed throughout our skin. For this tactile sense, we require receptors distributed throughout our body since we need to be aware of when an object meets our skin. When speaking of human vision, it is ideal to have our eyes positioned in the anterior region of our head, as everything about our body is designed to complete the most complex tasks in front of us. Lastly, electroreceptors used for electrosensing in weakly electric fish can be found all over the fish's skin (Nelson & MacIver, 1999). Receptor location is important, but receptor density is also an important factor to consider when trying to make sense of and how the fish encodes sensory input.

Receptor density plays a pivotal role in determining the acuity of a sensory system. For instance, the retina's fovea in the human eye is the region with the highest photoreceptor density, which provides exceptional acuity in the field of vision (Curcio et al., 1990). Similarly, the cochlear fovea in bats, which has a higher innervation density per octave (Zhang et al., 2015), is crucial for detecting the Doppler-shifted echo responses generated by their echolocation calls (Russell et al., 2003). Moreover, the pain fovea situated at the fingertips (Mancini et al., 2013) exhibits finer spatial resolution as one moves further distally along the limbs (Weissman-Fogel et al., 2012). Beyond acuity, receptor density also influences sensitivity in certain sensory systems. For example, olfactory sensitivity increases with receptor density (Apfelbach et al., 1991; Meisami, 1989). These examples collectively illustrate the existence of neural mechanisms and variations in receptor densities across multiple sensory systems, all optimized for sensing. These two concepts of acuity and sensitivity are the driving forces for this research project. Their role in electrosensing will be discussed at length throughout this thesis.

Electrosensory Systems

Electrosensing was first discovered in 1951 when H. W. Lissmann observed the *Gymnarchus niloticus*'s effortless navigation in both forward and backward directions in the dark. Electrosensing is a specialized sensory system found in various organisms, including weakly electric fish (Benda, 2020), and, can be categorized into two distinct types: passive and active electric sense. Passive electric sensing involves the use of an ampullary system to detect low-frequency external electric fields with remarkable sensitivity (Benda, 2020; Bullock et al., 1983). On the other hand, active electric sense entails the active generation of an electric field around the fish's body (Benda, 2020).

Equipped with thousands of electroreceptors, the active weakly electric fish can perceive perturbations within the generated electric field. These perturbations can be caused by nearby objects or living organisms with distinct electrical properties compared to the surrounding waters (Knudsen, 1975; Nelson & MacIver, 1999). Beyond this primary function, electrosensing serves various other purposes, including electrolocation, electronavigation (Benda, 2020) and electrocommunication (Carr, 1990).

Electric Organ and Electric Organ Discharge

The electric organ discharge (EOD) is the production of a dipolar electric field in the water around the fish (Benda, 2020). This discharge is generated by a specialized organ called the electric organ (Bennett, 1971). *Apteronotidae* subfamily including *Apteronotus albifrons* has an electric organ unlike most other weakly electric fish (Zakon et al., 1999). Their electric organ is composed of electromotor axons, compared to modified muscle fibres for other families and subfamilies of weakly electric fish (Zakon et al., 1999).

Electric fish generally exhibit two types of EOD: wave-type and pulse-type (Benda, 2020). Pulse-type electric fish produce an EOD intermittently, with each pulse being significantly narrower in duration than the interval between successive pulses (Benda, 2020). A well-known example of a pulse-type electric fish is the electric eel, renowned for its exceptionally high EOD amplitude, which can reach up to 860 V (de Santana et al., 2019). Another notable pulse-type electric fish is *Gnathonemus petersii*, characterized by its distinctive chin appendage (Bacelo et al., 2008).

In contrast to the electric eel, wave-type weakly electric fish lacks any potential danger associated with its EOD due to its wave-type EOD, which has an amplitude in the range of millivolts (Benda, 2020). Another characteristic shared by wave-type weakly electric fish, including *A. albifrons*, is the continuous nature of their time-varying electric organ discharge. *A. albifrons* exhibits a stable and regular frequency of approximately 1 kHz (Lissmann, 1951; Serrano-Fernandez, 2003).

Electroreceptors

To acquire information about the perturbations to the electric organ discharge, specialized receptors known as electroreceptors are required. In wave-type weakly electric fish, there are two primary categories of electroreceptors: ampullary and tuberous electroreceptors (Carr et al., 1982; Scheich et al., 1993).

Ampullary receptors detect and respond to low-frequency electric fields, particularly bioelectric fields generated by prey or other fish (Carr, 1990). In other words, ampullary electroreceptors responds to electric fields that are way lower in frequency compared to the electric organ discharge. Tuberous receptors, on the other hand, are tuned to the electric organ discharge's frequency. Tuberous receptors comprise two main subtypes: T-type and P-type (Carr et al., 1982; Franchina & Hopkins, 1996; Scheich et al., 1993). T-type electroreceptors act as a phase coder, providing information about the occurrence of an EOD (Carr et al., 1982). In contrast, P-type electroreceptors function as a probability coder. These probability coders respond to changes in local intensity of the EOD, which is crucial in electrolocation (Carr et al., 1982). In *A. albifrons*, the high frequency EOD presents a trade-off. Its high frequency (1khz) provides a higher electric image resolution by the probability coders by having a higher sampling frequency. However, this comes at the expense of making it more challenging to distinguish phase shifts with the phase coders since the intervals between every discharge is already short (Scheich et al., 1993).

The Electric Image

Contrary to the clear image we get with vision, the electrosensory system produces a blurry electric image. The profile of a "Mexican hat" is a common way to describe the electric image shape of a small nearby object (Budelli & Caputi, 2000). In other words, electroreceptors at the center of the object's projection on the skin will fire rapidly, then rapidly lower in firing frequency as you go outwards of that region. Several factors can influence this electric image, including the size and shape of the object, its distance relative to the fish and its electrical characteristics (Benda, 2020; Sicardi et al., 2000). Another important aspect that affects the electric image is the shape of the fish itself, as well as the tapered nature of the fish's body. For example, a simple tail bend can change the local field amplitude, and thus, may help with the discrimination of two nearby objects (Babineau et al., 2007; Heiligenberg, 1975). Considering all these factors makes analyzing and predicting behavior in response to a stimulus challenging.

Apteronotus albifrons

Apteronotus albifrons, commonly known as Black Ghost Knifefish (Nelson & MacIver, 1999) is a weakly electric fish that inhabit neotropical waters (see Figure 1 for a picture of *A. albifrons*). This fish is renowned for its remarkable ability to navigate through waters without visual cues (Benda, 2020). Omnidirectional swimming is a characteristic of *A. albifrons* (Lannoo & Lannoo, 1993). Interestingly, *A. albifrons* employs backward swimming to assess potential prey and ingest it. After backward swimming, a short forward lunge suffices to consume the prey (Lannoo & Lannoo, 1993; MacIver et al., 2001). In these cases of backward swimming, the initial location of prey is close to the tail or the trunk, suggesting electroreception is used for detection (Lannoo & Lannoo, 1993).

The distribution of electroreceptors on the body of *A. albifrons* isn't uniform (Carr et al., 1982; Franchina & Hopkins, 1996), suggesting that certain regions may be more sensitive to subtle signals or offer greater definition compared to others. Two distinct regions in *A. albifrons* that exhibits a higher electroreceptors density than the rest of the body are: the head, especially ventral regions (Carr et al., 1982), and the dorsal filament, which exclusively contains electroreceptors (Franchina & Hopkins, 1996). This raises the question: Is the dorsal filament advantageous for electrosensing?

Figure 1. Picture of Apteronotus albifrons.

The Dorsal Filament

The dorsal filament is a firmly attached structure located on the dorsal caudal-most edge of the trunk. The dorsal filament is devoid of bones, muscles and covered by an opaque mucus layer (Franchina & Hopkins, 1996). In general, weakly electric fish have an average origin location of the dorsal filament at approximately 48% of their body lengths from the snout, tapering gradually towards the tail without a distinct end point (Franchina & Hopkins, 1996). However, in *A. albifrons*, the dorsal filament originates on average at around 63% of the body lengths from the snout, making it the farthest origin among the Apteronotidae subfamily and compared to most other weakly electric fish (Franchina & Hopkins, 1996, see Figure 2 for visual representation of the location and the origin of the dorsal filament).

The dorsal filament is separated from the trunk by a high resistance barrier composed of two epithelial layers (Franchina & Hopkins, 1996). This barrier prevents currents, especially from nearby muscles, to transfer to the dorsal filament (Franchina & Hopkins, 1996), potentially enhancing the electroreception capabilities of this organ by minimizing potential interference.

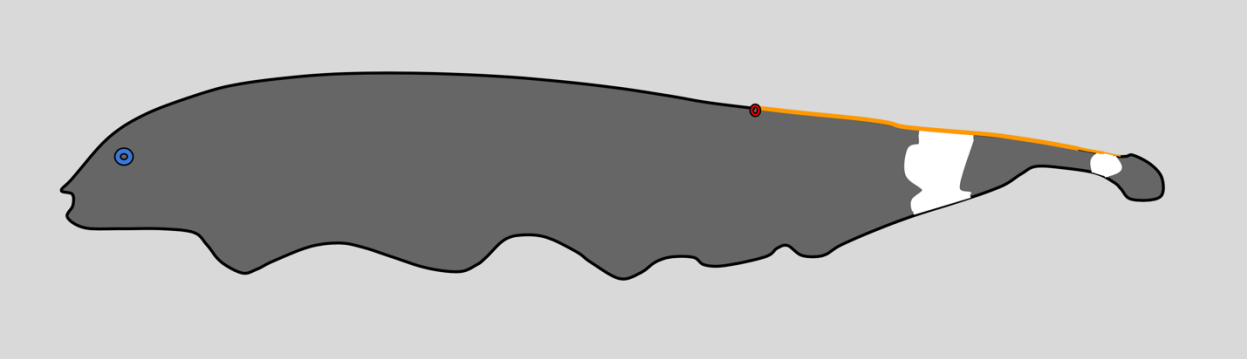

***Figure 2. Visual representation of the location and origin of the dorsal filament**. The orange line is the location of the dorsal filament, and the red dot is the origin.*

Electroreceptors on the Dorsal Filament

Electroreceptors found on the dorsal filament include both ampullary and tuberous electroreceptors (Franchina & Hopkins, 1996). Ampullary electroreceptors are situated near the junction of the dorsal filament and the trunk (Franchina & Hopkins, 1996). On the other hand, tuberous electroreceptors appear to be evenly distributed throughout the dorsal filament. (Franchina & Hopkins, 1996, see Figure 3 for a picture of these electroreceptors on the dorsal filament). The ratio of tuberous:ampullary electroreceptors ranges between 9:1 and 20:1 on the dorsal filament (Franchina & Hopkins, 1996).

In terms of receptor density, it is important to consider that the dorsal filament region is 2-3 times lower than the head (Carr et al., 1982). Consequently, the head likely serves as a primary electroreceptive region. On the trunk, the dorsum is the region that has the highest electroreceptors density with over 3 tuberous receptors/mm^2 compared to anywhere from 0.5 to 2.5 receptors/mm^2 for the rest of the trunk, depending on the specific region (Carr et al., 1982). However, it's important to consider that Carr's study (1982) didn't explicitly define the term "dorsal region" to include the dorsal filament. Furthermore, there's no mention of ampullary receptor density in that study. Franchina & Hopkins's (1996), on the other hand, observed a range of 3.9 to 6.4 tuberous electroreceptors per millimetre of length and 0.33 to 0.59 ampullary electroreceptors per millimetre of length on the dorsal filament. While these values don't provide a direct comparison to Carr's study (1982), they offer valuable insights into the composition of the dorsal filament. Overall, these findings support the notion that the dorsal filament serves as a structure for electroreception and possibly even an electrosensory fovea.

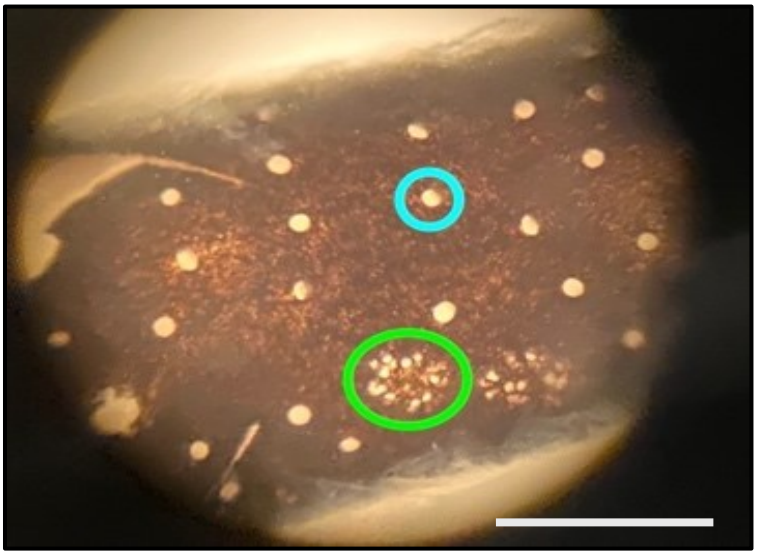

Figure 3. Top view picture of the dorsal filament from Apteronotus albifrons. *The blue circle shows a tuberous receptor, and the green circle shows an ampullary receptor. Scale bar: approximately 1mm.*

Foveal Regions in Electric Sensing

A foveal region in an electro-sensory system has been observed before. An example of such a fovea in *Gnathonemus petersii* is the chin appendage, commonly referred to as the Schnauzenorgan (Bacelo et al., 2008). This chin appendage serves a purpose of proximity electrosensing, allowing the fish to detect prey by moving it over surfaces, similar to how a human finger rubs over a surface to feel its texture (von der Emde, 2006).

The concept of an electrosensory fovea on the dorsal edge of *A. albifrons* is intriguing because no other sensory systems assist that region in sensory acquisition. Since electroreceptors are sensitive to stimuli originating from their direction of pointing (Benda, 2020), the dome geometry of the dorsal filament also suggests that it might make it a great candidate to acquire sensory information from a wide range of angles around the dorsal edge.

Previous studies focused on prey capture by dropping prey near the fish from the top of the tank (MacIver et al., 2001). However, this approach introduces bias since the prey is mostly over the fish. This prevents comparisons to stimuli originating from other directions, such as below the fish. Such an experiment would enable a fair comparison between reaction to stimuli originating from all directions around the fish. Understanding how a potential foveal region like the dorsal filament works can require either intricate biochemical analyses (Bacelo et al., 2008) or complicated behavioral experiments. Acquiring a large sample size for either approach can be time-consuming, involving multiple terminal experiments or require extensive time and patience.

Thesis Objectives

Determine if sensitivity to electrosensory stimuli varies with stimulus location.

Sensitivity to small signals plays a crucial role in sensory acquisition, and this project aims to determine which regions of the body are more sensitive to small signals compared to others. Specifically, the principal component of this analysis will be to compare the sensitivity to weak stimuli originating from regions close to the dorsal filament and other regions, such as the ventral regions of the trunk and the head. This will be achieved by strategically placing computer-controlled resistors around the fish, as explained in the following Methods section.

Determine if *A. albifrons* orients to stimuli at different locations in a manner that could increase sensory input from the dorsal filament.

The orientation and repositioning of *A. albifrons* when sensing a stimulus provides valuable insights into which body part the fish favours for electrosensing. In MacIver's study (2001), it was observed that weakly electric fish exhibit a slight rolling behavior towards their prey, positioning their dorsal side closer to the prey compared to the rest of their trunk. This behavior allows researchers to characterize the specific point at which the fish initiates a roll/reorientation maneuver for electrosensing. By measuring the fish's movements in response to stimuli located around its trunk, I will estimate the accuracy of orientation.

Methods

Stimulus

Resistor Ring

To deliver stimuli at various locations around the fish, eight computer-controlled resistors are strategically positioned in a ring configuration, spaced at 45-degree intervals. For future reference, resistor #1 is located at the top, and as you rotate clockwise, resistors #2 to #8 will follow in a sequential manner. A 3D-printed ring holds small carbon-tipped cables, which are connected to a ribbon cable responsible for transmitting the signal out of the tube. This approach eliminates the need for eight individual cables within the field of view, which could potentially hinder tracking using DeepLabCut (Mathis et al., 2018; Nath et al., 2019). Outside the tube's end of the resistor circuit is a single uninsulated metal wire wrapped around the exterior of the tube. See Figure 4 panel A for a visual representation of the resistor ring, see Figure 6 panel B for a picture of the resistor ring installed inside the tube and ribbon cable. A slight corrosion problem surfaced during testing, see Corrosion Problem in the appendices for more details.

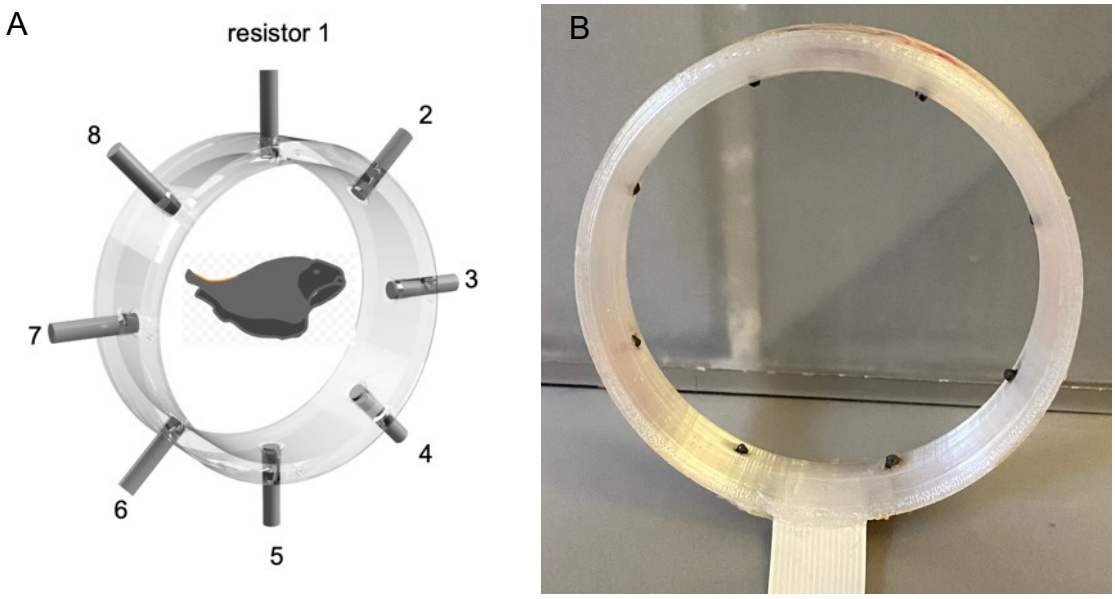

Figure 4. Visual representation of the resistor ring. *In panel A, fish is facing the open end of the tube in this scenario. Resistor numbering and location will be consistent with this organization throughout the thesis. In panel B, picture of the actual resistor ring.*

Stimulus Characteristics

The stimulus is generated using a shunting circuit of a carbon-tipped cable placed inside the tube and connected to a wire outside the tube. In between these two ends, a mechanical relay completes the circuit with a physical resistor. See Figure 5 for a visual representation of the stimulus circuit. This setup is based on a technique previously used in object perception for weakly electric fish and electric image analysis (Budelli & Caputi, 2000; Pedraja & Sawtell, 2024). Three test experiments using opto-couplers were conducted, but relays were reinstalled to make sure the stimulus worked as expected (see Opto-Coupler Experiment in the appendices for more details on these experiments).

In the first round of the experiment, the circuit resistance is set at a fixed value of 1.5kΩ. The primary objective was to create a strong stimulus to ensure that the fish could easily detect it. In the second round of experiments, the resistance values used are 1.5kΩ, 25kΩ, 50kΩ, 100kΩ, 250kΩ, 500kΩ, and 1mΩ (see the Resistor Configuration and True Value in the appendices for more details). As resistance increases, electrical contrast between the resistor and the surrounding tube wall decreases, resulting in a stimulus with a decreasing relative intensity.

In both rounds of the experiment, a control unstimulated state (sham) was set as an open circuit (the relays were activated, but they led to a channel with a physical air gap instead of a conductor or a physical resistor, see Figure 5 for a visual representation of the location of the air gap). These sham stimuli provide a control for variables like the clicking of the relays and to establish a baseline for no activation at all.

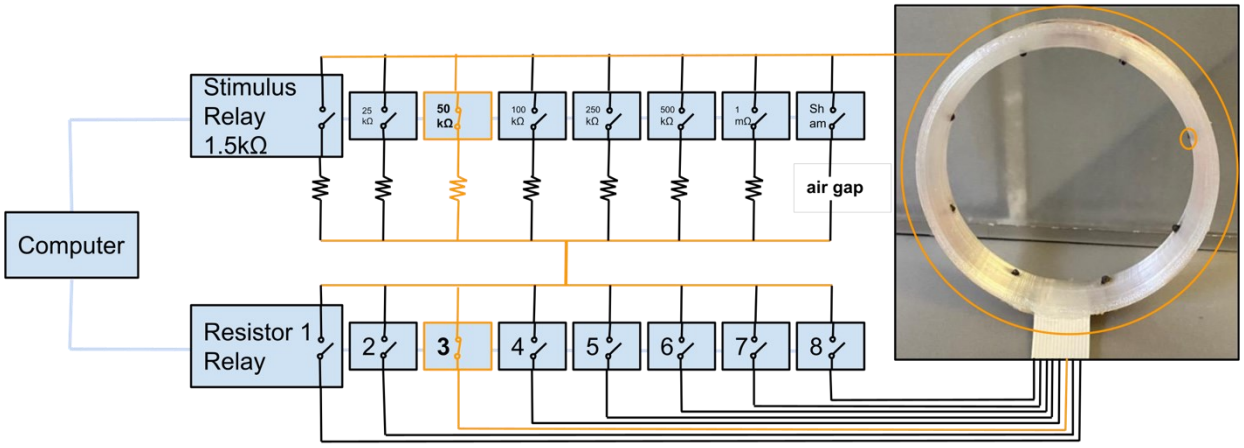

Figure 5. Shunting circuit for experimental stimulus. *The top row of relays selects the resistance value (stimulus intensity), while the bottom row selects the resistor location. All relays are controlled by a Raspberry Pi 4 via its GPIO programable pins. The orange circuit illustrates the path of an example stimulus: a 50kΩ intensity at resistor location 3. The orange circle around the resistor ring represents the metal wire that would be outside the tube. Note the sham stimulus as a physical air gap (approximately 1cm) in the circuit.*

Experimental Arena

Fish Tank

The fish tank is a square box 11 inches in both horizontal directions and containing 6 inches of water. The tank is designed to accommodate two mirrors at a 45-degree angle on adjacent sides. This arrangement enables simultaneous video capture of three points of view using a single camera mounted atop the tank, looking down at it. See Figure 6 panel A for a 3D representation of the fish tank.

Tube – Area of Interest

A transparent polycarbonate tube, measuring 3.5 inches in diameter and 10 inches in length, is positioned centrally and at a 45˚ angle in the experimental arena. Attached to one end of the tube is a perforated plastic sheet with an opening, while the other end is sealed with a transparent cap. A small leg beneath the tube elevates it from the tank's bottom, ensuring its level position. The side connected to the perforated plastic sheet serves as a barrier, restricting the fish's access to the corner of the tank or the tube while maintaining the entire water volume of the whole tank to dilute organic solutes. See Figure 6 for a 3D representation of the location of the tube in panel A and associated structures in panel B.

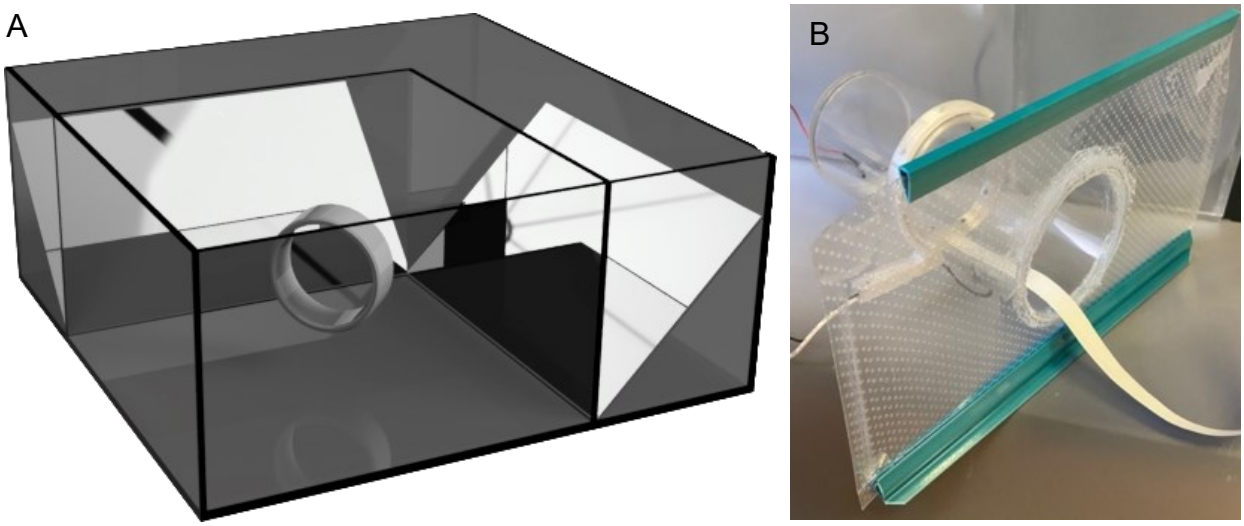

Figure 6. Visual representation of the experimental arena*. Panel A shows a 3D rendering of the experimental arena and the location of the mirrors. The white ring represents the location and orientation of the tube and resistor ring. Panel B shows a picture of the tube and related structures.*

Experimental Protocol and Sample Size

Experiment – Round 1

The objective of this round is to assess the fish's response to stimuli in all directions. One experiment consists in collecting 125 sham control samples, followed by 250 real stimuli, and then a second round of 125 sham control samples. The sequence of stimulus locations was randomized. In total, 11 experiments were conducted (fish length = 108.2mm +/- 10.4mm): 10 had identical protocols, while one additional experiment took significantly longer to complete (320 sham samples and 320 stimulus samples). Each experiment involved a different naïve fish. The total sample size was 5640 samples, 1067 samples were categorized as exits and an additional 4 samples needed to be removed due to the data structure (for more details, see Round 2 Setup Alterations). That is a total of 3.6 million video frames!

Experiment – Round 2

The objective of this round is to assess the fish's sensitivity to weaker stimuli in all directions. The higher the resistance of the resistor, the lower the electrical contrast compared to the tube walls. In this experiment, the same sham control and 1.5kΩ resistor from round 1 are reintroduced to compare the results with that round of experiments. These two resistor states were also randomized and mixed with the rest (see Stimulus Characteristics for all resistance values used in this round). Additionally, only four resistor locations (1, 3, 5, and 7) were used instead of eight to increase the sample size per location. Each resistance value was utilized 16 times at each of the four resistor locations, resulting in a total of 512 samples (sham & stimulus). A total of 22 experiments were conducted (fish length = 110.1mm +/- 8.3mm), with three having a lower sample count (258, 330, and 460 samples) due to a slower data acquisition frequency. Out of the 22 fish of the second round, 11 of them were used approximately five months prior in the first round of experiment. All other fish were not used in any behavioral experiments for at least 12 months prior to the second round of experiments. For more details on the experimental setup, refer to Round 2 Setup Alterations. The final sample size for round 2 is 10776 with 1260 samples categorized as exits. That is a total of 7.6 million video frames!

General Protocol

The fish are kept in a 12h/12h day/night cycle. On the day of the experiment for a fish, it was transported to the experimental arena at the beginning of the dark cycle and kept in the dark for the whole 10h acclimation and experiment. Water conductivity was kept at approximately 200 µS/cm +/- 20 µS/cm for the duration of the experiment. The water was completely changed with fresh new water for every new experiment. (ACVS protocol : Ble-3678-R1)

Data Acquisition & Automation

To record the videos, a Blackfly-S USB3 camera was used to record a square frame that captures the whole top of the fish tank at once (30 frames per second, 2048 pixels x 2048 pixels, see Machine Vision Camera in the appendices for more details). Then, some video preprocessing was required to separate the three views and prepare the videos for tracking (see Video processing in the appendices). Speaking of tracking, DeepLabCut (Mathis et al., 2018) was then used to get 2D tracking in each view. Once this 2D tracking is complete for each views, Anipose (Karashchuk et al., 2021), a python based complement to DeepLabCut, takes the three 2D tracking files to triangulate the views (see DeepLabCut & Triangulation in the appendices for more details) and produce one file that contains the 3D tracking coordinates. Between these two steps, a simple filtering algorithm was employed to help refine 2D tracking (see 2D Filtering in the appendices). Once all of that is done, the 3D position files are ready to be used for the analysis (see Splining, Distance and Angle Calculation & The "Big Data" Processing Step in the appendices). To verify data manipulations and calculations with the videos, a tool was developed to synchronize data points of interest with video and tracking (see The Dashboard in the appendices). In addition, to ensure accurate timing of stimulus onset and video recording, a visual confirmation using infrared LEDs was employed (see Resistor Video Confirmation Detection in the appendices). Data acquisition and processing were logged for each experiment (see Log Book in the appendices).

Prior to data acquisition, an automated mandatory 10-hour acclimation period was programmed for both rounds of experiments. This research project aimed to collect a large sample size and prevent human interaction by automating the experimental protocol. A Raspberry Pi 4 was used to accomplish that task. To achieve automation, a dedicated set of carbon-tipped cables was positioned at each end of the tube and connected to an amplifier to detect the electric organ discharge emitted by the fish. By periodically sampling the EOD, it is possible to determine when the fish was inside the tube (see Fish Location Based on OED Amplitude in the appendices). Once video recording began, a second verification of the EOD's amplitude was conducted just before the stimulus onset (see Sample Structure in the appendices). Between each stimulus, there was a mandatory waiting period of 8 to 12 seconds for the first round and 4 to 8 seconds for the second round (the actual time was randomized within this range) to allow the camera to save the video and provide a break for the fish. After collecting groups of five samples, a mandatory longer waiting period of 60 seconds was imposed to try to prevent the fish from becoming accustomed to the stimulus. Once the experiment completed, an LED indicator outside of the behavioral room indicated its completion (see Status LED Panel in the appendices). Finally, a few modifications to the experimental setup were required to accommodate the multiple stimulus intensities in round 2, more details can be found in Round 2 Setup Alterations of the appendices.

Even if the automated program verifies that the fish is in the tube before starting the stimulus, the fish can still exit the tube during the stimulus period. This occurred on a few occasions. These samples are excluded from the final dataset to prevent them from affecting the results and the analysis. These faulty samples were identified by tracking the location of all the body parts of the fish: when all body parts are located further than 30 mm from the resistor ring (towards the open end of the tube) and remained so for at least 1 second of the last 2 seconds of the stimulus phase, they were removed (see Filtering the Exits in the appendices for more details about their effects on the results).

In five out of eleven experiments in round 1, the resistor ring was rotated approximately 20 degrees counterclockwise (when looking at it from the open end of the tube) to position the ribbon cable over the EOD detector (and conceal it) to aid in tracking. The whole tube and resistor ring was rotated and repositioned properly in the second round of experiments.

Behavior Analysis Metrics

3D Distance and Detection

To determine if the fish detects the stimulus, this analysis relies on behavioral cues. One such possible cue is the rapid reversal, as explained by MacIver et al. (2001). This is the simple change in the longitudinal velocity of the fish from forward swimming to backward swimming. This cue was particularly useful in prey capture behavior analysis, as it allowed researchers to drop the prey near the fish. In the context of this research project, introducing the stimulus at a precise location to induce this behavior is challenging due to the fixed and automated nature of the experiment. While this criterion was tested for stimulus detection, it yielded poor detection contrast between the sham and stimulus samples and was not used for that reason (see Detection Based on Reversal Events in the appendices for the results of this reversal analysis).

In fish behavior, attraction and avoidance can indicate the detection of an object (Williams et al., 2023). In prey capture behavior analysis, 3D distance is a parameter used for weakly electric fish. As the fish attempts to capture a prey, the distance decreases (MacIver et al., 2001). In this analysis, 3D distance is defined as the distance between the activated resistor for that sample and the closest point on the fish. This closest point on the fish is technically on the central axis of the fish at either 0%, 25%, 50%, 75% or 100% of the fish's body length and can vary in time as the closest proportion change. Therefore, 3D distance will be the primary criterion used in this research project to identify stimulus detection.

As shown in Figure 7, the "closest distance" parameter appears to demonstrate a reaction to the stimulus as it varies in time. To count a sample as a detection event, the fish must get 50% closer than its initial distance (at the onset of the stimulus) and remain under that threshold for a minimum of 1.5 seconds. The fish has the 4 seconds of stimulation and 1.5 second post-stimulus to complete this task.

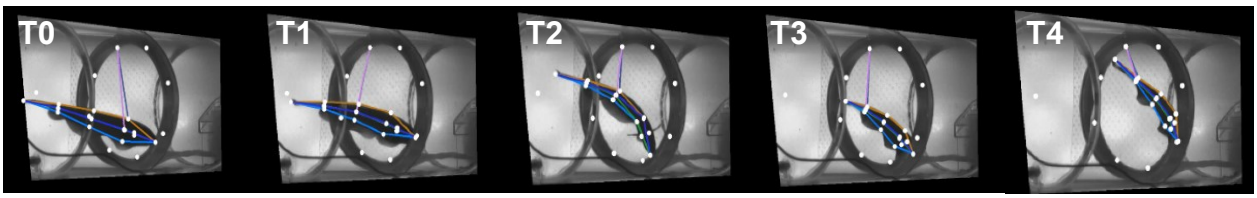

Figure 7. Distance demonstration. *Left to right shows the progression. Resistors 1 is activated in this demonstration. The pink line represents the closest distance to the closest center label. Pictures are taken at 1 second intervals with the first one taken at the stimulus onset (T0) and the last one at the stimulus offset (T4). Smallest closest distance can be seen at T4.*

Fish Proportions

For comparison purposes, the fish's body is separated into four distinct longitudinal segments. The first segment encompasses the head, defined as everything before 25% of the fish's body length. The second segment includes everything between 25% and 60% of the body length, named the mid-trunk. The third segment is the dorsal filament. According to Franchina & Hopkins (1996), the dorsal filament originates at 63% of the body length and gradually tapers towards the tail without a distinct end. Therefore, in the analysis, the dorsal filament is defined to start at 60% and end at 95%. Finally, the last segment (tail) is considered from 95% to 100% of the body length. These main proportions are especially important in the detection frequency analysis. See Figure 12 between panels C and D for a visual representation of these main proportions with colors.

Roll Reorientation

A roll reorientation in prey capture behavior is described as the reorientation of the fish's dorsal surface toward the prey (MacIver et al., 2001). To calculate the roll angle, a function developed by Anipose (Karashchuk et al., 2021) is utilized. This function, known as the "axis angle," requires three points in three-dimensional space. Two of these points define a vector around which the third point will be positioned, thereby determining the rotation angle relative to the Z-axis (see Two Angle Calculations in the appendices for a detailed explanation of this angle calculation). In this case, two mid points constitutes the central axis of the fish, and a third top dorsal label is the last point. Subsequently, to determine the relative roll angle between the fish and the resistor, the third point is replaced with the resistor, and the difference between the roll and resistor angles provides the relative roll angle. See Figure 8 for demonstration of roll.

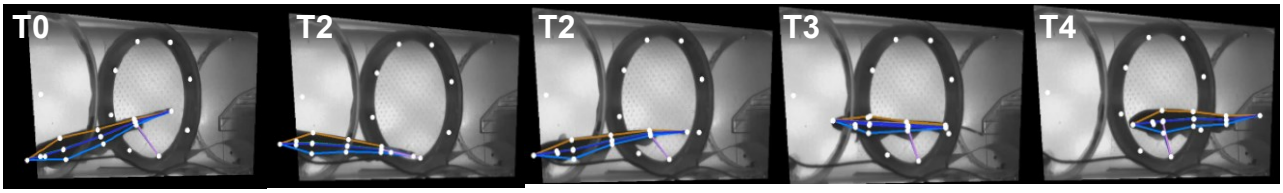

***Figure 8. Roll demonstration**. Left to right shows the progression. Resistors 5 is activated in this demonstration. Pictures are taken at 1 second intervals with the first one taken at the stimulus onset (T0) and the last one at the stimulus offset (T4). Roll behaviour is mostly happening in panels T2 & T3. Lowest relative roll angle value can be seen at T3.*

Minimizing False-Positive Detection Events

False positives are inevitable, especially with large datasets of behavioral experiments like this one. This is because there is always a chance that the fish spontaneously performs the behavior that defines the detection metrics. In total, 180 false positives were picked up from the sham samples across both rounds (5.2% false positive detection frequency). Threshold values can be found in 3D Distance and Detection. The reduction of this value is challenging since there are a few parameters in the detection metrics that can affect it. In addition, making a stricter detection parameters increases the chances of having false negatives since a sample that should count might be right outside of the stricter acceptable window and become a false negative. An example of this is making the distance to the resistor 75% closer instead of 50% closer, which would help with the false positive frequency by removing some of them. However, parameters that strict might have an even bigger impact on the stimuli samples by removing a larger proportion of them. Due to the large nature of sample size in this dataset, the limitation of false positive at the expense of potentially having more false negatives was the driving force in the decision of the detection metrics.

Manual Behavior Identification

Manually analyzing the behavior of fish for each sample is a possibility in behavior analyses, but it's time-consuming and not ideal. This is because visually observing the behavior can be biased, leading the researcher to report what they think the subject is doing without any objective measurement in some cases. For this reason, the previously explained quantitative behavior analysis is used for the Results, but this manual behavior identification was used as a confirmation of the automated analysis.

This manual behavior identification step was not conducted blindly and information such as sham/stimulus, resistor location and onset time were known. Ideally, a blinded version of this analysis would be more insightful and provide a fair comparison between the sham and the stimuli samples. However, the decision to use this technique was based on the nature of the tool used for this analysis (see The Dashboard in the appendices for more details), which was originally designed to observe videos and verify data points. In total, 177 sham samples and 165 stimuli samples were observed and analyzed across all fish from the initial round of the experiment.

For detailed observations and respective counts, refer to Manual Behavior Analysis in the appendices.

Statistical Analyses

Linear mixed models (LMM) and generalized linear mixed models (GLMM) are the primary statistical modelling techniques employed in this analysis. For more details on the models and assumptions, refer to the Additional statistical analysis in the appendix. To begin, a Kolmogorov-Smirnov Test was conducted to compare the distribution of closest proportions in Stimulus Origin Distribution section to a flat distribution. In the 3D Distance Reaction section, a linear mixed model (LMM 1) was used to compare the sham and the stimulus dataset from round 1. In the General Detection Frequency section, a generalized linear mixed model (Binomial GLMM 2) was used because the dependent variable is a binomial dataset. Another linear mixed model (LMM 2.1) was used in this section to compare the non-detections from the stimulus and the sham of round 1. Similarly, four generalized linear mixed models (Binomial GLMM 3.1, Binomial GLMM 3.2, Binomial GLMM 3.3 & Binomial GLMM 3.4) were used in the Dorsal Filament & Head Detection Frequency section. This dataset from round 2 was divided two separate ways. The first way was into two groups to compare the head and the dorsal filament regions individually. The other way was to separate the data from resistor 1 and resistor 5. Finally, two similar linear mixed models (LMM 4.1 & LMM 4.2) were used in the Post-Detection Reorientation section to analyze roll reorientation in both rounds of experiments separately.

In all mixed models, the fixed effects sham/stimulus and resistor location are categorical. Resistance (stimulus intensity), longitudinal body proportion and initial distance are continuous. Random effect of fish number is categorical and random effect of sample number (time) is continuous. The modelling was performed using the Lme4 package in R (Bates et al., 2014). See Table 1 for statistical equations of these models.

Model name	Model equation
LMM 1	`Distance_difference ~ Sham_Stim + Resistor + Initial_distance + (1| Fish_number) + (1|Sample_number)`
Binomial GLMM 2	`Detection ~ Resistor + Resistance + Sham_Stim + (1|Fish_number) + (1|Sample_number)`
LMM 2.1	`Distance_difference ~ Sham_Stim + (1|Fish_number) + (1|Sample_number)`
Binomial GLMM 3.1 & Binomial GLMM 3.2	`Detection ~ Resistor + Resistance + Sham_Stim + (1|Fish_number)`
Binomial GLMM 3.3 & Binomial GLMM 3.4	`Detection ~ Closest_initial_proportion + Resistance + Sham_Stim + (1|Fish_number)`
LMM 4.1	`Relative_angle_difference ~ Resistor + (1|Fish_number)`
LMM 4.2	`Relative_angle_difference ~ Resistor + Resistance + (1|Fish_number)`

Table 1. Statistical modelling equations.

Results

Stimulus Origin Distribution

The experimental setup ensures distribution of the stimulus location all around the fish. Figure 9 panels A and B illustrate the distribution of the initial stimulus location (T0, onset of the stimulus) of all samples, including the sham samples. Notably, the advantage of having the stimulus as a ring of resistors (for more details, refer to Stimulus) is the uniform distribution of detectable stimulus around the fish. Figure 9 panels C and D similarly show the distribution of the stimulus's closest body proportion on the fish at the onset (see Figure 10 panel A for a schematic showing an example of the closest proportion on the fish). Since the fish can't be perfectly aligned in the resistor ring every time, this results in increased chances where the head or tail would be closest to the activated resistor at the onset compared to other body proporitons. In addition, the distribution isn't perfectly uniform across all body positions between 5% and 95% for both rounds of experiments ($p<0.001$, Kolmogorov-Smirnov Test). Due to this variation across longitudinal proportions, subsequent analyses, like the detection frequency, will normalize the number of events based on the total possible events for that longitudinal proportion.

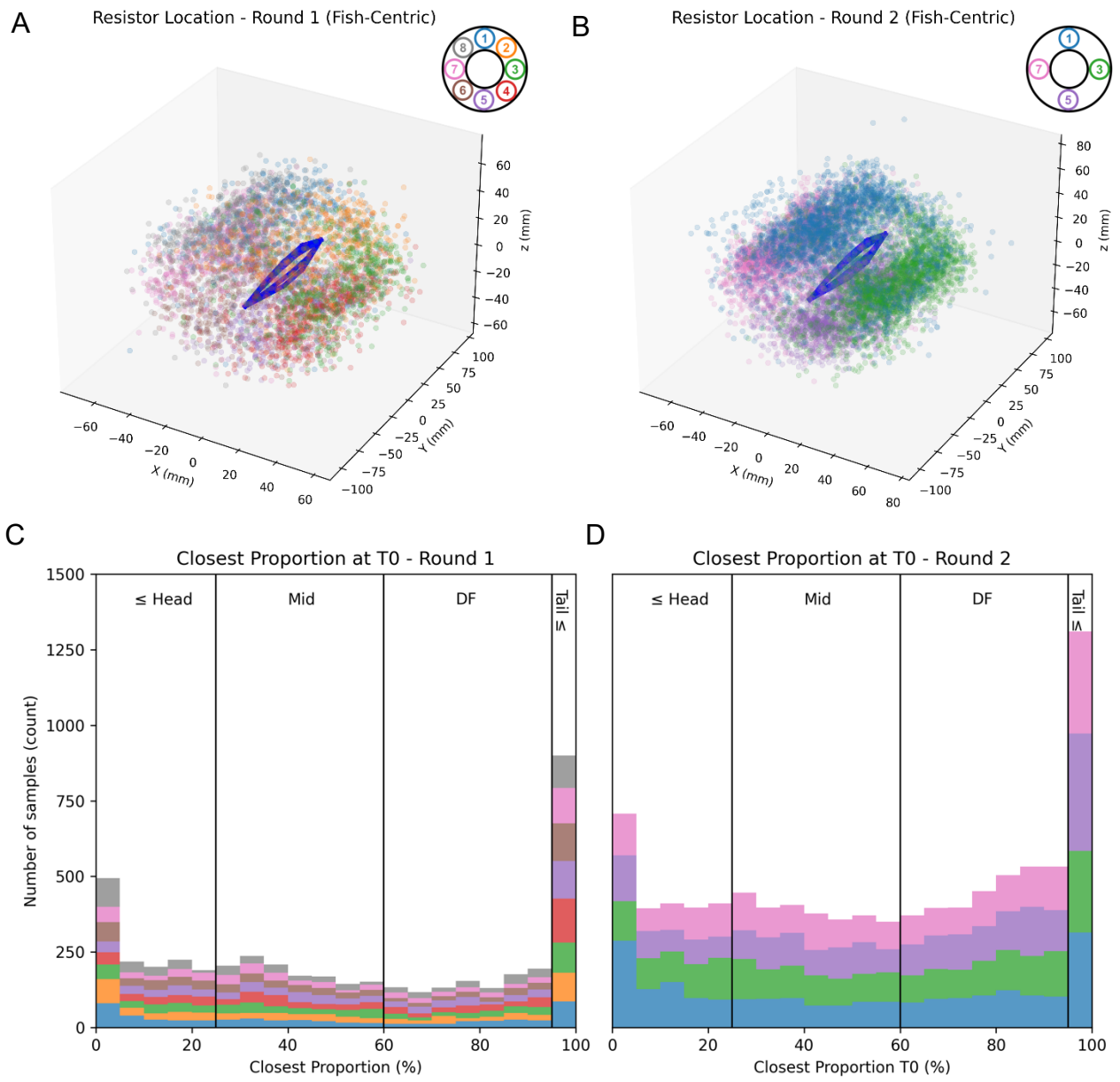

Figure 9. Stimulus location is distributed around the fish. *The relative position of the resistor at the onset of the stimulus is depicted for all eight resistors in panel A (round 1) and four resistors in panel B (round 2). This figure assumes that the fish is straight and parallel with the tube but this is not always the case. The resistor's location is relative to the center of the fish at 50% body length. The orientation of the fish in the tube is also accounted for; in this scenario, the fish is facing towards the capped end of the tube. The fish's roll angle is considered but not pitch or yaw. In panels C and D, the distribution of the stimulus closest proportion is presented as a stacked histogram for both rounds 1 and 2, respectively. Each bin represents 5% of the body length.*

3D Distance Reaction

Fish-resistor distance decreases after the stimulus onset. Figure 10 panels B and C show a clear difference between sham and stimulus samples from the first round of experiments (LMM 1, $p<0.001$). For the stimuli samples, the distance reduction is evident after the stimulus onset (T0) and stabilizes near T1.5 (1.5 seconds after stimulus onset). This time point will be used for further analyses. Interestingly, when comparing the distance distribution between the pre-stimulus phase (unimodal Gaussian distribution, 40.67±12.14mm) and after one second of stimulation (bimodal Gaussian distribution, 15.98±7.47 mm & 40.67±12.14mm), there is a clear reduction in distance for a portion of the data points (see Distance Distribution – Round 1 in the appendices for more details). Additionally, the farther the fish is from the activated resistor at the onset, the longer the distance it can travel. This initial distance effect on distance difference (T1.5 – T0) is observed in this dataset (LMM 1, $p<0.001$). For an equivalent figure to Figure 10 panels B and C with the raw data including the post stimulation phase, see Raw Distance 3D With After. Also, for an equivalent figure to Figure 10 panels B and C for round 2, see Raw 3D Distance – Round 2.

Figure 10 panels D through I show the closest proportion's location in the resistor ring plane. There is a clear difference between the sham and the stimulus samples in the panels F and G ("after" time point). In the sham, the distribution of location remains random and in the stimulus samples, there is visually a preference for the activated resistor. The same movement towards the resistor is consistent across all the higher resistors, with only a slight reduction in distance difference for resistors 5 and 6 ($p<0.01$, LMM 1). A version of these three stimuli heat maps subfigures (Figure 10 panels E, G & I) with fixed body positions can be found in Position in Resistor Ring – Fixed Body Position of the appendices.

This 3D distance reaction shows a strong behavioral response to the stimulus. As explained in Behavior Analysis Metrics, this 3D distance response will be used as a proxy for stimulus detection.

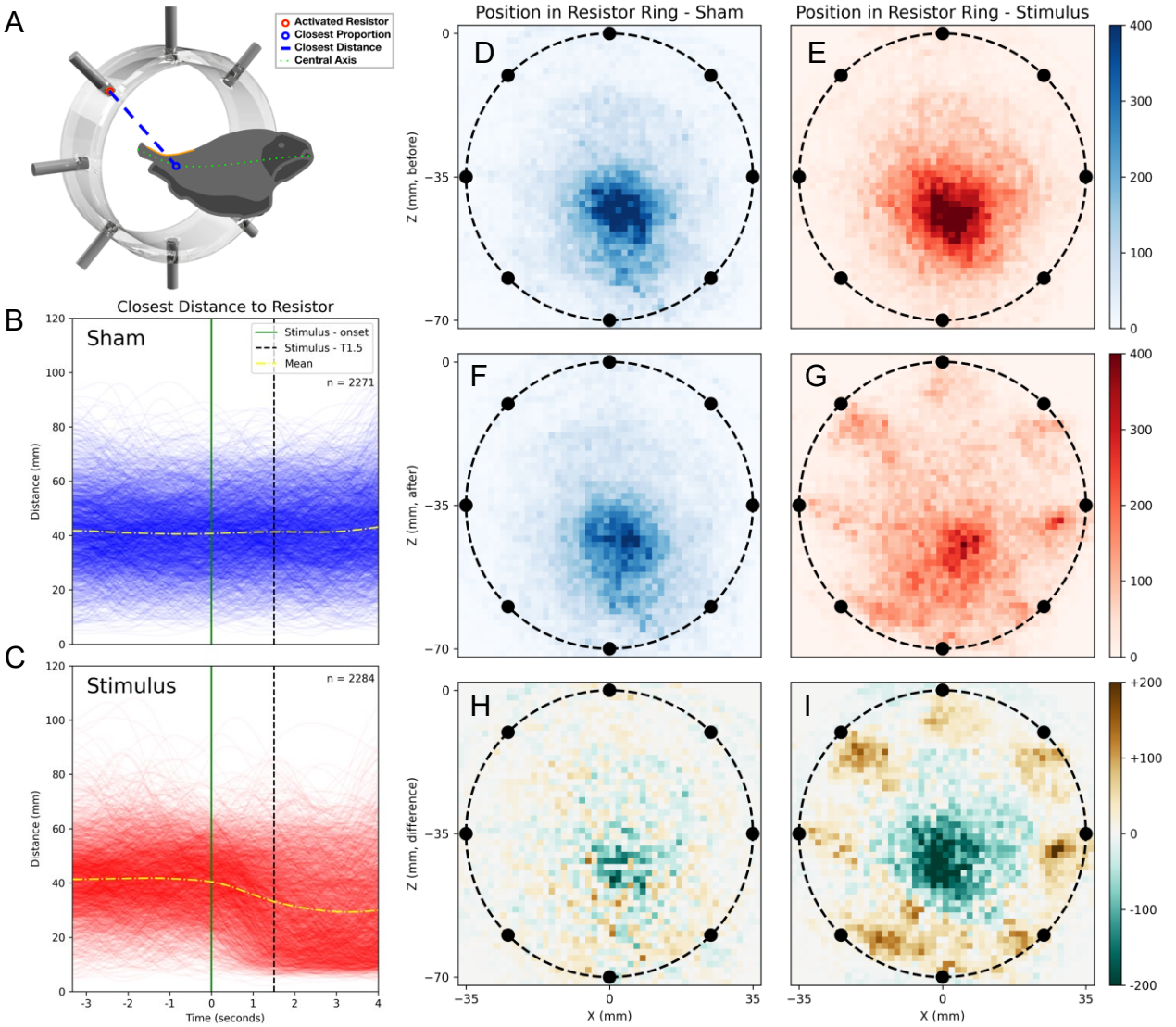

Figure 10. Fish-resistor distance in response to the stimulus. *Fish-resistor distance is measured as the distance between the resistor and point on the fish that is closest (i.e. this is a floating-location on the central axis of the fish); see panel A for a schematic. The raw traces of closest distance in time for round 1 are shown in panels B through I. The green vertical line indicates the stimulus onset (T0), and the dotted black vertical line represents the T1.5 timepoint (1.5 sec after stimulus onset). The yellow dotted-dashed line represents the mean of all samples. Panels D and E show the fish's position in the 2D plane of the resistor ring for 60 frames (2 seconds) preceding the stimulus onset (before). Panels F and G show the same as D and E, but for 60 frames (2 seconds) following T1.5 (after). Panels H and I display the difference in bin counts between T0 and T1.5. The ring and black dots in panels D through I represent the resistor ring and resistor location, the corresponding color bars are included on the right.*

General Detection Frequency

Detection frequency decrease with decreasing stimulus intensity. Detection of the stimulus is based on 3D distance and detection events can only be categorized as detections or non-detections. When comparing the non-detections from the stimuli samples of round 1 (Figure 11 panel A) to the sham samples (Figure 10 panel B), there is a resemblance. When comparing both groups statistically, there is no statistical difference between them (LMM 2.1, $p=0.141$). In Figure 11 panel B, the raw closest distance samples from round 1 that didn't count as detections were removed. The leftover detections samples are clearly showing a reaction to the stimulus.

As mentioned in Stimulus Characteristics, stimulus intensity is inversely proportional to resistance. Figure 11 panel C shows the overall detection frequencies for multiple stimulus intensities and the sham samples, which are significantly different (Binomial GLMM 2, $p<0.001$). Additionally, as stimulus intensity decreases, the detection frequency decreases (Binomial GLMM 2, $p<0.001$). Surprisingly, even the weakest stimulus intensity at 1mΩ is still detectable and over twice as many detections compared to sham samples. The data from the first round of experiments and the second round are both presented and yield similar results for the same stimulus intensity. Out of the 10 635 stimuli samples, 3 030 samples across both rounds of experiments were counted as detections. See Detection VS. Non-Detection Raw 3D Distance in the appendices for the same graphs as panels A & B but for round 2, including the panels for sham samples.

Figure 11 panel D shows the average detection frequency for each resistance value at each resistor location in round 2. Overall, there is a similar detection frequency between stimuli coming from the top and bottom resistors (Binomial GLMM 2, $p=0.732$). However, there is a decrease in detection frequencies for the side resistors compared to the top and bottom (Binomial GLMM 2, $p<0.001$). This suggests that there is an overall dorsal-ventral bias in detection frequency compared to lateral stimuli.

Taken together, these results show that fish respond to stimuli with an approach and these responses are dependent on stimulus intensity. We now consider how these responses vary with initial fish location as a step towards understanding the role of the dorsal filament in detection.

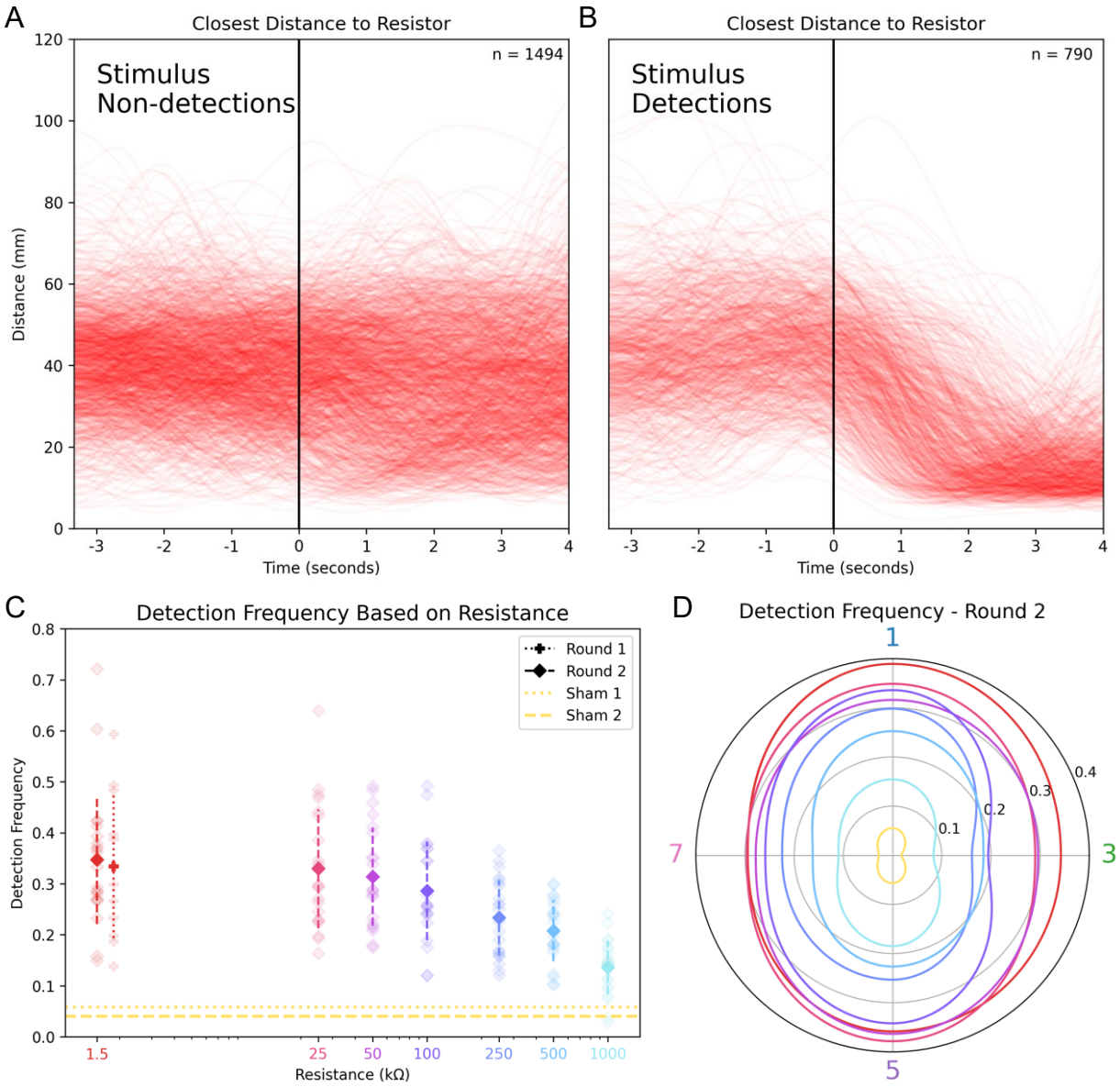

Figure 11. Detection frequency decreases with stimulus intensity. *In panels A and B, the raw distance data for the initial round of experiments is divided into two categories: non-detection and detection events respectively. In panel C, the normalized average detection frequency across fish is displayed for each resistance value (mean ± standard deviation) and for both rounds of experiments. Please note that the x-axis is logarithmic. In panel D, the average detection frequency (across fish) at each resistor location for round 2 is shown for each stimulus intensity. The exact detection frequency at a resistor location corresponds to the value at the intersection of plotted line and the resistor's corresponding quadrant line. The colors correspond to the colors in panel C. See Detection Based on Resistance – Count for the count version of panels C and D.*

Dorsal Filament & Head Detection Frequency

Sensitivity is higher for stimuli over the dorsal filament and under the head. Comparing locations near the head and the dorsal filament with the rest of the body give valuable insight on the sensitivity distribution to electrical stimuli. When compared to the head, the overall detection frequency of the dorsal filament region is reduced by 10% on average (across stimulus intensities, see Detection Frequency - Dorsal Filament VS. Head in the appendix for visual representation of the differences). However, this doesn't compare specifically the dorsal sensitivity of the dorsal filament to the head, but it includes all regions around the trunk at that location.

In most cases, the fish is oriented upright, with its dorsal face facing the top of the tube, as illustrated in Figure 12 panel A. When comparing dorsal regions, detection frequencies from stimuli coming from the top (resistor 1) are not significantly different across all longitudinal proportions ($p=0.15$, Binomial GLMM 3.3, see Figure 12 panel B and C). However, when looking at detection frequencies for ventral regions with the lowest resistor location (resistor 5), there is a decrease in detection frequency as you go from rostral regions (head and mid-trunk) towards the tail ($p<0.001$, Binomial GLMM 3.4, see Figure 12 B and D). This is similar for the ventral side of the dorsal filament region, which has a lower detection frequency compared to more rostral regions (see Figure 12 panel B). For both the head and dorsal filament, the detection frequency decreases as stimulus intensity decreases ($p<0.001$, Binomial GLMM 3.1, Binomial GLMM 3.2, Binomial GLMM 3.3 & Binomial GLMM 3.4), which is consistent with observations from General Detection Frequency.

When stimuli are located above the dorsal filament (resistor 1) at the onset of the stimulus, the detection frequency is significantly higher compared to other locations around the same region of the trunk (resistors 3, 5 and 7, $p<0.001$, Binomial GLMM 3.1, see Figure 12 panel B for resistors 1-5 comparison and Detection Frequency – Principal Body Regions in the appendices for all four resistors). This supports a slightly higher sensitivity to all stimulus intensities with the dorsal filament compared to ventral and lateral areas of the same region. For the head, the detection frequency from the sides and top resistors are not significantly different ($p=0.417$ for resistor 3 and $p=0.075$ for resistor 7, Binomial GLMM 3.2, see Detection Frequency – Principal Body Regions in the appendices for all four resistors). Interestingly, there is a significant increase in the detection frequency for the resistor 5 at the head region compared to resistor 1 ($p<0.001$, Binomial GLMM 3.2, see Figure 12 panel B).

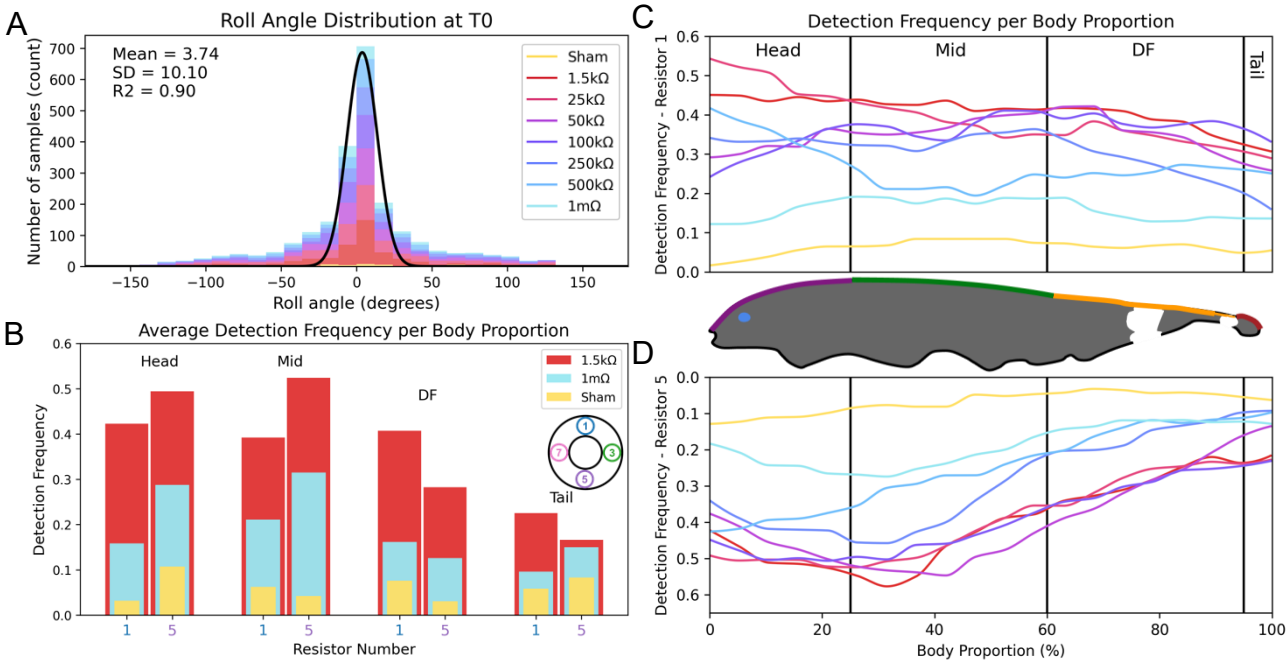

Figure 12. Detection frequency across body proportions. *Panel A presents the distribution of roll angles for all detection samples from round 2 at the onset (T0). Panel B presents the average detection frequency across fish for each major body proportions (closest at T0) for resistors 1 and 5. The weakest and strongest stimulus intensities (1.5kΩ and 1mΩ) and sham are included. Average detection frequencies across fish along the longitudinal axis of the fish is presented separately for resistor 1 (panel C) and resistor 5 (panel D). Note that panel D has a reversed Y axis.*

Post-Detection Repositioning

After detection, the fish repositions its head closer to the activated resistor. As illustrated in Figure 13 panel A, the fish undergoes a significant repositioning relative to the resistor. In most cases, the head moves closer to the resistor. This is also evident in Figure 13 panel C and D, where the average fish movement between T0 and T1.5 is illustrated when resistors are activated around the fish.

The distribution of detection threshold crossing timing is distinct between the dorsal filament and the head regions. Notably, there is a visual increase in latency for detections made from more caudal regions, as shown in Figure 13 panel B. In other words, the distribution peaks for each major proportion shift to the right (increase in time) as initial closest proportion moves towards the tail. This suggests that it takes more time for the fish to reach 50% closer to the resistor when using more caudal regions. On a side note, when initial distance is increased, the minimum time it takes for a sample to cross the threshold also increases (see Distribution of Threshold Crossing – Round 1 in the appendices for more details). When considering the change in closest proportion, as depicted in Figure 13 panel A, the fish overall prefers to reposition its head closer. This repositioning takes some time and in situations where the fish would prioritize this over reducing the distance, it could explain the increased latency in Figure 13 panel B.

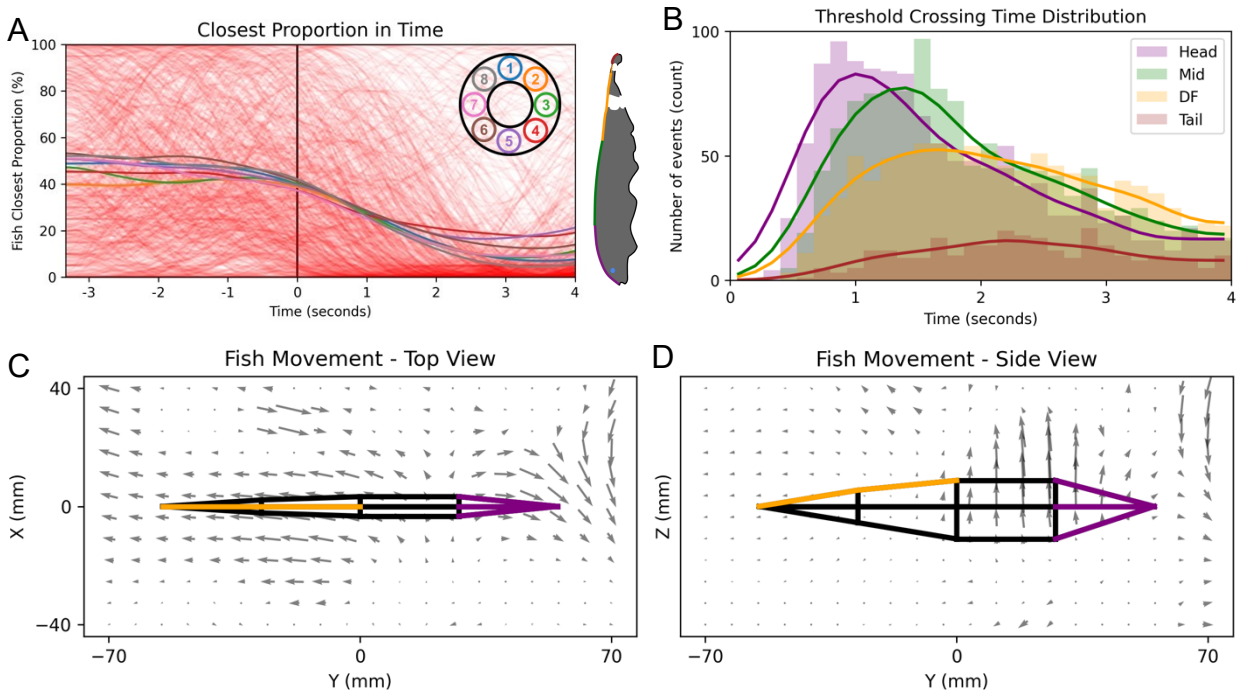

Figure 13. Post-detection movement. *Panel A presents the raw closest proportion (in percentage of the body length) in time for detection samples from round 1, along with the mean traces for each resistor. Panel B shows the distribution of threshold crossing times for all detection samples across both rounds of experiments. The data is separated by which body proportion was closest at the onset of the stimulus. In panels C and D, quiver plots illustrate fish movement after stimulus onset for both rounds of experiments. A 10mm slice of the datapoints located in the center of the Z axis and of the X axis were selected for figure C and D respectively prior to smoothing. Arrows shown are proportional to movement between T0 and T1.5. Measurements are relative to the center of the fish at 50% body length. See Quiver Plots – Sham the appendices for a visual representation of the datapoints used for the quiver plots and for the sham version of these quiver plots. See Quiver Plots – 3D Non-Smooth in the appendices for a 3D version of non-smooth quiver plots.*

Post-Detection Reorientation

Some reorientation behavior is observed for stimuli located more ventrally. Looking at the roll reaction to the stimulus may be an indicator of what location around the fish is preferred for sensing. The relative roll angle can be measured at the onset of the stimulus and again 1.5 second after to quantify reorientation (see Figure 14 panel A for a visual representation of this calculation). In Figure 14 panel B, the average trace for resistors located more ventrally show a slight decrease in the relative roll angle.

Figure 14 panel C (round 1) and D (round 2) present the average difference in relative roll angle between T0 and T1.5 for various conditions. In round 1, when selecting all detection events when the dorsal filament is closest to the resistor at the onset, there is a slight decrease in relative roll angle on average for resistors 4 and 5 compared to resistor 1 ($p=0.002$ and $p= 0.013$ respectively, LMM 4.1). A similar observation can be made for round 2, where there is also a decrease in relative roll angle for resistor 5 ($p=0.002$, LMM 4.2), and the stimulus intensity didn't affect this result($p=0.569$, LMM 4.2). This supports the idea that a slight reorientation can occur after the onset of a stimulus when it's initially located under the dorsal filament region.

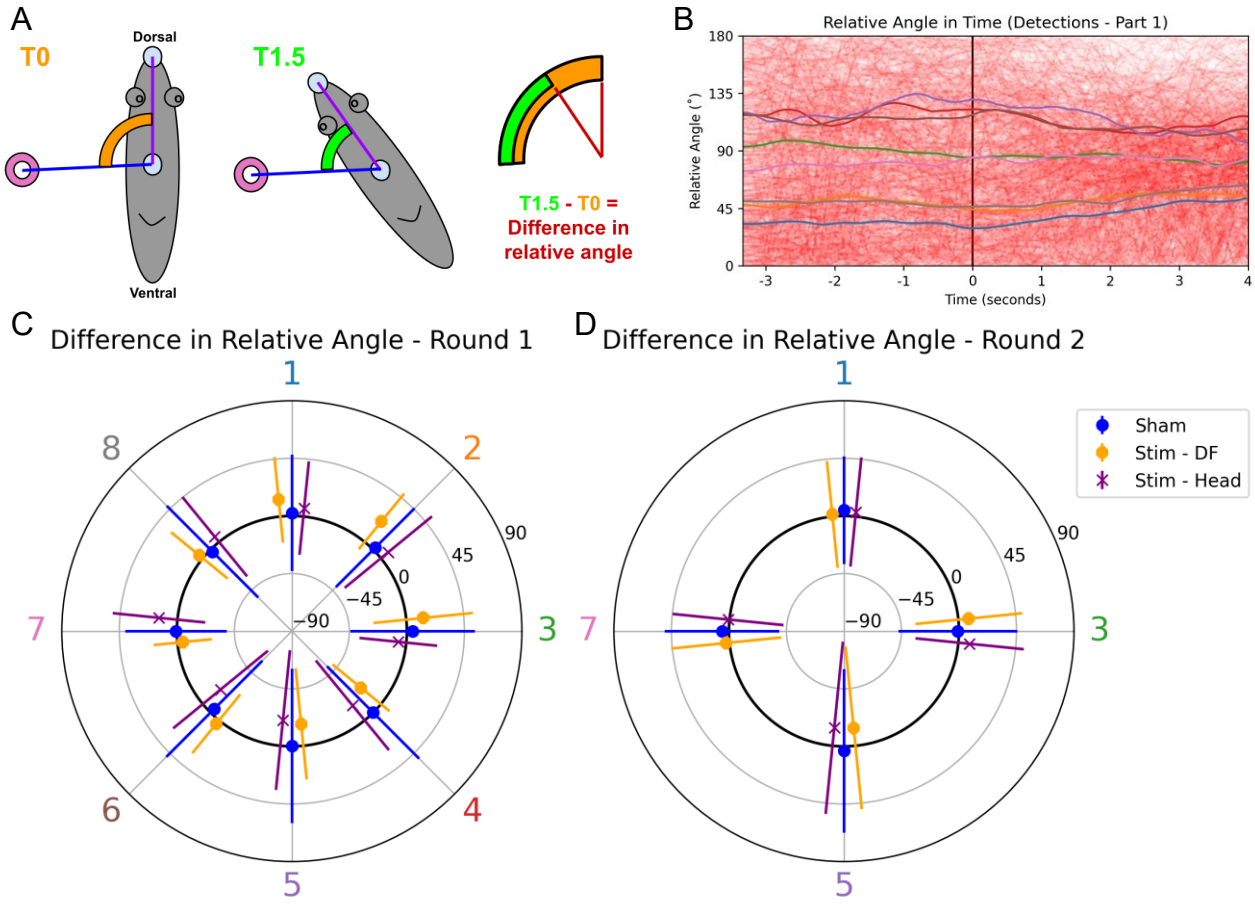

Figure 14. Post-detection reorientation. *Panel A presents a schematic of the difference in relative roll angle calculation used in panels C and D. Fish is facing the reader in panel A. Panel B displays the raw relative roll angle traces (at 50% of the fish's body length) in time for all detection samples of round 1, along with the mean traces of each resistor (see panel C for color map of the resistors). Panels C and D show the difference in relative roll angle between T0 and T1.5. Sham samples are included as a baseline. Panel C presents the overall difference in relative angle (mean ± standard deviation across fish) for round 1 where the closest proportion at the onset was the head (purple) or the dorsal filament (orange). Panel D shows the same data as panel C for round 2.*

Discussion

Result Summary

The first objective was to determine if sensitivity to electrosensory stimuli varies with location. The primary reaction observed was a reduction in the distance between the fish and the resistor, making it a clear and straightforward choice for detection proxy. The dorsal filament yields a higher detection frequency compared to ventral areas of the same region, while the head also generally offers a high detection frequency (see Dorsal Filament & Head Detection Frequency, Figure 12). The detection frequency is directly proportional to stimulus intensity.

The second objective was to determine if the fish reorients in a manner that could increase sensory input from the dorsal filament. Upon the stimulus onset, the fish undergoes a slight reorientation on average in response to stimuli positioned beneath it, consistent with a repositioning of the dorsal filament towards the stimulus (see Post-Detection Reorientation, Figure 14). In addition, the fish eventually repositions its head closer to stimuli regardless of initial closest proportion (see Post-Detection Repositioning, Figure 13).

The large sample size of this experiment enabled the exploration of fish behavior in simple and effective ways. Systematically analyzing fish behavior to stimuli originating from ventral locations was not previously done in prey capture studies (MacIver et al., 2001) since adding a live prey at those angles would be challenging. The experimental arena ensured even distribution of stimuli around the fish's body, particularly allowing the analysis of the reactions to stimuli from a ventral aspect (see Stimulus Origin Distribution, Figure 9).

Electrosensory Sensitivity of the Dorsal Filament & Head

The first prediction was that detection frequency would be higher when the dorsal filament was closest at stimulus onset compared to corresponding (caudal) ventral regions, which was the case (see Dorsal Filament & Head Detection Frequency). Interestingly, in these situations, the initial distance of resistor #1 (top) was on average slightly further away from the fish compared to the three other resistor locations (approximately 5 to 10 mm, see Average Distance at T0 – Round 2 of the appendices). This is an important consideration since the electric field intensity drops with distance cubed (Benda, 2020). Taken together, these observation supports the notion that the dorsal filament enhances the detection of stimuli, even in scenarios with weak stimulus intensity and increased distance.

As mentioned for *Apteronotus albifrons* in the introduction, another region with a high electroreceptor density compared to the rest of the body is the head, specifically ventral regions of the head. In general, when stimuli are closest to the head at the onset, there is an overall increase in detection frequency compared to other locations. In addition, within the head region itself, the detection frequency varies: the highest detection frequency is found for stimuli originating from beneath the fish (ventral locations). This observation also supports the idea that a higher electroreceptor density enhances electrodetection capacity as the chin has the highest electroreceptor density in the head region.

Following up with this receptor density effect on detection frequency, for stimuli originating from resistor 5 (under the fish), there is a decrease in detection frequency as you go from rostral to caudal regions. An interesting coincidence is the fish's body shape, which starts at a certain width and thickness near the head and becomes narrower and thinner as it gets closer to the tail. Less surface area means less room for electroreceptors. Since detection frequency is reduced in the same manner as the ventral skin's surface area when going towards the tail, this suggests that the dorsal filament could compensate with electrosensory sensitivity in more dorsal caudal regions.

Sensory Acuity of the Dorsal Filament

The second prediction was that the fish would reorient the dorsal filament towards the activated resistor to optimize sensing. While some reorientation was observed when analyzing the average reorientation in Post-Detection Reorientation, it was not always consistent or close to a full roll reorientation towards the bottom resistors (resistors 4,5 & 6). On the other hand, the measurement used (difference in relative roll angle) is only sampling at two timepoints (T0 & T1.5), which might not be fully representative of the complete reorientation happening. Looking at continuous differences in relative roll angle in time in conjunction with other metrics like distance and longitudinal velocity might give a better insight into the actual roll observed in this dataset.

Manual Behavior Observations

Among the numerous Manual Behavior Identification observations, in the sham stimulus samples, a common pattern emerged: the fish simply randomly swam in the tube without any interest in the resistor after the stimulus onset, which is to be expected in a non-stimulus setting. In addition, there were 15 samples where the fish coincidentally ended up near the activated resistor, potentially triggering the detection algorithm to count it as a detection event. Finally, some other interesting observations were made, including instances where the fish was sleeping or playing with a bubble at the top of the tube, which played a significant role in investigating the limitations of the experimental setup.

Repositioning and Reorientation Behavior

Post Detection Repositioning and Threshold Crossing

Post-detection reaction primarily involves a reduction in the closest distance, as discussed earlier. Additionally, the fish repositions its head closer to the activated resistor, which was clearly demonstrated in Post-Detection Repositioning. Detection threshold crossing times seems to increase as the closest proportion at stimulus onset gets closer to the tail. This is to be expected when the fish repositions the head before getting closer to the resistor since that first step takes time to accomplish. In over 77 samples from the Manual Behavior Identification, the head remained the final investigative region for the stimulus, irrespective of the initial proportion. This strongly supports the observations from the Post-Detection Repositioning results.

A statistical analysis which looked at the effect of initial closest distance and initial closest proportion on threshold crossing time was conducted. However, the overdispersion of the data did not allow for an appropriate analysis (see LMM 5 for more details).

Challenges with Reorientation Analysis

When analyzing individual traces of relative roll angle between the resistor and the top of the fish, there are relatively high noise levels in the data, which significantly impacts the analysis (see Figure 14 panel A). Two main factors can play a role in this noise level: the tracking technique and the fish's behavior itself. Furthermore, as points comprising the angles approach each other, such as the top label and its corresponding center label, variations in angle values become amplified. This is likely partially the cause of the noisy relative roll angle data.

An alternative relative roll angle method involving two vectors was also tested. One vector consisted of a center label and its corresponding top label, while the other vector was between the top label and the resistor. The angle between these two vectors could have served as an approximation of the relative roll angle. This method was straightforward to explain, but the uncertainty in the actual position of the resistor prevented its implementation. The Anipose-Axis angle constrains the location of the resistor by considering the fish's orientation. This eliminated some uncertainty in the relative roll angle presented in the Post-Detection Reorientation results. See Two Angle Calculations in the appendices for a more detailed explanation of the limitations.

Reorientation Asymmetry Between Resistors 4 & 6

In Figure 14 panel C, there is a slight difference in reorientation between resistors 4 and 6, which is also picked up in the statistical analysis. Technically, they should yield similar results since their relative angle from the top resistor are the same. However, in 5 experiments of the first round, the resistor ring was rotated, as explained in Tube – Area of Interest. This is likely the reason behind the asymmetry in the reorientation frequency for resistors 4 and 6.

Conclusion

Behavioral studies are an excellent way to gain insights into the usage of sensory structures. However, communication challenges are especially hard when in non-human interactions. To overcome this limitation, creative experimental approaches, like behavioral experiments, are essential to collect compelling data.

This research project focused on the dorsal filament of the weakly electric fish *Apteronotus albifrons*. It was hypothesized that a higher electroreceptors density would enhance sensitivity and acuity to stimuli compared to other locations around the trunk. As previously discussed, this region is particularly effective at detecting stimuli of varying intensities compared to the rest of the trunk. Moreover, signs of reorientation, which involve repositioning the dorsal filament towards lower stimuli, were observed. These conclusions, based on quantitative behavioral measures, suggest a distinct preference for this region especially for stimulus detection. To further explore these findings, additional experiments could be conducted to investigate whether the results change when the dorsal filament is prevented from being used (see Bonus Manipulation Experiment Ideas in the appendices for more details).

Bibliography

Alhazmi, F. H. (2020). White-matter integrity and hearing acuity decline in healthy subjects: Magnetic resonance tractography. *The Neuroradiology Journal*, *33*(3), 236–243. https://doi.org/10.1177/1971400920913868

Apfelbach, R., Russ, D., & Slotnick, B. M. (1991). Ontogenetic changes in odor sensitivity, olfactory receptor area and olfactory receptor density in the rat. *Chemical Senses*, *16*(3), 209–218. https://doi.org/10.1093/chemse/16.3.209

Babineau, D., Lewis, J. E., & Longtin, A. (2007). Spatial Acuity and Prey Detection in Weakly Electric Fish. *PLoS Computational Biology*, *3*(3), e38. https://doi.org/10.1371/journal.pcbi.0030038

Bacelo, J., Engelmann, J., Hollmann, M., von der Emde, G., & Grant, K. (2008). Functional foveae in an electrosensory system. *Journal of Comparative Neurology*, *511*(3), 342–359. https://doi.org/10.1002/cne.21843

Bates, D., Maechler, M., Bolker, B., Walker, S., & Christensen, R. H. B. (2014). *lme4: Linear Mixed-Effects Models using "Eigen" and S4*. https://doi.org/10.32614/CRAN.package.lme4

Benda, J. (2020). The Physics of Electrosensory Worlds. In B. (Ed.) Fritzsch & H. (Volume E. Bleckmann (Eds.), *The Senses: A Comprehensive Reference* (Vol. 7, pp. 228–254). Elsevier.

Bennett, M. V. L. (1971). Electric Organs. In *Fish Physiology* (Vol. 5, pp. 347–491). https://doi.org/10.1016/S1546-5098(08)60051-5

Budelli, R., & Caputi, A. A. (2000). The Electric Image in Weakly Electric Fish: Perception of Objects of Complex Impedance. *Journal of Experimental Biology*, *203*(3), 481–492. https://doi.org/10.1242/jeb.203.3.481

Bullock, T. H., Bodznick, D. A., & Northcutt, R. G. (1983). The phylogenetic distribution of electroreception: Evidence for convergent evolution of a primitive vertebrate sense modality. *Brain Research Reviews*, *6*(1), 25–46. https://doi.org/10.1016/0165-0173(83)90003-6

Carr, C. E. (1990). Neuroethology of Electric Fish. *BioScience*, *40*(4), 259–267. https://doi.org/10.2307/1311262

Carr, C. E., Maler, L., & Sas, E. (1982). Peripheral organization and central projections of the electrosensory nerves in gymnotiform fish. *The Journal of Comparative Neurology*, *211*(2), 139–153. https://doi.org/10.1002/cne.902110204

Curcio, C. A., Sloan, K. R., Kalina, R. E., & Hendrickson, A. E. (1990). Human photoreceptor topography. *The Journal of Comparative Neurology*, *292*(4), 497–523. https://doi.org/10.1002/cne.902920402

Dalesio, N. M., Barreto Ortiz, S. F., Pluznick, J. L., & Berkowitz, D. E. (2018). Olfactory, Taste, and Photo Sensory Receptors in Non-sensory Organs: It Just Makes Sense. *Frontiers in Physiology*, *9*. https://doi.org/10.3389/fphys.2018.01673

de Santana, C. D., Crampton, W. G. R., Dillman, C. B., Frederico, R. G., Sabaj, M. H., Covain, R., Ready, J., Zuanon, J., de Oliveira, R. R., Mendes-Júnior, R. N., Bastos, D. A., Teixeira, T. F., Mol, J., Ohara, W., Castro, N. C. e, Peixoto, L. A., Nagamachi, C., Sousa, L., Montag, L. F. A., … Wosiacki, W. B. (2019). Unexpected species diversity in electric eels with a description of the strongest living

bioelectricity generator. *Nature Communications*, *10*(1), 4000. https://doi.org/10.1038/s41467-019-11690-z
Franchina, C. R., & Hopkins, C. D. (1996). The Dorsal Filament of the Weakly Electric Apteronotidae (Gymnotiformes; Teleostei) Is Specialized for Electroreception. *Brain, Behavior and Evolution*, *47*(4), 165–178. https://doi.org/10.1159/000113236
Günel, S., Rhodin, H., Morales, D., Campagnolo, J., Ramdya, P., & Fua, P. (2019). DeepFly3D, a deep learning-based approach for 3D limb and appendage tracking in tethered, adult Drosophila. *ELife*, *8*. https://doi.org/10.7554/eLife.48571
Heiligenberg, W. (1975). Theoretical and Experimental Approaches to Spatial Aspects of Electrolocation. In *J. temp. Physiol* (Vol. 103).
Karashchuk, P., Rupp, K. L., Dickinson, E. S., Walling-Bell, S., Sanders, E., Azim, E., Brunton, B. W., & Tuthill, J. C. (2021). Anipose: A toolkit for robust markerless 3D pose estimation. *Cell Reports*, *36*(13), 109730. https://doi.org/10.1016/j.celrep.2021.109730
Knudsen, E. I. (1975). Spatial aspects of the electric fields generated by weakly electric fish. *Journal of Comparative Physiology ? A*, *99*(2), 103–118. https://doi.org/10.1007/BF00618178
Lannoo, M. J., & Lannoo, S. J. (1993). Why do electric fishes swim backwards? An hypothesis based on gymnotiform foraging behavior interpreted through sensory constraints. *Environmental Biology of Fishes*, *36*(2), 157–165. https://doi.org/10.1007/BF00002795
Lissmann, H. W. (1951). Continuous Electrical Signals from the Tail of a Fish, Gymnarchus niloticus Cuv. *Nature*, *167*(4240), 201–202. https://doi.org/10.1038/167201a0
MacIver, M. A., Sharabash, N. M., & Nelson, M. E. (2001). Prey-capture behavior in gymnotid electric fish: motion analysis and effects of water conductivity. *Journal of Experimental Biology*, *204*(3), 543–557. https://doi.org/10.1242/jeb.204.3.543
Mancini, F., Sambo, C. F., Ramirez, J. D., Bennett, D. L. H., Haggard, P., & Iannetti, G. D. (2013). A Fovea for Pain at the Fingertips. *Current Biology*, *23*(6), 496–500. https://doi.org/10.1016/j.cub.2013.02.008
Mathis, A., Mamidanna, P., Cury, K. M., Abe, T., Murthy, V. N., Mathis, M. W., & Bethge, M. (2018). DeepLabCut: markerless pose estimation of user-defined body parts with deep learning. *Nature Neuroscience*, *21*(9), 1281–1289. https://doi.org/10.1038/s41593-018-0209-y
McDaid, O., Stewart-Knox, B., Parr, H., & Simpson, E. (2007). Dietary zinc intake and sex differences in taste acuity in healthy young adults. *Journal of Human Nutrition and Dietetics*, *20*(2), 103–110. https://doi.org/10.1111/j.1365-277X.2007.00756.x
Meisami, E. (1989). A proposed relationship between increases in the number of olfactory receptor neurons, convergence ratio and sensitivity in the developing rat. *Developmental Brain Research*, *46*(1), 9–19. https://doi.org/10.1016/0165-3806(89)90139-9
Nath, T., Mathis, A., Chen, A. C., Patel, A., Bethge, M., & Mathis, M. W. (2019). Using DeepLabCut for 3D markerless pose estimation across species and behaviors. *Nature Protocols*, *14*(7), 2152–2176. https://doi.org/10.1038/s41596-019-0176-0
Nelson, M. E., & MacIver, M. A. (1999). Prey capture in the weakly electric fish Apteronotus albifrons: sensory acquisition strategies and electrosensory

consequences. *Journal of Experimental Biology*, *202*(10), 1195–1203. https://doi.org/10.1242/jeb.202.10.1195
Pedraja, F., & Sawtell, N. B. (2024). Collective sensing in electric fish. *Nature*, *628*(8006), 139–144. https://doi.org/10.1038/s41586-024-07157-x
Russell, I. J., Drexl, M., Foeller, E., Vater, M., & Kössl, M. (2003). The Development of a Single Frequency Place in the Mammalian Cochlea: The Cochlear Resonance in the Mustached Bat *Pteronotus parnellii*. *The Journal of Neuroscience*, *23*(34), 10971–10981. https://doi.org/10.1523/JNEUROSCI.23-34-10971.2003
Scheich, H., Bullock, T. H., & Hamstra, R. H. (1993). Coding Properties of Two Classes of Afferent Nerve Fibers: High-Frequency Electroreceptors in the Electric Fish, Eigenmannia. In *How do Brains Work?* (pp. 149–170). Birkhäuser Boston. https://doi.org/10.1007/978-1-4684-9427-3_18
Serrano-Fernandez, P. (2003). Gradual frequency rises in interacting black ghost knifefish, Apteronotus albifrons. *Journal of Comparative Physiology A: Sensory, Neural, and Behavioral Physiology*, *189*(9), 685–692. https://doi.org/10.1007/s00359-003-0445-8
Sicardi, E. A., Caputi, A. A., & Budelli, R. (2000). Physical basis of distance discrimination in weakly electric ÿsh. In *Physica A* (Vol. 283). www.elsevier.com/locate/physa
Stafford, L. D., & Welbeck, K. (2011). High Hunger State Increases Olfactory Sensitivity to Neutral but Not Food Odors. *Chemical Senses*, *36*(2), 189–198. https://doi.org/10.1093/chemse/bjq114
von der Emde, G. (2006). Non-visual environmental imaging and object detection through active electrolocation in weakly electric fish. *Journal of Comparative Physiology A*, *192*(6), 601–612. https://doi.org/10.1007/s00359-006-0096-7
Weissman-Fogel, I., Brayer-Zwi, N., & Defrin, R. (2012). Spatial resolution of the pain system: a proximal-to-distal gradient of sensitivity revealed with psychophysical testing. *Experimental Brain Research*, *216*(2), 181–190. https://doi.org/10.1007/s00221-011-2924-4
Williams, K., Goddard, P., Wilborn, R., Bryan, D., & Rooper, C. (2023). Fish behavior in response to an approaching underwater camera. *Fisheries Research*, *268*, 106823. https://doi.org/10.1016/j.fishres.2023.106823
Zakon, H., Mcanelly, L., Smith, G. T., Dunlap, K., Lopreato, G., Oestreich, J., & Few, W. P. (1999). Plasticity of the electric organ discharge: implications for the regulation of ionic currents. *Journal of Experimental Biology*, *202*(10), 1409–1416. https://doi.org/10.1242/jeb.202.10.1409
Zhang, S. Q., Li, S. L., Zhu, H. L., & Yan, L. Y. (2015). Specialized features of the outer hair cell shapes in the cochlear fovea of bats. *Genetics and Molecular Research*, *14*(3), 9530–9542. https://doi.org/10.4238/2015.August.14.16
Zimmerman, A. B., Lust, K. L., & Bullimore, M. A. (2011). Visual Acuity and Contrast Sensitivity Testing for Sports Vision. *Eye & Contact Lens: Science & Clinical Practice*, *37*(3), 153–159. https://doi.org/10.1097/ICL.0b013e31820d12f4
Zingaretti, P., Petta, A. M., Cruciani, G., & Spitoni, G. F. (2019). Tactile sensitivity, tactile acuity, and affective touch: from childhood to early adolescence. *Somatosensory & Motor Research*, *36*(1), 90–96. https://doi.org/10.1080/08990220.2019.1604334

Appendix

Additional Methods

Machine Vision Camera

A Blackfly-S USB3 camera from FLIR Teledyne recorded all official video footage for this research project. The region of interest was set at 2048 by 2048 pixels and recorded at 30 frames per second. MJPG compression resulted in an AVI format video. The software, SpinView (version 3.2.0.57), provided by FLIR Teledyne, was used for this purpose.

During a regular experiment with these settings, the camera generated on average 193380 frames, with a range of +/- 35920 frames per experiment, for round 1. For round 2, the average number of frame recorded was 208720, with a range of +/- 10376 frames. The average frame count for each part is represented by the mean value, while the standard deviation indicates the range of variation. The file size for the recorded videos was on average 73.74 GB +/- 13.90 GB for round 1 and 73.94 GB +/- 3.70 GB for round 2. Additionally, a separate computer was dedicated to storing the videos.

A notable feature of this camera is its ability to control it externally using GPIO connections. In this project, the camera was controlled by a Raspberry Pi, which managed the entire experimental protocol. Complement to Data Acquisition & Automation.

Fish Location Based on OED Amplitude

A carbon-tipped wire is positioned on each end of the tube through small holes in the bottom, allowing water to contact the carbon end and transmit the electric signal from the EOD to the wires. The signal is amplified 100X and fed through the microphone pin of an audio jack to convert it to an audio signal. A defined threshold determines if the fish is in or out of the tube. See Figure 15 panels A and B for a visual demonstration of the EOD detection and see panel C for a picture of the EOD detection setup. Complement to Data Acquisition & Automation.

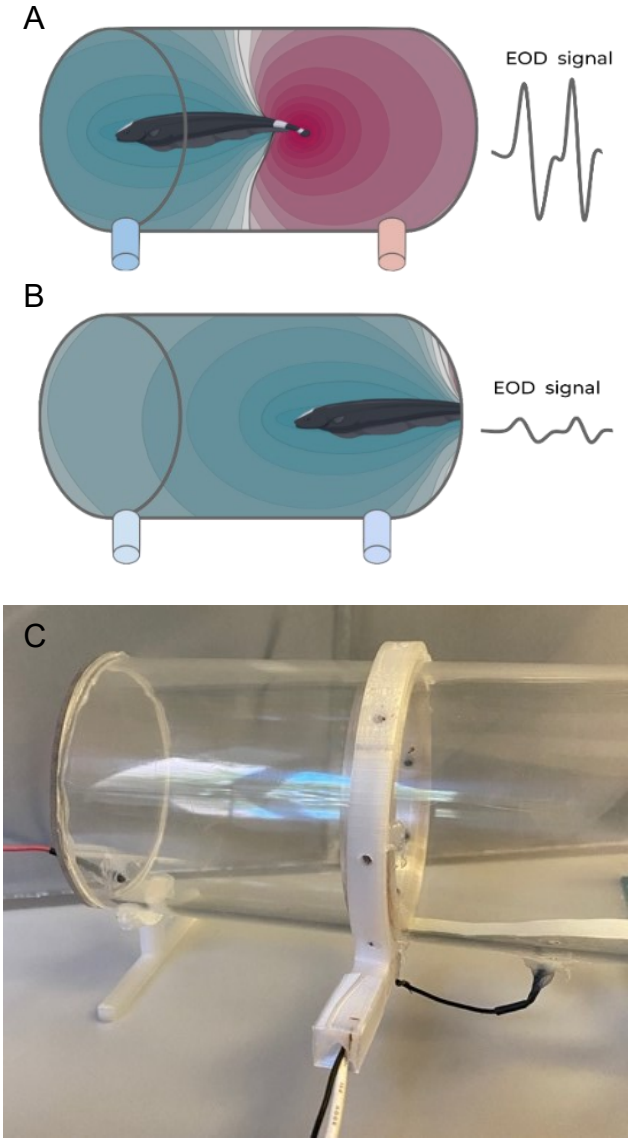

Figure 15. EOD amplitude reading based on fish. *Panel A shows a situation when the fish is located fully in the tube and panel B shows a situation where the fish in only partially in the tube. Panel C shows a closeup picture of the EOD detector setup. Red wire is at the caped end and black wire is at the open end of the tube.*

Sample Structure

To initiate a sample, the Raspberry Pi 4checks if the fish is in the tube and starts camera recording. A 4-second observation period precedes the activation of the resistor. The system checks again to ensure the fish remains in the tube before activating the stimulus. An additional observation period follows the stimulus, providing a before/after of the onset, useful for analysis. Complement to Data Acquisition & Automation.

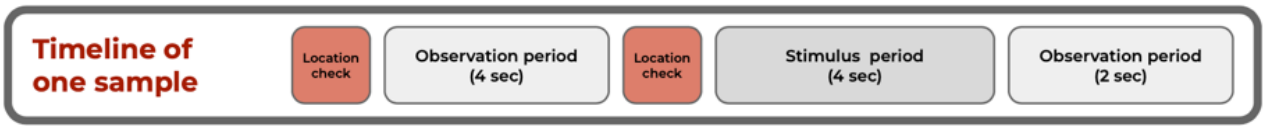

Figure 16. Timeline of one sample.

Status LED Panel

As the experiment progresses, the script sends progress data (acclimation, fish location, and script status) to a background script that updates the Status LED array outside the experiment room every 5 seconds (see Figure 17). A short flash of the lower LED confirms the script's successful running. This data is exchanged in real time between the two scripts in the form of a small data frame. Complement to Data Acquisition & Automation.

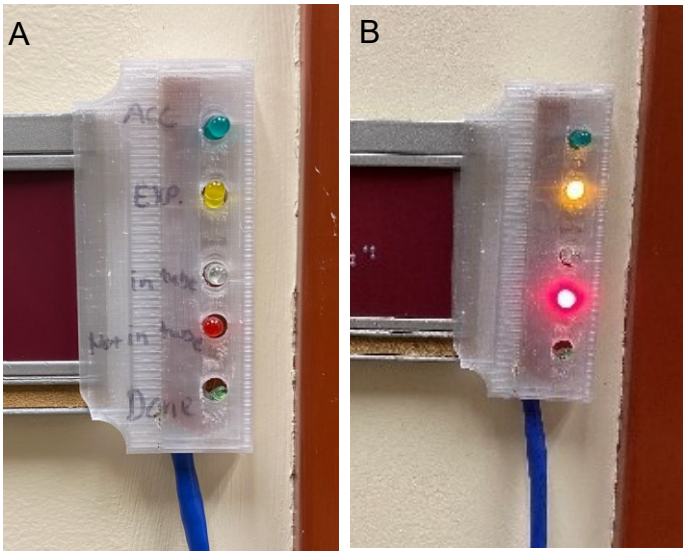

Figure 17. Status indicator pictures. *Panel A shows the labelling of each LED. Panel B shows an example where the experiment is started, and the fish is outside the tube.*

Round 2 Setup Alterations

The Raspberry Pi's IO pins required greater flexibility in the second round, leading to the use of two 3-to-8 decoders. Fewer pins were needed to run a decoder and select resistors location, while allowing for resistance selection with another decoder. Initially, opto-couplers were planned to replace relays, but diode-like effects in the opto-coupler circuit prompted a switch to relays for safety. Three full-length text experiments were conducted with opto-couplers, and a brief analysis is provided in this appendix (Opto-Coupler Experiment).

For the second round, the structure of the raw data produced is combined instead of separating the sham dataset and the stimuli dataset like in round 1. That previous structure unfortunately resulted in four unusable samples in total for round 1 (one sample per fish: 207, 208, 210 and 213). Complement to Data Acquisition & Automation.

Corrosion Problem

During testing prior to round 1, corrosion on the connections in the resistor ring caused short circuits between resistors, necessitating repairs and enhanced waterproofing. Testing involved testing for conductivity between each resistor and between each resistor and their projection on the control board. Regular testing ensured the issue was resolved and didn't happen again after the incident. Complement to Resistor Ring.

Video processing

Cropping Coordinates and Resistor Locations

A clicking software was made to manually click on specific locations in raw videos. The code has four main uses (see Figure 18 for visual of these uses):

1. Video masking: Masking uninteresting regions for enhanced tracking.
2. Video cropping: Coordinates for cropping the 3 separate views.
3. IR-LED stimulus confirmation: Coordinates for cropping the IR-LED array and LED locations in the frame.
4. Resistor location: Coordinates for resistor locations in the frame.

Complement to Data Acquisition & Automation.

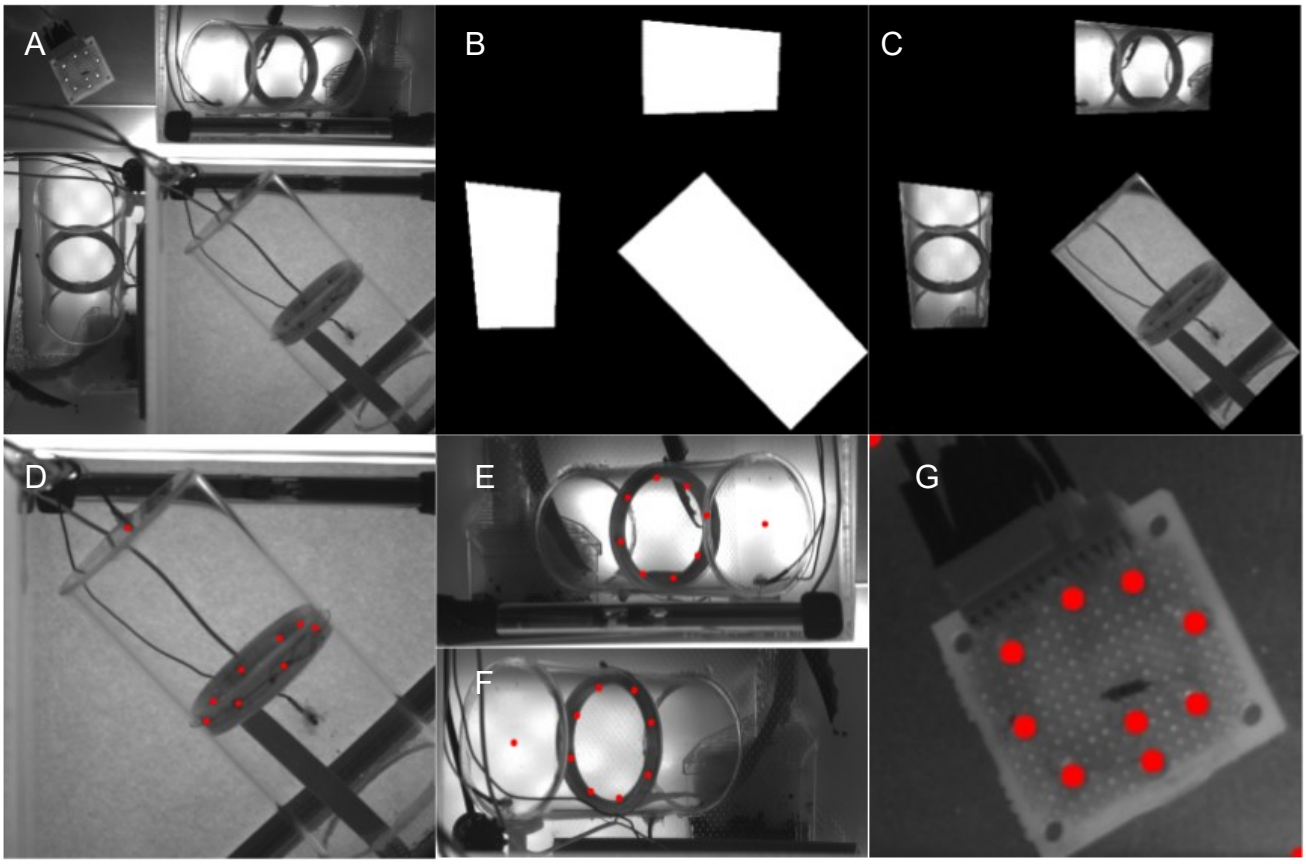

Figure 18. Video processing and cropping preview. *Panel A is a preview of the raw video stream. Panel B is a preview of the mask. Panel C is a preview of the video with the mask. Panel D through F shows the location of the resistors in the cropped views. Panel G is a preview of the IR LED array for Round 1 (see Figure 20 for a picture of round 2's IR LED Array).*

OpenCV functions

The raw video with the 3 views and the video confirmation of the resistors needs processing before DeepLabCut analysis. Multiple OpenCV functions crop the views into separate files, mask irrelevant areas, and mirrors and rotate the side views. These steps ensure each view is considered an independent camera for triangulating positional data. The same process without masking is done for calibration videos to ensure camera calibration matches the video parameters. A parallel video of the cropped IR LED array is produced.

The mirroring function (camB and camC) cancels the mirror effect from the two mirrors. Figure 19 shows the mirroring effect on the camera views. The panel A shows the two side cameras that would be expected if the “fictional cameras” were placed on each side. Complement to Data Acquisition & Automation.

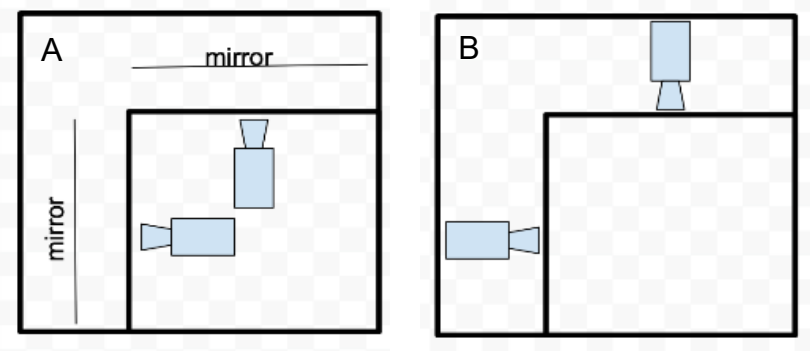

Figure 19. Camera mirroring. *Panel A is the view without the mirroring function and the panel B is the corrected side view.*

Resistor Video Confirmation Detection

Instead of relying on the Raspberry Pi's logged timing, a small infrared LED array in the camera's unused corner lights up with the resistor's activation (see Figure 20 for a picture of the LED array). While videos are processed, the infrared LED array is visually analyzed. Pixel values at the LED's location are compared to a threshold to detect ON. The exact frame number, resistor number, and resistance value are saved for data analysis. This allows precise timing of resistor activation with video recording. Complement to Data Acquisition & Automation.

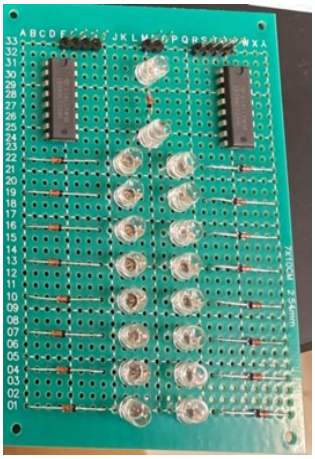

Figure 20. Video confirmation circuit board. *Configuration for round 2.*

Log Book

The log book tracks data acquisition and processing steps and important settings for reproducible results. For instance, the experiment script log file contains trial details like date and fish number, as well as EOD detector threshold and sample counts. The pre-DLC processing script log file records video processing options like masking and correction. Log files also help verify if an experiment needs reprocessing due to script modifications. For a given script, a main log was saved in a main log folder, and individual log files for each experiment were created as needed. Complement to Data Acquisition & Automation.

Tracking

DeepLabCut

Tracking fish movements, especially skinny ones like *A. albifrons*, is challenging. Tracking labels are placed on the snout, tail, and at 25%, 50%, and 75% of the body on the top, bottom, left, and right to build a 3D shape. Figure 21 illustrates the tracking label locations.

To ensure the DeepLabCut (Mathis et al., 2018; Nath et al., 2019) model accurately understands label positioning, 10630 frames were manually labelled across three views. Tracking isn't perfect, but it's sufficient for these experiments. Three different models (Resnet-50, Resnet-101, and Resnet-152) were trained for 1 million iterations each to aid tracking. The highest likelihood for each label is retained for the final 2D pose files, which are combined with interpolated data to replace lower likelihood labels (explained in 2D Filtering). DeepLabCut was ran on WSL2 (Ubuntu 22.04.3 LTS) on a Windows 11 personal computer. Complement to Data Acquisition & Automation.

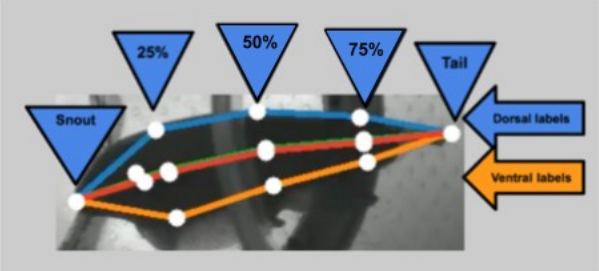

Figure 21. Location of tracking labels

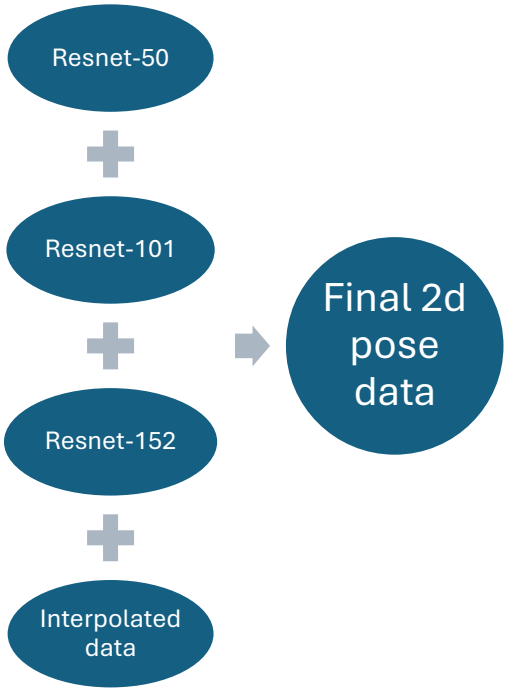

Figure 22. Diagram for 2D tracking.

2D Filtering

A simple function removed lower likelihood data points for linear interpolation. The threshold was set to 0.83, based on Figure 23 showing interpolated values (possible repairs) at different likelihood thresholds. The peak from camera view A was used, which was the highest peak at approximately 0.83. Complement to Data Acquisition & Automation.

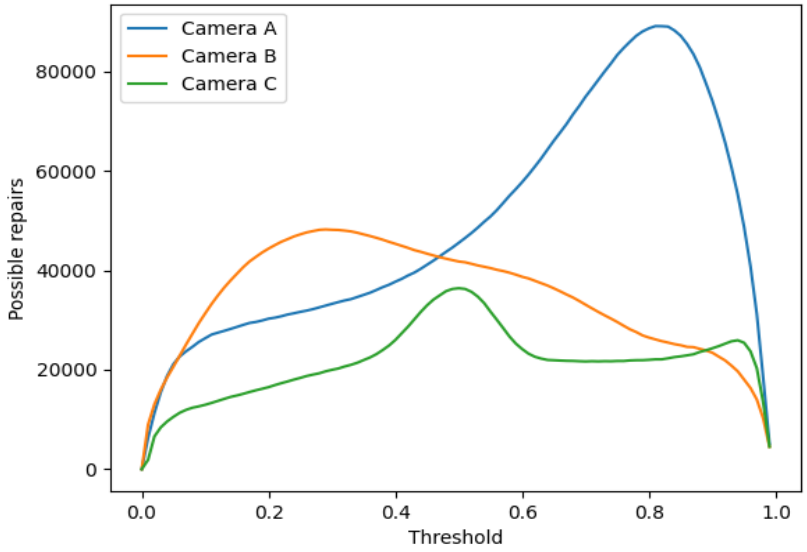

Figure 23. Interpolated points based on likelihood threshold. *This figure is based on the data from fish 201 from round 1.*

Triangulation

Triangulation of the three views (3 x 2D tracking) is the second step after calibration to get 3D tracking for analysis (see Calibration for more details). To accomplish this, an Anipose (Karashchuk et al., 2021) function triangulates all three 2D data points to produce a 3D tracking dataset. The error is limited by the accuracy of the 2D tracking, but as camera views are added, error is reduced by 10-30% per camera view (Günel et al., 2019), which is why three camera views were used instead of two. Complement to Data Acquisition & Automation.

Calibration

Camera calibration triangulates 2D tracking files into a single 3D label position file. The calibration video must match the 2D video input to DeepLabCut for accuracy. Matching parameters included cropping field of view, mirroring side views, and rotation on a side view. For both rounds, a 10-minute calibration video of a 10x7 checkered board was recorded to ensure optimal camera calibration. The board must be visible in all camera views and frames. Complement to Triangulation.

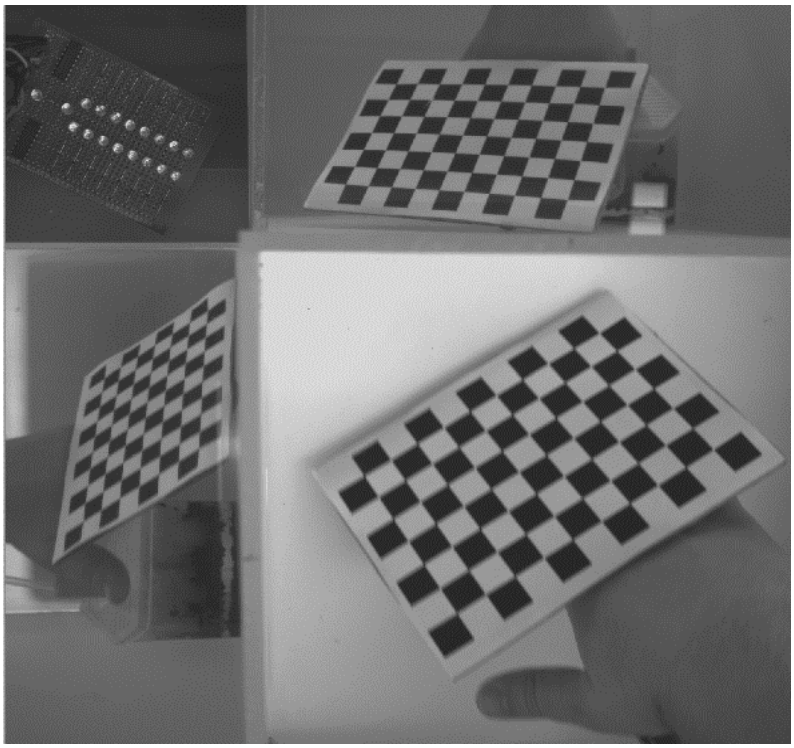

Figure 24. Snapshot of one frame from a calibration video. *A 7 by 10 checkerboard is used for calibration.*

Post-triangulation Data Processing

Splining, Distance and Angle Calculation

The splining function interpolates a line of points in the center of the fish to determine the closest proportion to the resistor with higher resolution than the original labels. It calculates the distance from each label to the resistor. Multiple angle calculations are done in this step also.

These functions could have been easily done directly in The “Big Data” Processing Step but are kept separately since this was developed before and is already working properly. Complement to Data Acquisition & Automation.

The “Big Data” Processing Step

Organizing data on a “per sample” basis is important to be ready for analysis. This step fetches and reformats data like closest distance, closest body part, orientation, and multiple angle calculations from multiple data frames. Using timing data from the LED activation step, it includes 100 frames before the stimulus onset, the whole stimulus length (120 frames), and an additional 45-frame post-stimulus for each sample. In the final data frames, each row represents a sample with the sample number, experiment step, resistor number, and resistance value for round 2. This facilitates easy access to raw data for further analysis. Multiple calculations and a smoothing function are happening at this stage to reduce noise. Calculation functions presents an overview of the calculations done in this step. Complement to Data Acquisition & Automation.

Calculation functions

Function name	Summary - Description
Closest Distance Function	Calculates the distance between the closest proportion on the fish and the activated resistor and records the XYZ position for visualization (Figure 10).
Snout and Dorsal Filament Function	Calculates the distance between the head and dorsal filament relative to the resistor.
Maximum Y Value Function	Extracts the maximum Y value of all center body parts to filter out samples when the fish exits the tube (see Filtering the Exits).
Spline Closest Distance Function	Spline data is used to refine the closest proportion, also determining the closest distance and body part.
Fixed Roll Angle Function	Calculates the roll angle and relative angle of the fish relative to the activated resistor using two methods: plane roll angle and vector angle (for more details, see Two Angle Calculations)
Swimming Function	Calculates the longitudinal velocity, acceleration, and swimming direction of the fish. This was used in the reversal analysis (Detection Based on Reversal Events)
Distance From End of Tube Function	Calculates the distance from the end of the tube and the fish's orientation. This function also calculates the relative position between the center of the fish and the activated resistor (used in Figure 9).

Table 2. Calculation function summary & description.

The Dashboard

The dashboard, a custom-made tool, visualizes data, videos, and tracking synchronously. It includes a 3D representation of the original tracking, spline, and other informations. The dashboard also offers three separate 2D views with tracking, resistor location, and masking. Ten graphs update in real time as the video progresses, and a list of data points updates with each frame. The code can display different information on the graphs and data list. The 2D and 3D tracking code was adapted from Anipose's (Karashchuk et al., 2021) code for tracking. The dashboard was used for manual behavior identification and to verify calculations from "Big Data" processing due to its adapted data frame format. Video encoding followed the same process as Pre-DLC processing. See Figure 25 for a snapshot of the dashboard. Complement to Data Acquisition & Automation.

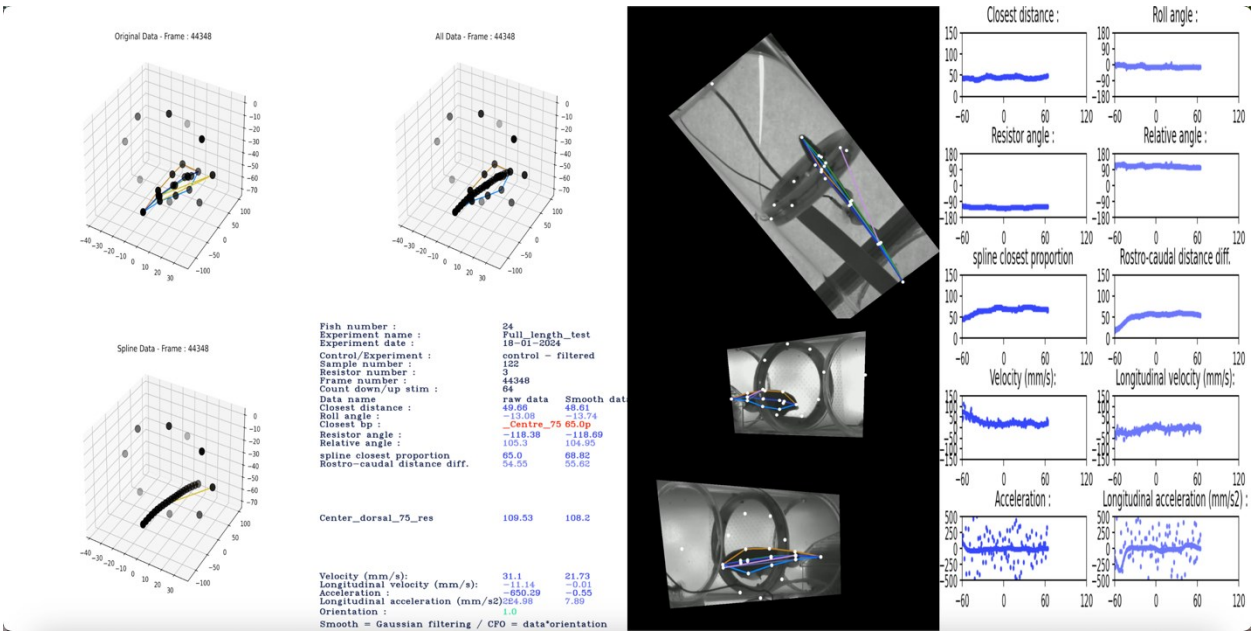

***Figure 25. Snapshot of one frame of the dashboard**. This is from a test experiment not included in the final official dataset.*

Filtering the Exits

The EOD detection system ensures that the fish is present in the area of interest before recording starts and the stimulus onset. However, since the tube lacks a door that closes off the tube, the fish can leave after the stimulus onset, resulting in the inclusion of unhelpful data points. For instance, the raw 3D distance data shows samples with an immediate increase in distance after the stimulus onset for both the sham and stimulus groups (see the purple box in Figure 27, first row). To address this issue, a filtering algorithm checks if all body parts of the fish are farther than 30 mm from the resistor ring and for at least 30 frames of the last 60 stimulus frames (30 frames per second). This filtering process reduced the number of samples for the stimulus from 2818 to 2294 and for the sham from 2821 to 2278 in the initial round of experiments. The results of this filtering can be observed in the second row of Figure 27. Now, the control data appears normal, with a similar visual distribution of data points before and after the sham stimulus onset.

When comparing the average distance per fish before and after the stimulus onset in Figure 26, there's a clear difference between the filtered and unfiltered. This difference is especially clear for the sham, where the slopes appear randomized after filtering, expected since there's no stimulus.

To verify the effectiveness of the filtering algorithm, visual inspection was conducted on 15 samples from three different fish. All verified samples demonstrated the correct filtering results. Complement to Data Acquisition & Automation.

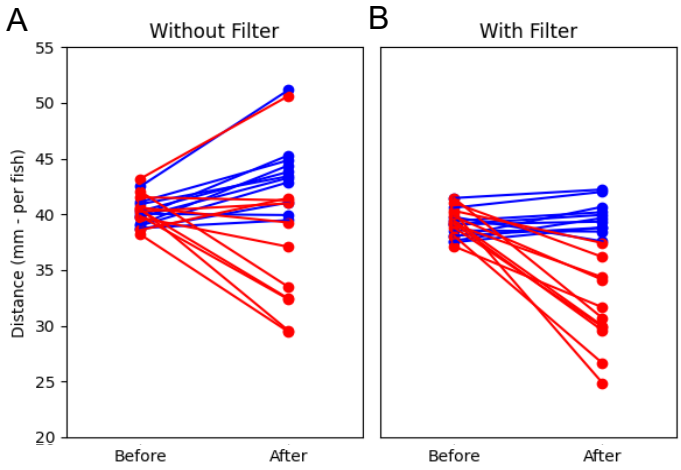

***Figure 26. Comparison between the filtered dataset and the unfiltered for exits**. The average distance before and after is represented for the sham (in blue) and the stimuli samples (in red). Panel A is for the unfiltered dataset and panel B is for the filtered dataset. All the data is from the first round of experiment. Before is T0 and after is at T1.5.*

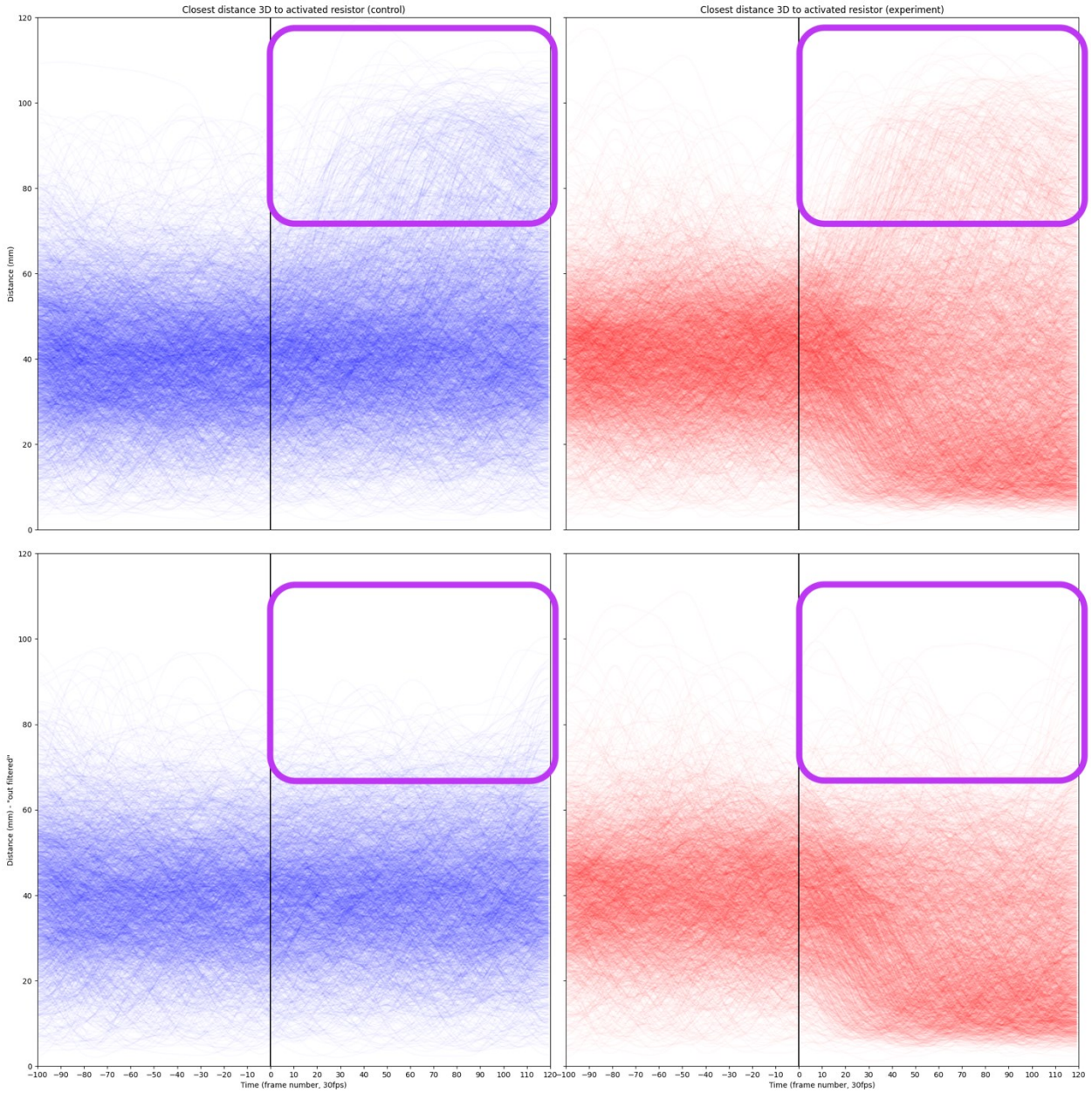

Figure 27. Unfiltered raw data VS. filtered raw fata for the exits. *Left blue graphs represents the sham, right red graphs are the stimulus samples. First row is unfiltered, second row is filtered. Data is from round 1. Purple boxes indicate the datapoints of interest.*

Resistor Configuration and True Value

To be able to achieve the desired resistance values for the second round of the experiment, multiple combinations of physical resistors were used as shown in the Table 3. All resistors have a tolerance of +/- 5% indicated by the gold band. Complement to Stimulus Characteristics.

Nominal resistance value	Resistance real value (measured)	Physical resistor configuration
Infinite (control)	Infinite (air)	
1.5 kΩ	1.478 kΩ	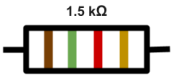
25 kΩ	24.77 kΩ	
50 kΩ	49.48 kΩ	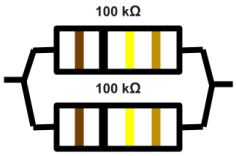
100 kΩ	99.0 kΩ	
250 kΩ	248.0 kΩ	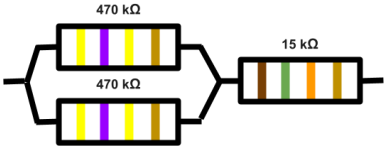
500 kΩ	512.1 kΩ	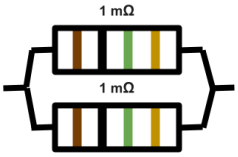
1 mΩ	1.038 mΩ	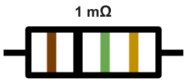

Table 3. Resistor configuration and true measured resistance values.

Two Angle Calculations

Two angle calculations were tested in the reorientation analysis: the Anipose-Axis angle and the alternative center-dorsal-resistor angle. The Anipose-Axis angle involves using the axis-angle function from Anipose (Karashchuk et al., 2021) for the fish itself and resistor, calculating the difference between them, and obtaining a relative roll angle. The center-dorsal-resistor angle is simpler, calculating a 3D angle between three points. However, this technique has a limitation: the resistor label which is not on the fish can be anywhere around the center-dorsal axis, giving the same angle value. This means that in some cases, the resistor could be positioned over the dorsal edge of the fish, but since the center-dorsal axis could be more rostral or caudal, it tends to give a relative angle that approaches 90°. There is technically a conical shape for the resistor to be on, but there's no way to determine if it's over the dorsal edge or more towards the side. See Figure 28 for a visual representation and demonstration of both angles. For an example-based explanation of the Anipose-Axis angle, see Axis Angle Calculation - Explanation. Complement to Roll Reorientation.

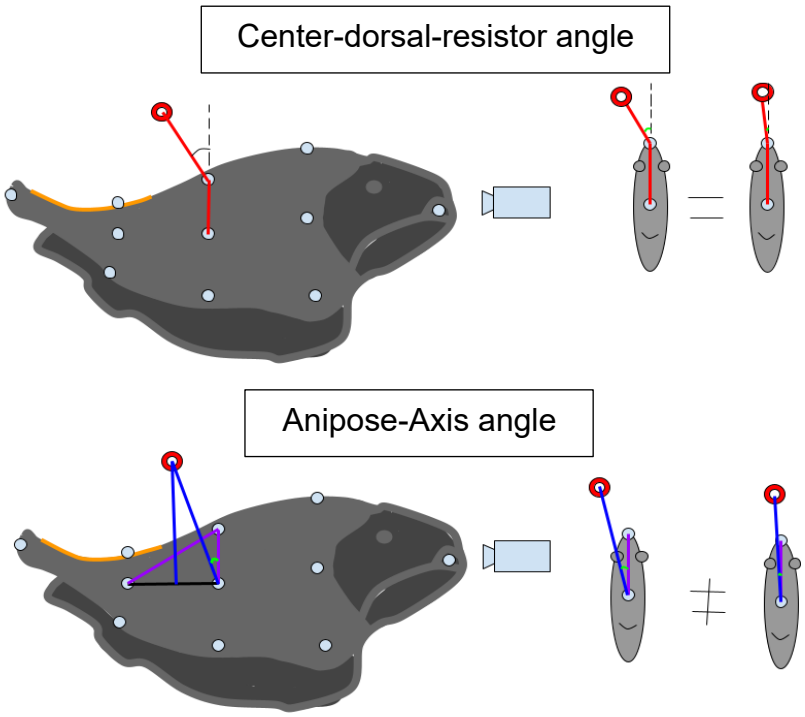

Figure 28. Visual representation of both angle calculation.

Axis Angle Calculation - Explanation

The axis-angle calculation function provided by Anipose involves defining two vectors with a common point. The first vector defines the axis of rotation, while the second vector, attached to one of the rotation axis points, defines the angle. This angle is relative to a parallel vector to the applicate (z-axis).

Here's a scenario to illustrate how it works (while following Figure 29):

- Take the snout and center labels at 25% of the body length to form the axis of rotation.
- The top 25% label and the center 25% label form the "lever" and provide the angle of rotation around the other vector.
- Panel B shows the labels, vectors, and the parallel vector moved through the center 25% label.
- To measure the angle, rotate the 3D space to align the snout label (in green) over the center 25% label (in red). The snout should hide or be in front of the center 25% label, which also hide the red line, allowing us to calculate the angle of rotation around that axis. It should look like panel C.
- With the angle protractor on top of the whole thing (ensure aspect ratios are equal in all axes), use the applicate parallel vector as the reference and the "lever" to find the angle value. In this case, the correct angle is 101˚.

This simplified explanation shows how it could be found manually. If the lever were on the right, the angle value would be negative. Since the 3D environment's reference is resistor 1, the top of the 3D environment is the true top in the experimental arena. Complement to Two Angle Calculations.

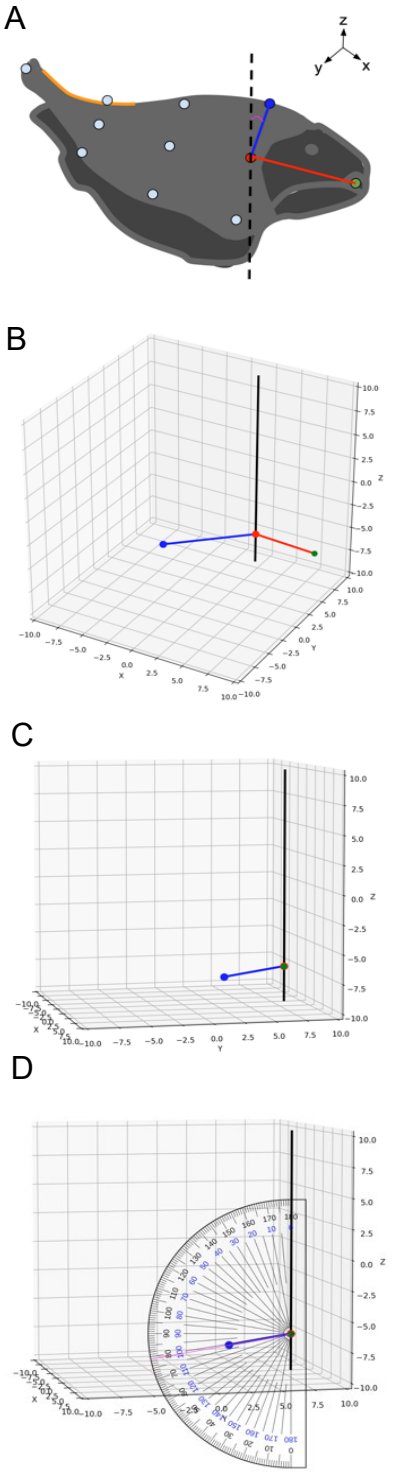

***Figure 29. Axis angle visual example**. Fish orientation in panel A is not representative of panels B – D.*

Bonus Manipulation Experiment Ideas

Manipulation experiments proposed previously were not conducted. The goal was to prevent the dorsal filament's use for electrosensing. One way was to use an insulating gel to block the electric field from reaching the electroreceptors, preventing sensing. Another was to use a local anesthetic to block neuronal signals from leaving the dorsal filament and reaching the brain. Figure 30 shows the proposed manipulation experiments. Complement to Conclusion.

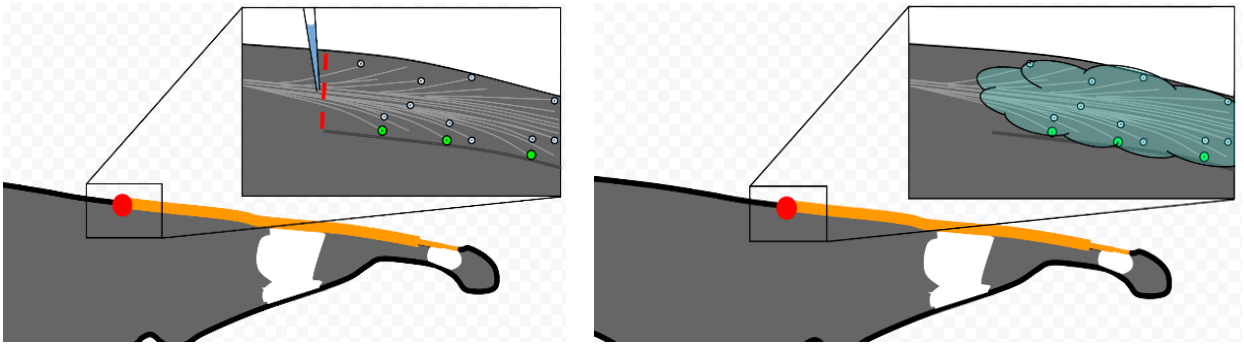

Figure 30. Visual representation of the proposed manipulation experiments.

Additional Results & Data Exploration

Manual Behavior Analysis Tables

This section shows the count for each observation from the Manual Behavior Identification. In the stimulus portion of these results, my subjective approximation of the chances of a detection is included. Figure 31 shows an overview of the results of this step.

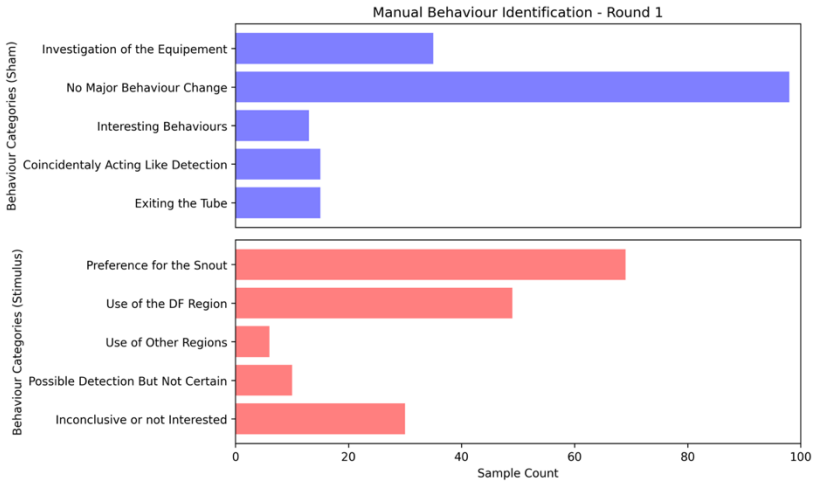

Figure 31. Manual behaviour identification overview. *General grouping of behaviors. Data summary from round 1.*

Sham Samples

Behavior description	Count
Investigation of the equipment	
Head pocking around the ring	29
Nose poking the EOD detector	4
Fish investigating the ribbon, no reaction to resistor	2
No major change on behavior	
Feeling around, no particular interest in resistor	83
Mostly stationnary	9
Small back and forth swimming, no major movement	4
Goes close to the resistor but keeps swimming past it	3
Weird behaviors	
Playing with a bubble	9
Fish sleeping	2

Feeling the edge of the exit of the ring with the snout	2
Coincidentaly acting like detection	
Coincidently ends up with the snout relatively close to the resistor	11
Coincidently ends up with the DF relatively close to the resistor	3
looks like sudden acceleration towards resistor ring at random time	1
Exiting the tube	
Fish not interested in the resistor, ends up exiting the tube	9
Not fully entered, just re-exited the tube.	5
Feeling around, no particular interest in resistor, ends up exiting the tube	1

Table 4. Manual behavior raw observations for sham samples.

Stimulus Samples

Behavior description	Count
Preference for the snout	
Nose poking the correct resistor, lots of short back and forth after activation (99% chance of detection)	45
Nose poking and sensing with the side of the head (95% chance of detection)	10
Backward scan then rapid nose poking at a distance (75% chance of detection)	4
Delayed backward scan then repositionning the snout slightly closer (80% chance of detection)	3
Head gets slightly closer to resistor after multiple seconds (40% chance of detection)	3
Snout already close, nose poking and then getting away (60% chance of detection)	2
Lots of right-left moovement, then the head gets closer (75% chance of detection)	2
Use of the dorsal filament region	
Fish reposition the caudal region closer to the resistor and sensing it (95% chance of detection)	11
Possible detection with DF region but appears to scare the fish and exits the tube (55% chance of deteciton)	10
Detection when close to DF, then repositions the snout closer (95% chance of detection)	8
Possible detection with dorsal filament region getting slightly closer (60% chance of detection)	5

Fish repositions the DF closer to the resistor and lowers the body to make the stimulus higher (95% chance of detection)	4
No major change in behavior but tail seems to do circles (50% chance of detection)	4
Possible detection with dorsal filament region slightly closer but then going back to original position (60% chance of detection)	3
Slight rotation of the body, approximatly a 90 degree rotation (95% chance of detection)	1
Detection with the DF already close, then quickly done with it (90% chance of detection)	1
Fish elevates the DF closer to the higher resistor (90% chance of detection)	1
After 2 sec, fish mooves forward but keeping the DF closer to the stimulus compared to the head (60% chance of detection)	1
Use of other regions	
Starts feeling around the resistor with the side of the body (85% chance of detection)	7
Possible detection but not certain	
Possible detection with dorsal filament region slightly closer, but exiting the tube (25% chance of detection)	6
Fish was mooving fast and then stalled near the exit of the tube (75% chance of detection)	2
Possible detection but fish is preocupied by the bubble at the top (45% chance of detection)	1
Possible detection but preocupied by the ribbon (30% chance of detection)	1
Inconclusive or not interested	
Not getting closer but not exiting (10% chance of detection)	8
On the way out, not stopping (<5% chance of detection)	7
Fish not going close to resistor and not interested in it (<5% chance of detection)	6
No major change in behavior, lots of rapid small moovements before and after (15% chance of detection)	5
Mostly out of the tube, not entering (<5% chance of detection)	4

Table 5. Manual behavior raw observations for stimuli samples.

Raw Distance 3D With After – Round 1

Figure 32 presents the same data as Figure 10 panels B and C, but it also includes the post-stimulus phase. Notably, immediately after the stimulus ends, there are numerous samples indicating an increase in the 3D distance to the resistor, which is similar to exit events (as discussed in Filtering the Exits). This is because the exit filtering algorithm only considers samples that exhibit exit behaviors within the last two seconds of the stimulus phase (frames 60 to 120).

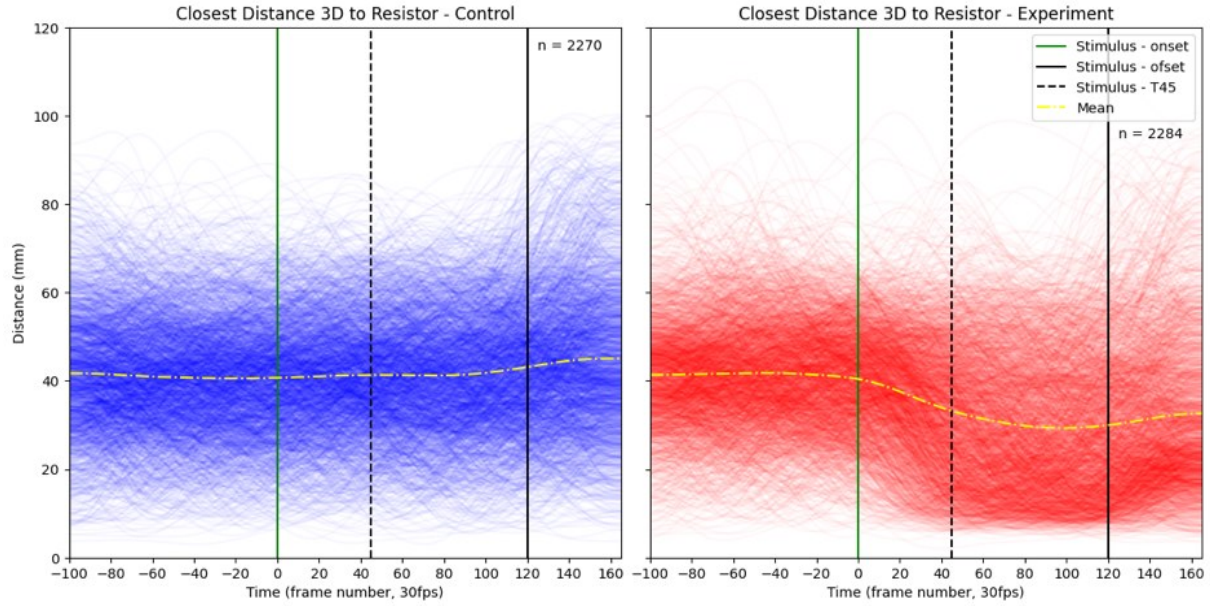

Figure 32. Raw 3D Distance in time for round 1 with the post stimulus phase. *T45 is the same as T1.5 in this figure. This figure was produced prior to converting x-axes to seconds, which explains the use of video frames (30 frames per second).*

Raw 3D Distance – Round 2

In Figure 33, eight individual graphs show the raw 3D distance before and after the stimulus onset for eight different stimulus intensities, including the sham. As the stimulus intensity decreases, the lower opacity in the lower regions suggests a less intense response. A version of this figure separating the detection events from the non-detection events can be found in Detection VS. Non-Detection Raw 3D Distance. Complement to 3D Distance Reaction.

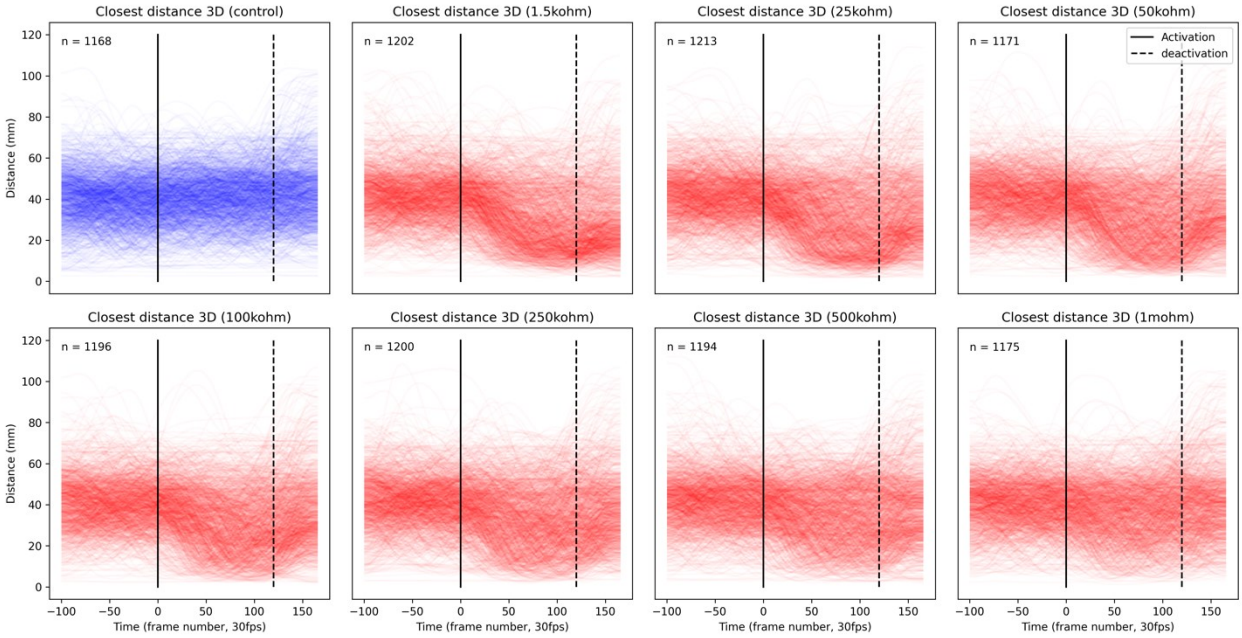

Figure 33. Raw distance traces by stimulus intensity from round 2.

Position in Resistor Ring – Fixed Body Position

Figure 34 is equivalent to Figure 10 panels E, G, and I, but uses fixed body locations instead of the closest proportion on the fish's midline. Most movement in the resistor ring plane appears to occur with the head and anterior regions of the fish's body. The head is the only region with hot spots on the resistors, and the label at 25% body length forms a clear ring around the center of the resistor ring. Other body parts remain close to the center of the resistor ring after the stimulus onset. Taken together, this supports that the head is clearly the preference to sense the stimulus once detected.

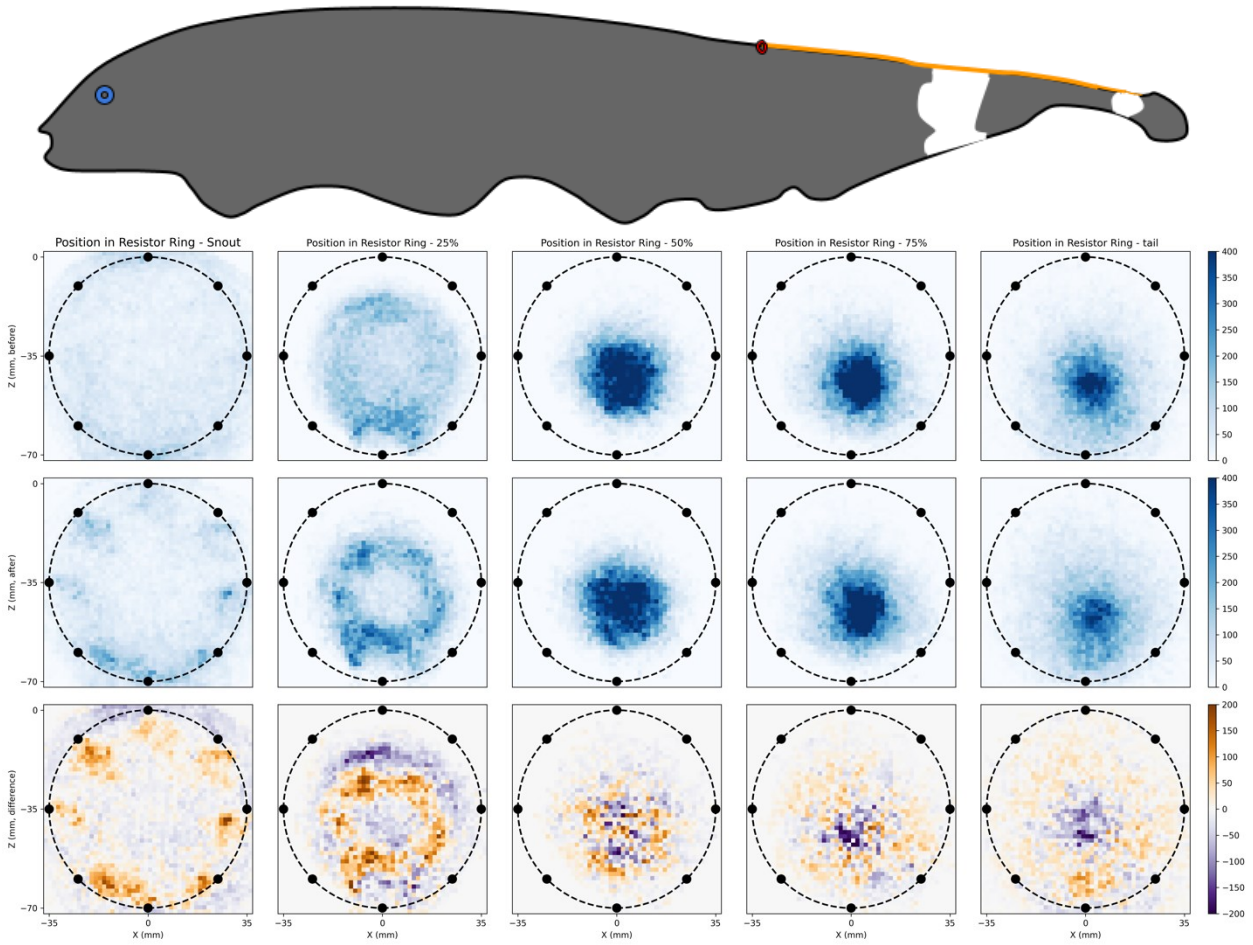

Figure 34. Ring plane position with fixed body locations. *Each column represents a fixed position on the fish. The first row shows datapoints for 60 frames before the stimulus onset. The second row shows datapoints for 60 frames after 1.5 seconds of stimulation. The last row shows the difference between the first two rows. This figure only uses round 1 stimulus samples.*

Detection VS. Non-Detection Raw 3D Distance

To verify the detection algorithm's accuracy, Figure 35 separate detection samples (based on the detection criteria) from non-detection samples in the raw 3D distance data of the second round of the experiment for each resistance value. Detection events in stimuli samples are the true positives, detection events in sham samples are false positives. This is crucial since the detection results relies on this data. (Figure 11 provides an equivalent figure of the experiment data from round 1.) Top left panel shows the detections for the sham samples are the false positives of round 2. This is a complement to General Detection Frequency.

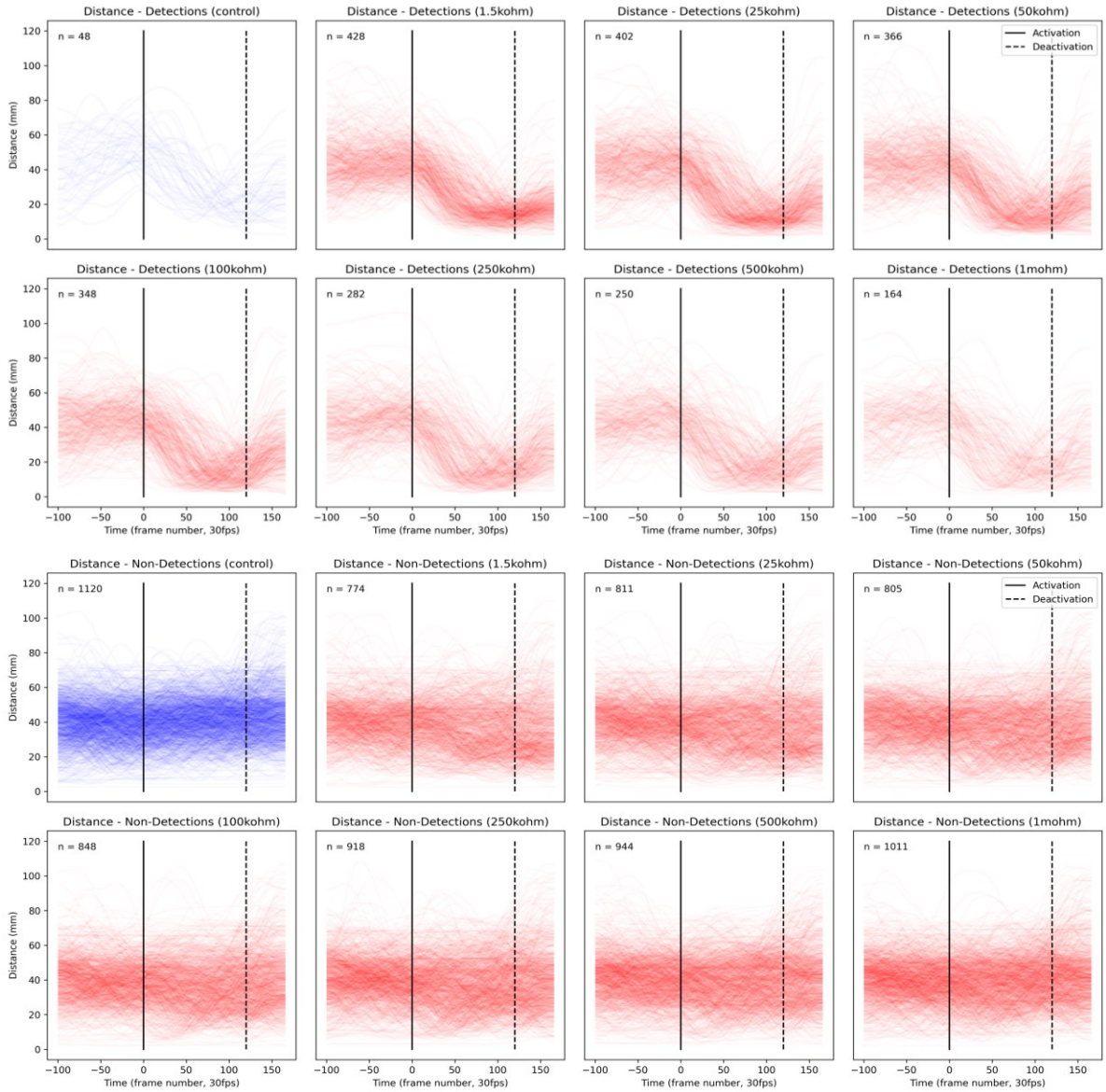

Figure 35. Detection VS. Non-Detection round 2. *The eight superior panels show the detection for each resistance and the eight bottom panels show the non-detections. In this figure, "control" is the same as sham.*

Detection Frequency – Time Effect

Figure 36 and Figure 37 show the distribution of detection events in time. This analysis aims to determine if there's a time effect on detection frequency. Figure 36 suggests a slight reduction in frequency after 200 samples (stimulus phase of round 1).

Figure 37 indicates a possible slight reduction in detection events with time for most stimulus intensities in round 2. However, this effect didn't significantly impact the detection frequency as discussed in Binomial GLMM 2. Complement to Binomial GLMM 2.

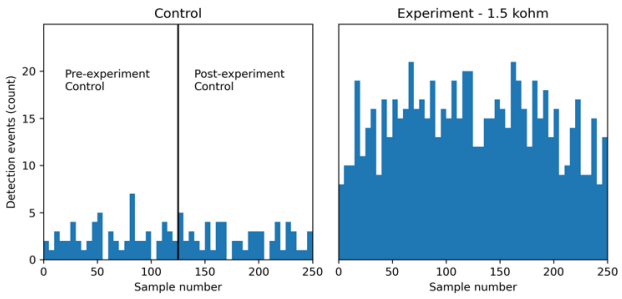

Figure 36. Distribution of detection events in time (sample number – round 1). *Comparison between the sham and the stimulus for round 1. Fish 201 for round 1 is excluded because the increased sample size doesn't align with the vertical line separating the control and the same issue for additional samples past #250.*

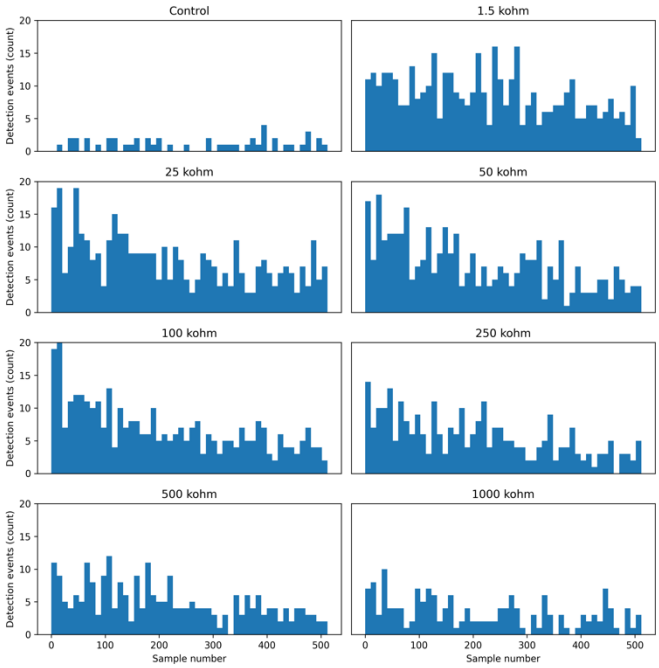

Figure 37. Distribution of detection events in time (sample number – round 2). *Comparison between all resistance values and the control.*

Detection Based on Reversal Events

Based on MacIver et al. (2001), a rapid reversal indicates a possible detection event. Detection means the fish perceives the stimulus. A reversal is a change in swimming velocity direction, from forward to backward or vice versa. Rapid reversal behaviors were observed during Manual Behavior Identification on a few occasions. In this analysis, a reversal is counted if the fish switches from a forward velocity over 25 mm/s to a backward velocity under -25mm/s. Complement to 3D Distance and Detection.

Reversal Analysis – Round 1

Figure 38 illustrates the distribution of reversal events, including both forward and backward events. The analysis predicted a higher reversal frequency immediately after stimulus onset, suggesting a detection response. However, the reversal frequency in panels A trough C doesn't increase visibly after the stimulus, making it a poor indicator of detection.

Overall, the stimulus phase has a higher reversal frequency than the sham. Panels D and E show the reversal frequency in time. During samples 125 to 375 (stimulus phase), there's a higher reversal count per bin, which was also visible in panels A through C. After the stimulus phase, the reversal frequency seems to roll off and return to a lower level, suggesting the higher activity stimulus phase makes the fish more active than the calm control phases, which show a basal reversal frequency.

Code Verification

To test the code, an artificial dataset with a sine wave of multiple amplitudes was used to see if it correctly detects each peak as a reversal. As expected, the sine waves below the threshold weren't identified as reversal events, while those with a high enough amplitude were detected correctly.

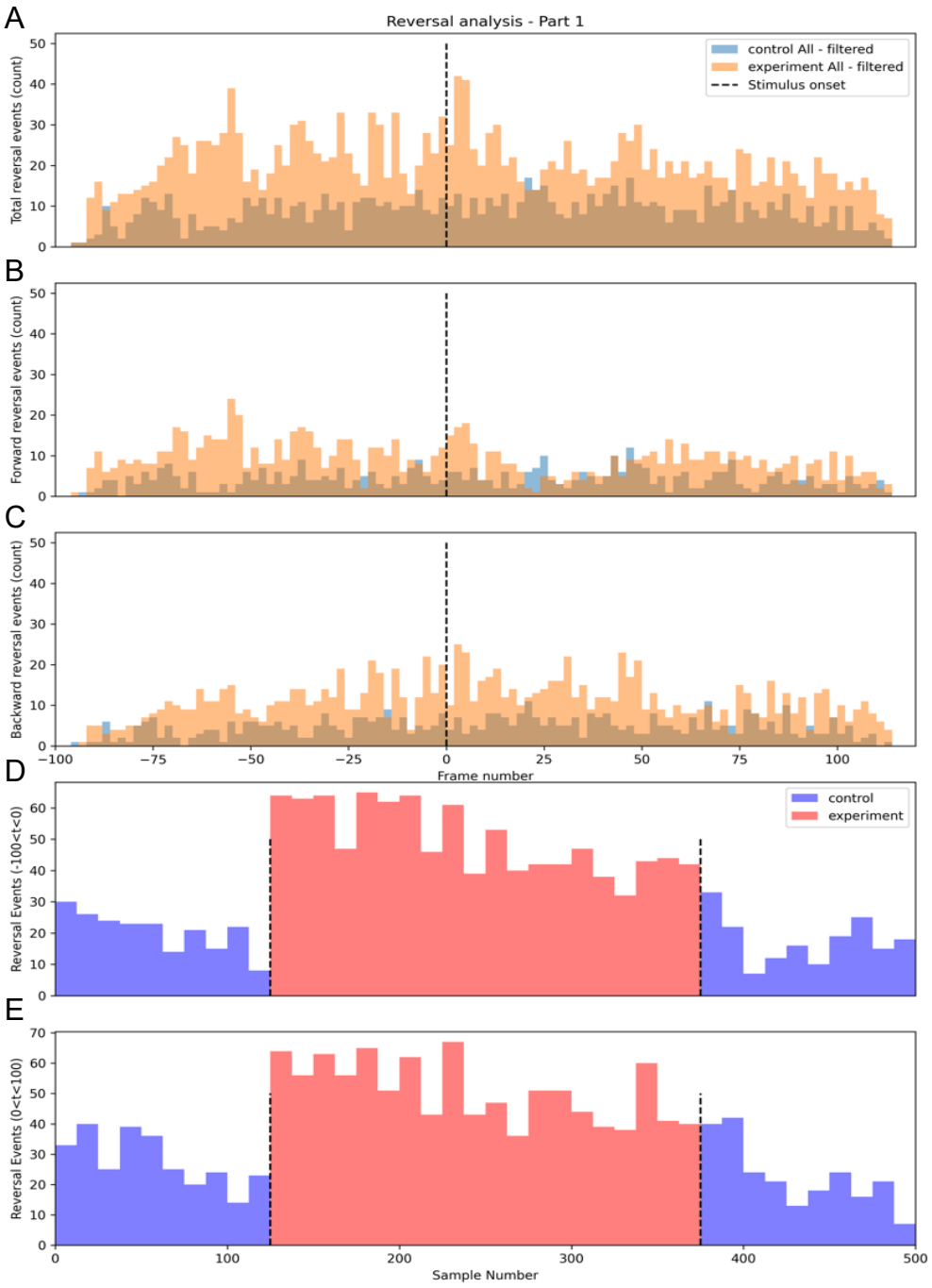

Figure 38. Reversal analysis - round 1. *Panel A show all reversal events for each timepoint during a sample. Panels B and C separate forward and backward reversals. Panels D and E show reversal event distributions in time during the experiment. Panel D counts reversal events in 100 frames before the stimulus onset, and Panel E counts events in 100 frames after the onset.*

Reversal Analysis – Round 2

Figure 39 shows data from round 2, specifically sham samples and the stimulus at 1.5kΩ, like round 1. The sample order is randomized, and there's no dedicated control or experiment period. Panel D shows a higher reversal frequency in the first hundred samples, which reduces slightly after. This suggests the novelty of resistor activation interests the fish and increases the reversal frequency.

Looking at the distribution of reversal events over time of a sample, there's a slight increase in backward reversal frequency right after the stimulus onset (Figure 39 panel C). This is surprising as it was barely visible in round 1 (Figure 38 panel C). However, the bump is so small that id didn't make sense to use this technique as detection proxy.

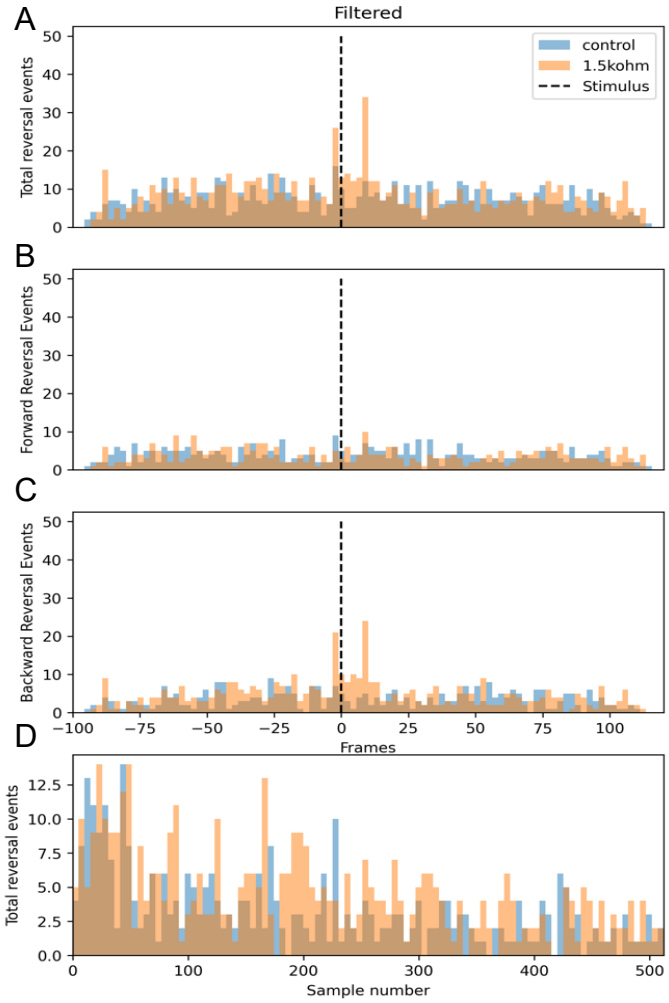

Figure 39. Reversal analysis - round 2*. Panels A show all reversal events for each timepoint during a sample. Panels B and C separate forward and backward reversals. Panel D shows reversal event distribution over time during the whole experiment.*

Distance Distribution – Round 1

The distance distribution in Figure 40 uses 100 frames prior to stimulus onset and after 1 second of stimulation for all stimulus samples (detections and non-detections) of the stimulus samples from round 1. Panel A show the raw data distribution of the distance during these timeframes. It shows that many data points from the stimulus phase remain in a similar distribution to the pre-stimulus data points, while some shifts to the left, indicating a reduction in distance.

Panel B shows a single Gaussian distribution fitted for the pre-stimulus data points and a bimodal Gaussian with free variables fitted for the stimulus data points. Panel C shows a unimodal Gaussian fitted to the pre-stimulus data. The mean and standard deviation from the pre-stimulus data were used to fix one of the two Gaussian distributions in the bimodal distribution for stimulus data points, while the other was left with free variables.

Overlaying the Gaussian curves from panel C onto the raw distribution in panel A shows a good fit for both pre-stimulus and post-stimulus data points, with an R^2 value of 1.0 for the pre-stimulus and 0.95 for the post-stimulus. This result shows a clear difference between the pre-stimulus and stimulus distance datasets, with a shift of many data points towards a smaller distance. This suggests that there is a clear reduction in distance for a great portion of the data points and the rest of them remains like the pre-stimulus distribution. This analysis was useful in determining the detection metrics. Complement to 3D Distance Reaction.

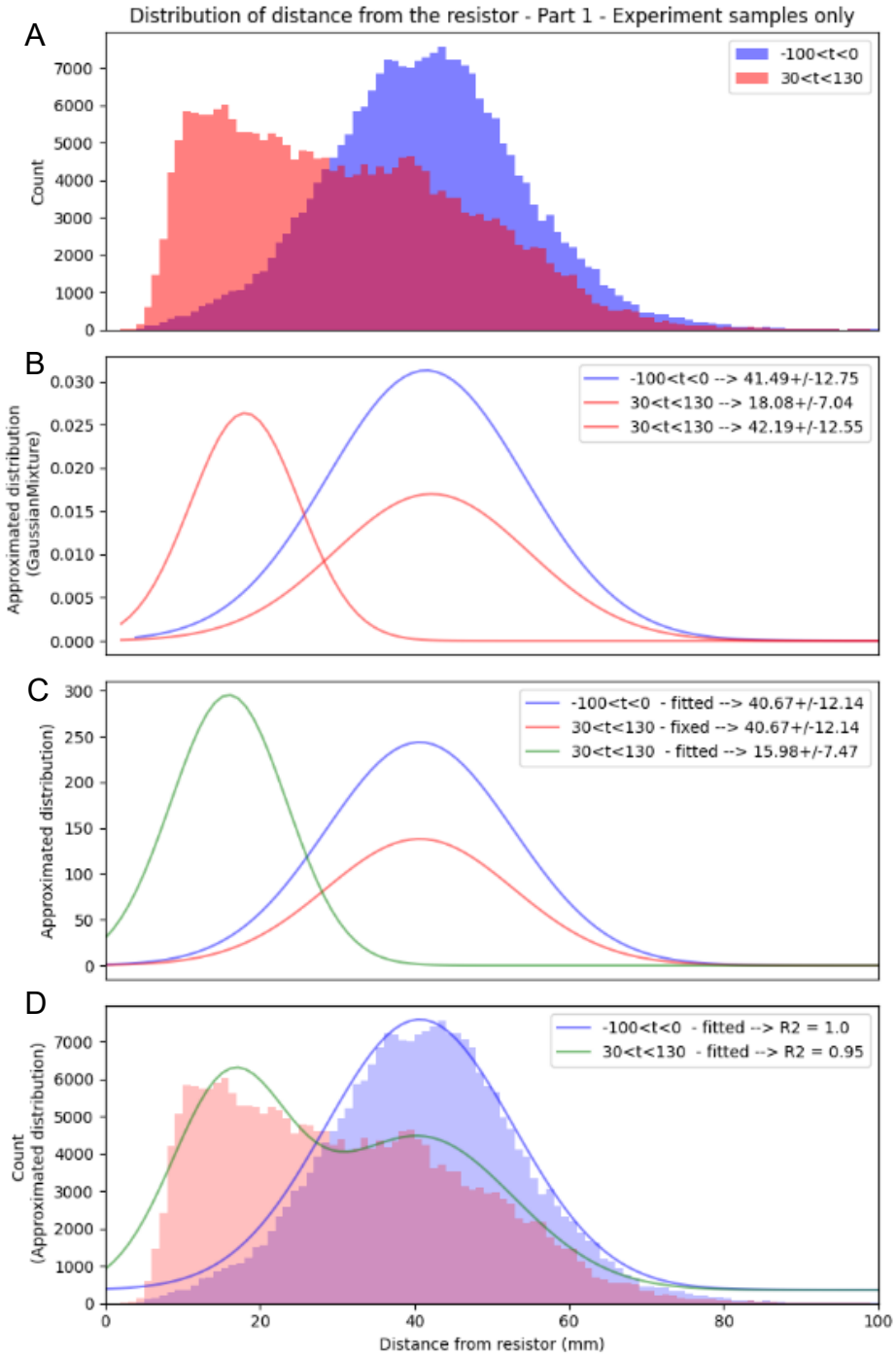

Figure 40. 3D distance distribution and Gaussian fitting. *Panel A shows the raw 3D distance distribution of all samples from the stimulus samples of round 1. Blue represents 100 frames before stimulus onset, while red represents 100 frames after 1 second of stimulus. Panel B presents a simple Gaussian fit with a unimodal distribution for the pre-onset and a bimodal distribution for the stimulus. Panel C shows a unimodal distribution for the pre-stimulus and a bimodal Gaussian for the post-onset with one of the Gaussian parameters fixed to the pre-stimulus fit. Panel D overlays the Gaussian curves from panel A on the distribution. In the legends "100<t<0" and "30<t<130" are values of time, in frame number.*

Distribution of Threshold Crossing – Round 1

Figure 41 shows the distribution of the frame number when the threshold for detection is crossed. It shows that there is a minimum delay of 14 frames for this round of experiments (467 ms) before getting any signs of detection. In other words, it takes a minimum of 467 ms to accomplish the task of moving 50% closer to the resistor, assuming detection happened instantly. As initial distance increase, there is a slight increase in delay before the first threshold crossing for that 10 mm category. This is a complement to Post-Detection Repositioning.

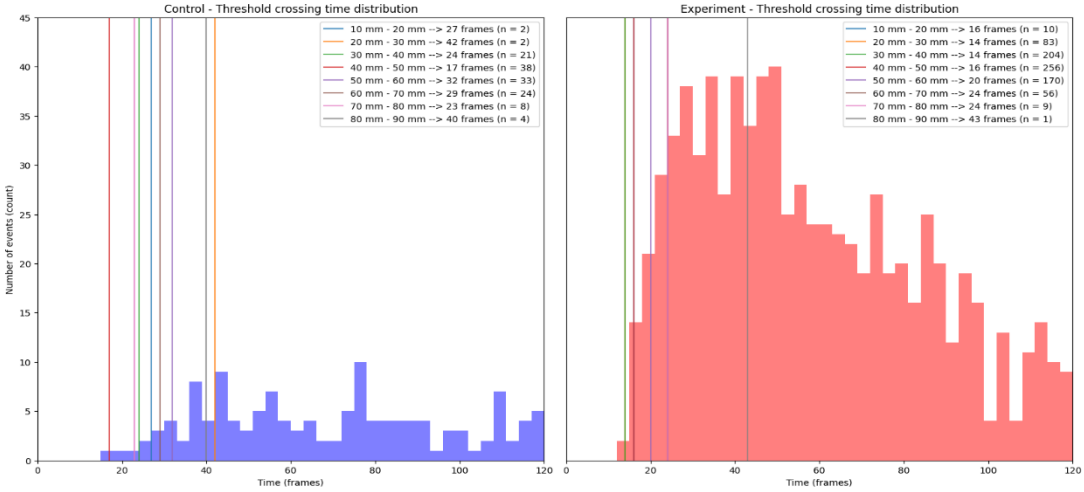

Figure 41. Threshold crossing distribution for all detection samples of round 1*. Vertical lines indicate the fastest threshold crossing for a given initial distance group.*

Quiver Plots – 3D Non-Smooth

Figure 42 is the original version of the quiver plots from Figure 13. This version was not used since it is harder to see the flow of the arrows. Note that this version represents the repositioning of the resistor, as opposed to the fish's movement in Figure 13.

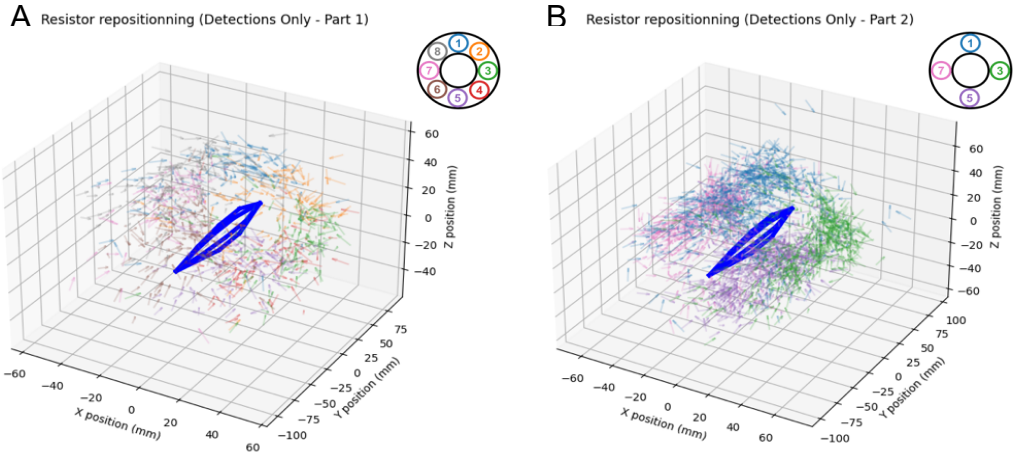

Figure 42. Original 3D quiver plots for both round of experiments. *Panel A is for round 1 and panel B is for round 2. Arrows are pointing in the direction that the resistor is repositioned and not the fish's movement.*

Quiver Plots – Sham

Figure 43 panels C and D are the sham equivalent to Figure 43 panels C and D. Figure 43 panels A and B are showing which data points are used prior to smoothing in the quiver plots. No obvious patterns can be observed in the sham quiver plots, as fish movement is random.

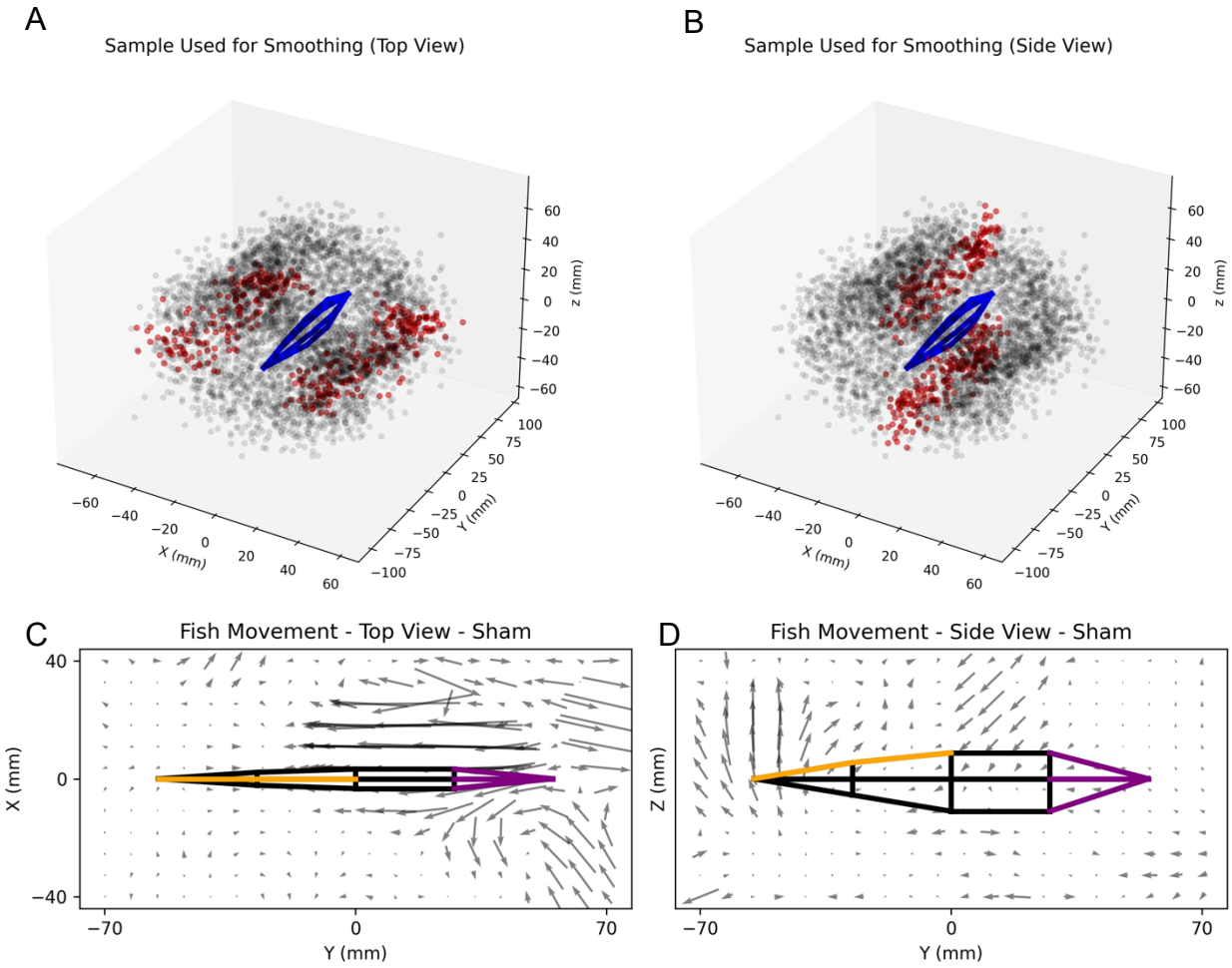

Figure 43. Quiver plots of sham samples. *Panels A and B are showing the initial location of the samples used in the 2D quiver plots in this figure and in Figure 13 panels C and D. These 3D scatter plots show all samples of the first round of experiments, and the red dots are the samples used for the 2D quiver plots. A 10mm slice in the center of the Z axis and of the X axis for figure A and B respectively were selected prior to smoothing. Panels C and D show the sham equivalent of the quiver plots of Figure 13. Arrows represent the fish movement if the resistor was at that location relative to the fish. Only data from round 1 are used in all 2D quiver plots.*

Orientation in the Tube – Round 1

Figure 44 shows the distribution of the orientation of the fish in the tube at the onset of the stimulus. In the stimulus phase, the fish seems to prefer facing the open end of the tube. Complement to: Post-Detection Reorientation

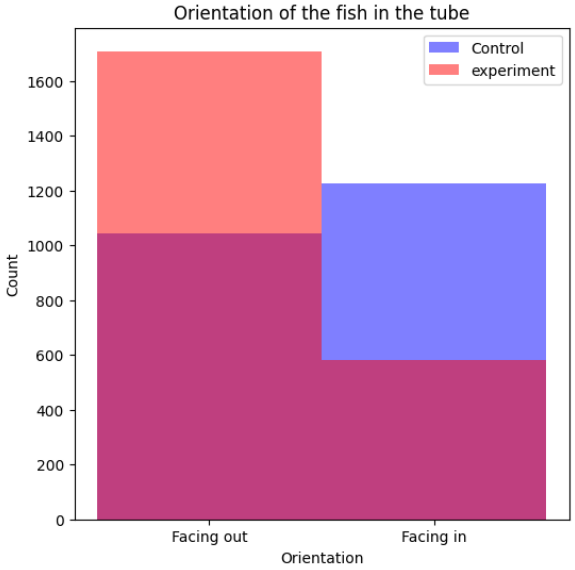

Figure 44. Orientation of the fish in the tube at T0.
Data from round 1 only.

Detection Based on Resistance – Count Version

Figure 45 panel A is the count version of the data from round 2 in Figure 11 panel C. Figure 45 panel B is the count version of Figure 11 panel D. Complement to General Detection Frequency.

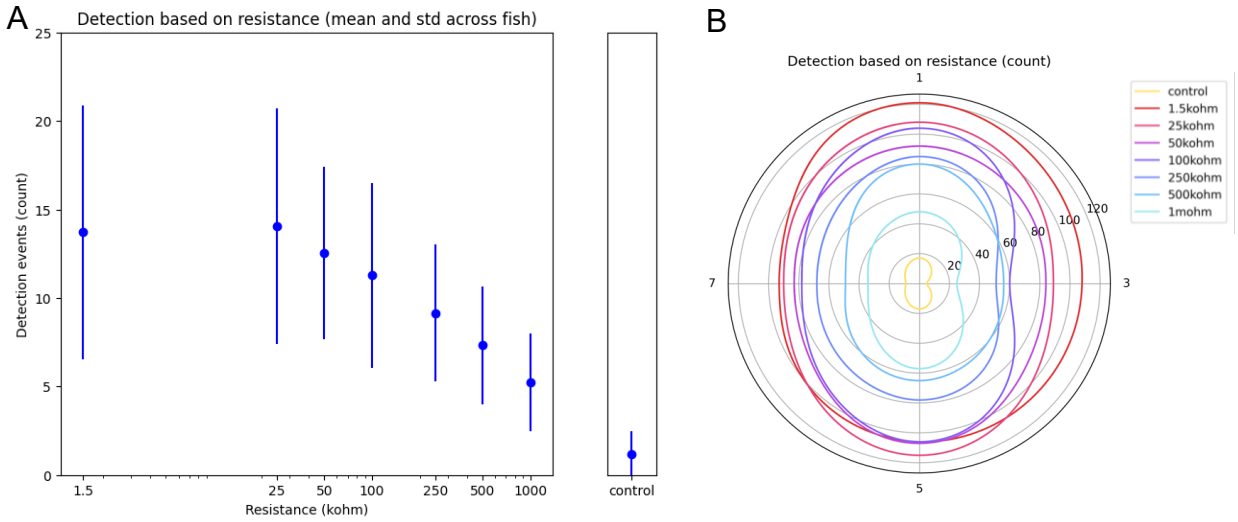

Figure 45. Count version of detection based on resistance plots. *Average detection count for each resistance value in panel A. Panel B is total count per resistor location and resistance value.*

Detection Frequency - Dorsal Filament VS. Head

Figure 46 presents the overall detection frequency for both regions of interest: the head and the dorsal filament. This complements Dorsal Filament & Head Detection Frequency.

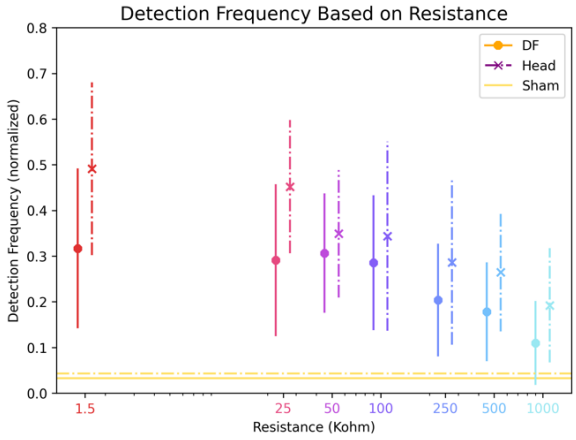

Figure 46. Dorsal filament and head average detection frequency. *Normalized average detection frequency across fish is displayed for each resistance value (mean ± standard deviation) for the dorsal filament region and for the head region. The horizontal yellow lines at the bottom is the mean detection frequency for the sham samples of both regions. Please note that the x-axis is logarithmic.*

Average Distance at T0 – Round 2

Figure 47 shows the average distance between the head and resistors or dorsal filament and resistors for detected samples. Dorsal Filament & Head Detection Frequency show an increase in the detection frequency from resistor 1 when using the dorsal filament, but the data at that same location shows an increased distance compared to other resistor locations. This is interesting since increased distance reduces stimulus intensity (Benda, 2020). The head's distance distribution shape is mainly oval, with increased distance for both sides compared to the top and bottom resistors. Complement to Electrosensory Sensitivity of the Dorsal Filament & Head.

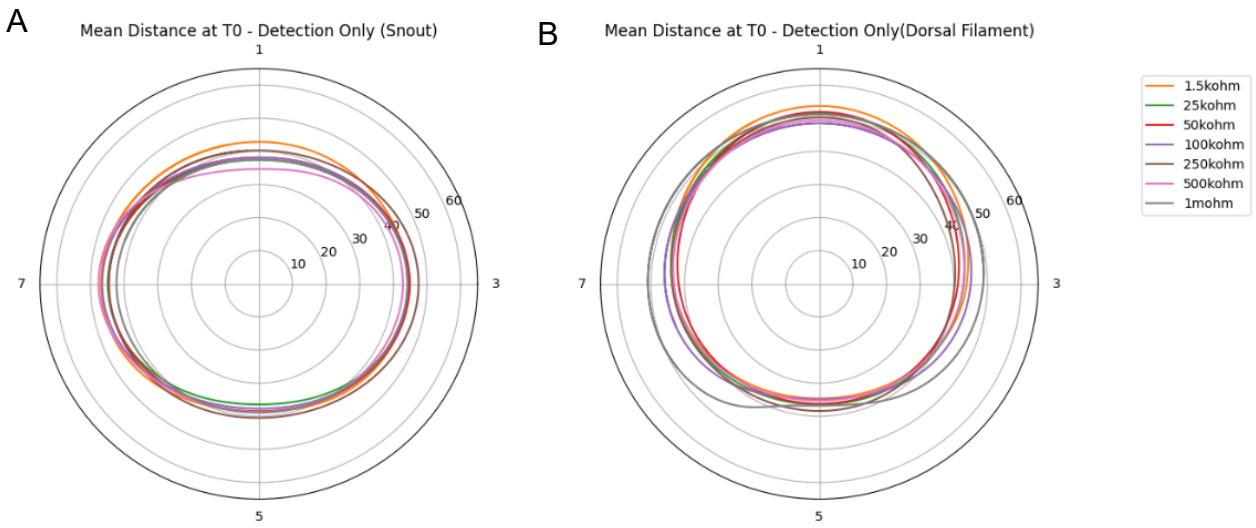

Figure 47. Average distance of the dorsal filament and the head at T0. *Average distance (mm) between the closest proportion and the head (panel A) and the dorsal filament (panel B) at the onset of the stimulus for the detection samples.*

Detection Frequency – Principal Body Regions

Figure 48 shows the detection frequency for four principal body regions. This is a complement to Dorsal Filament & Head Detection Frequency.

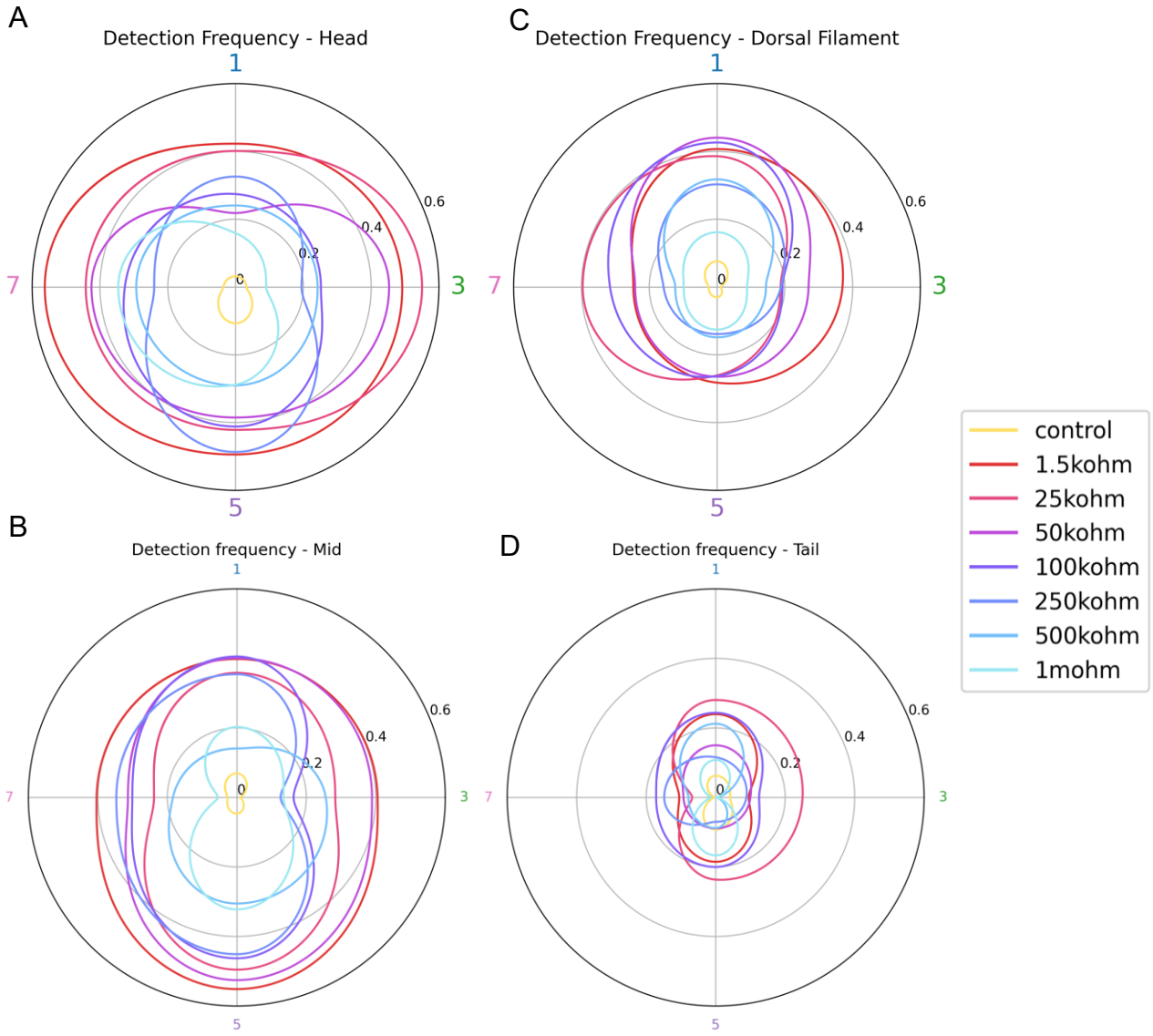

Figure 48. Detection frequency for the four principal body parts. *Each panel display the average detection frequency across fish at each resistor location and resistance value for the four principal regions. The proportion is selected by which proportion is closest at T0. The exact detection frequency at a resistor location corresponds to the value at the intersection of the corresponding quadrant line and the plotted lines.*

Opto-Coupler Experiment

Prior to the second round of experiments, three test experiments were conducted with opto-couplers instead of mechanical relays. Here's a brief analysis of the dataset. See Table 6 for details on the dataset.

Info	Notes
Protocol	Same as round 2 except resistor location
Resistor locations	2,4,6 & 8
Number of experiments	3
Number of samples total	1536
Number of exits	214
Number of usable samples	1322

Table 6. Opto-coupler analysis dataset summary.

Opposite resistors to round 2 were used in this dataset because the resistor ring was connected backward.

Figure 49 panel A shows the detection frequency for each resistance intensity and the sham. All resistance values have visually higher detection frequencies than the sham, indicating that the fish can detect stimuli from opto-couplers. Panels B and C show the detection frequency at each resistor location. Surprisingly, there's a major asymmetry, with almost no detection at resistor #4. Unfortunately, there is no way to verify that all the connections are correct since the experimental setup was modified to accommodate the relays instead. However, this is the likely reason that the detection frequency at resistors 4 and 8 are significantly lower.

In conclusion, opto-couplers may be useful as a switching system for stimulus delivery in behavioral experiments with weakly electric fish. However, more experiments to test their perception from the fish's perspective are needed to determine if they transport electrical current as expected.

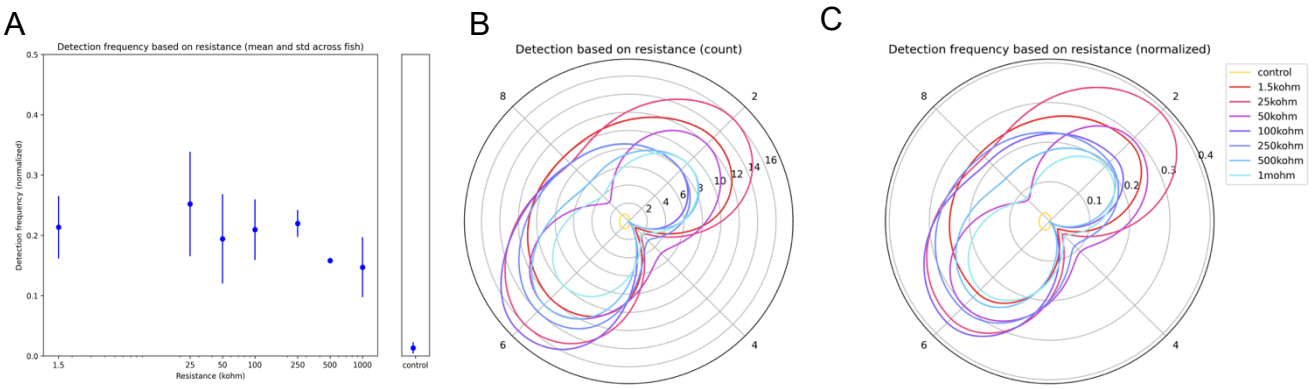

Figure 49. Opto-coupler analysis. *Opto-coupler detection frequency and dose response. Panel A is the normalized dose response curve. Panel B is the count at each location and panel C is the normalized frequency.*

Additional statistical analysis

LMM 1

Formula : distance_difference ~ control_exp + resistor + dist_before + (1| Fish_number)+ (1|Sample_number)

LMM1 is a linear mixed model examining the distance difference between T0 and T1.5 for round 1. It has three fixed effects: control vs. experiment, resistor number/location, and distance before. Random effects include sample number/time and fish number. See the result section for the fixed effects: 3D Distance Reaction.

To use a linear mixed model, the dependent variable's distribution must be normal. A Gaussian curve fits the distribution in Figure 50, and the high r2 value indicates a good fit. The "Normality of Residuals" panels in Figure 51 further support this.

Homoskedasticity of variance is also assumed. The "Homogeneity of Variance" panel in Figure 51 shows a flat reference line, suggesting this criterion is met.

Only the inter-individual variance (fish number) explains some of the variance. The "Normality of Random Effect (fish)" panel in Figure 51 shows some points off the line, and the left panel of Figure 52 shows the variance of this random effect. The "summary" function from R indicates that fish number explains some of the variance (ranova function, Pr(>Chisq) < 0.001). However, the second random effect (sample number) doesn't show a significant effect (ranova function, Pr(>Chisq) < 0.943).

Finally, a simple dispersion test confirms that the data isn't over/under-dispersed, which is good (Figure 53).

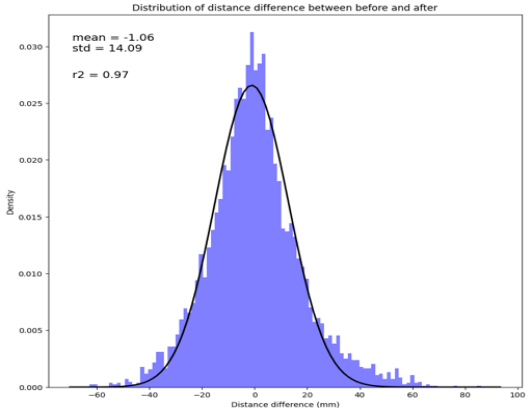

***Figure 50. Distribution of the dependent variable distance difference**. Data from LMM1.*

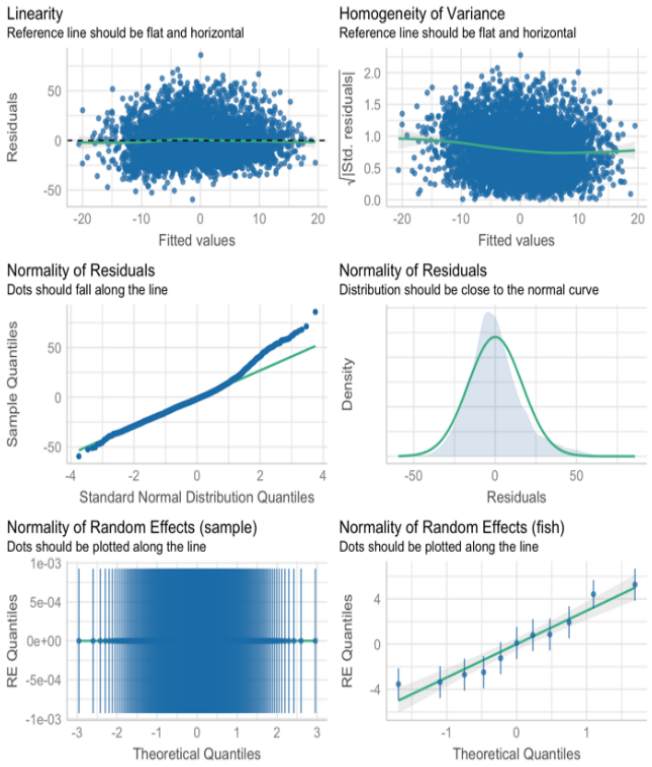

Figure 51. Diagnostic figure for LMM 1, output from R.

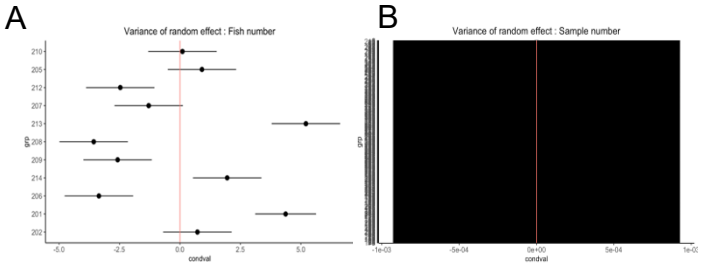

Figure 52. Variance of random effects of LMM 1. *Panel A is the variance of the random effect "Fish number" and panel B is the time effect or "Sample number".*

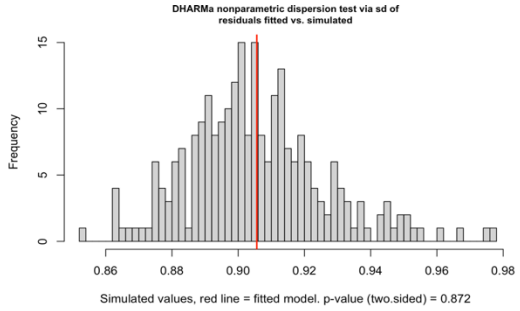

Figure 53. Dispersion test results for LMM 1, output from R.

Binomial GLMM 2

Formula : detection ~ resistor + Resistance + control_exp + (1|Fish_number) + (1|Sample_number)

This binomial GLMM 2 is a generalized linear mixed model for round 2 detection events. Since the dataset is binomial, the generalized form with the “binomial” family is needed. The fixed effects are resistor number, resistance, and sham vs. stimulus. The random effects are fish number and sample number. See the result section for the fixed effects: General Detection Frequency.

Only the inter-individual variance (fish number) explains some of the variance, as shown Figure 54. The random effect for sample number explains barely any variation. The distribution of detection events for both rounds is in Detection Frequency – Time Effect.

A simple dispersion test shows that the data isn’t over/under-dispersed (Figure 55), which is good.

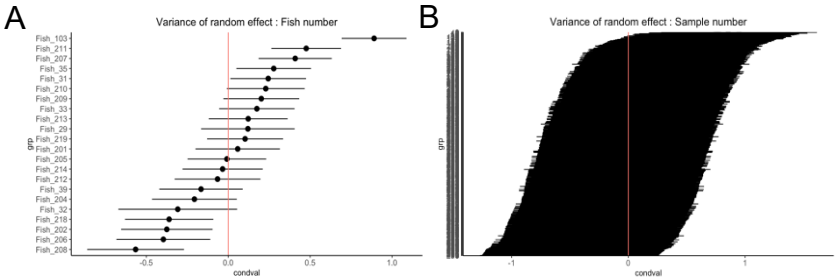

Figure 54. Variance of random effects of GLMM 2. *Panel A is the variance of the random effect "Fish number" and panel B is the time effect or "Sample number".*

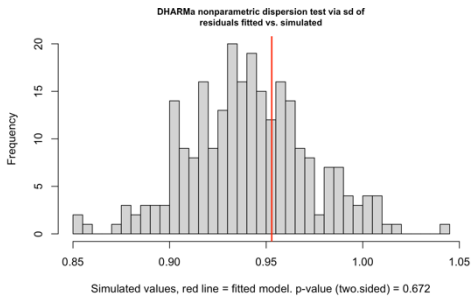

Figure 55. Dispersion test result figure for GLMM 2.

LMM 2.1

What?	Notes
Formula :	distance_difference ~ control_exp + (1|Fish_number) + (1|Sample_number)
Experiment Round	Round 1
Complement to :	General Detection Frequency
Assumption : Normality	Satisfied (see panels "Normality of residuals" from Figure 56)
Assumption : Homoskedasticity	Satisfied (see panel "Homogeneity of Variance" from Figure 56)
Variance of RE : Fish number	Accounts for some variance (see Figure 57)
Variance of RE : Sample number	Doesn't account for any variance (see Figure 57)
Dispersion test :	Satisfied (see Figure 58)

Table 7. Summary of LMM2.1.

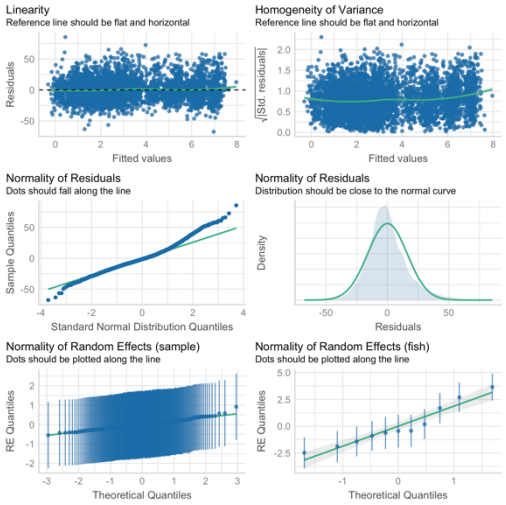

Figure 56. Diagnostic figure for LMM2.1.

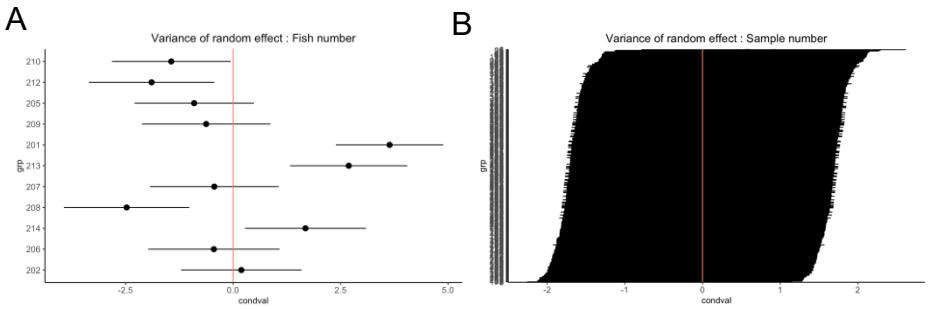

Figure 57. Variance of random effects of LMM 2.1*. Panel A is the variance of the random effect "Fish number" and panel B is the time effect or "Sample number".*

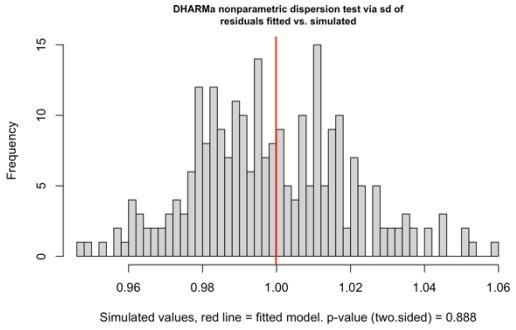

Figure 58. Dispersion test figure for LMM 2.1.

Binomial GLMM 3.1

What?	Notes
Data Subset :	Proportion (T0) = Dorsal Filament
Formula :	detection ~ resistor + Resistance + control_exp + (1|Fish_number)
Experiment Round	Round 2
Complement to :	Dorsal Filament & Head Detection Frequency
Assumption : Binomial data	Satisfied
Variance of RE : Fish number	Accounts for some variance (see Figure 59)
Dispersion test :	Satisfied (see Figure 59)

Table 8. Summary of GLMM 3.1.

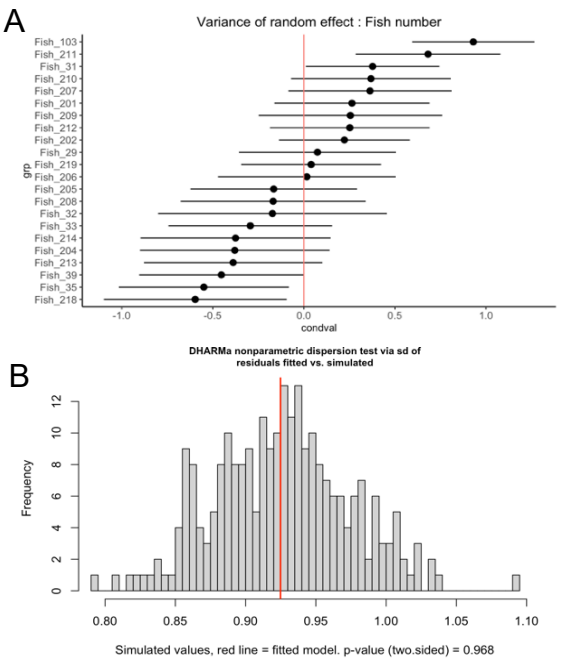

Figure 59. Variance of RE and dispersion test of GLMM 3.1 *Panel A shows the variance of the random effect "Fish number" for GLMM 3.1. Panel B shows the dispersion test figure for GLMM 3.1.*

Binomial GLMM 3.2

What?	Notes
Data Subset :	Proportion (T0) = Head
Formula :	detection ~ resistor + Resistance + control_exp + (1|Fish_number)
Experiment Round	Round 2
Complement to :	Dorsal Filament & Head Detection Frequency
Assumption : binomial data	Satisfied
Variance of RE : Fish number	Accounts for some variance (see Figure 60)
Dispersion test :	Satisfied (see Figure 60)

Table 9. Summary of GLMM 3.2.

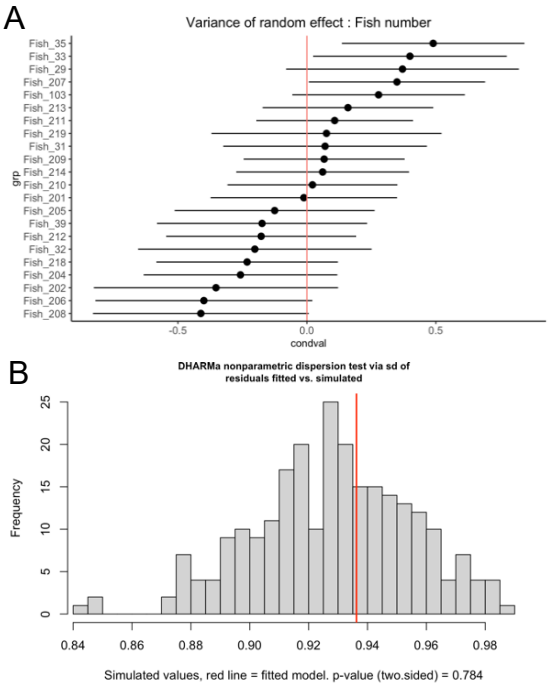

Figure 60. Variance of RE and dispersion test of GLMM 3.2. *Panel A shows the variance of the random effect "Fish number" for GLMM 3.2. Panel B shows the dispersion test figure for GLMM 3.2.*

Binomial GLMM 3.3

What?	Notes
Data Subset :	Resistor 1 only
Formula :	detection ~ prop_t0_percent + Resistance + control_exp + (1|Fish_number)
Experiment Round	Round 2
Complement to :	Dorsal Filament & Head Detection Frequency
Assumption : binomial data	Satisfied
Variance of RE : Fish number	Accounts for some variance (see Figure 61)
Dispersion test :	Satisfied (see Figure 61)

Table 10. Summary of GLMM 3.3.

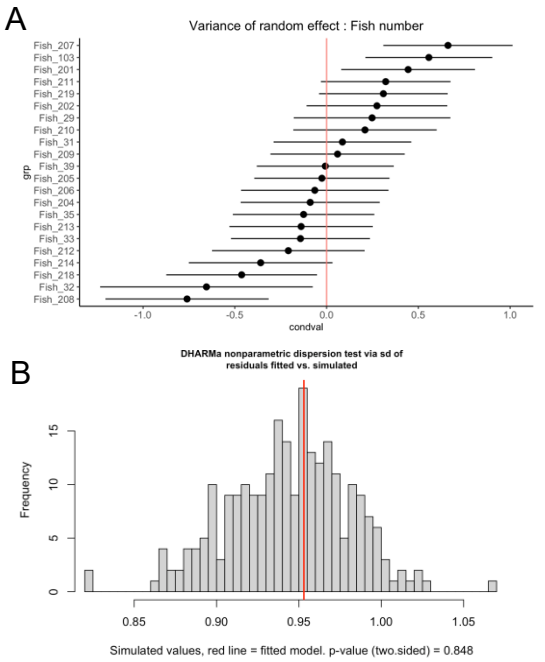

Figure 61. Variance of RE and dispersion test of GLMM 3.3. *Panel A shows the variance of the random effect "Fish number" for GLMM 3.3. Panel B shows the dispersion test figure for GLMM 3.3.*

Binomial GLMM 3.4

What?	Notes
Data Subset :	Resistor 5 only
Formula :	detection ~ prop_t0_percent + Resistance + control_exp + (1|Fish_number)
Experiment Round	Round 2
Complement to :	Dorsal Filament & Head Detection Frequency
Assumption : binomial data	Satisfied
Variance of RE : Fish number	Accounts for some variance (see Figure 62)
Dispersion test :	Satisfied (see Figure 62)

Table 11. Summary of GLMM 3.4.

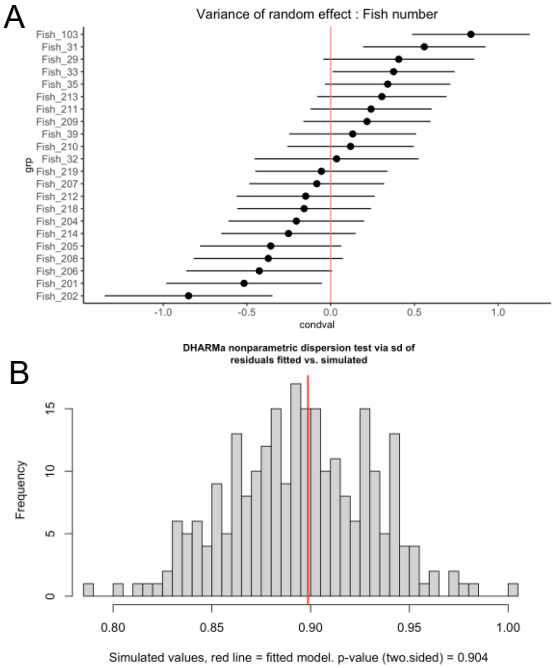

Figure 62. Variance of RE and dispersion test of GLMM 3.3. *Panel A shows the variance of the random effect "Fish number" for GLMM 3.4. Panel B shows the dispersion test figure for GLMM 3.4.*

LMM 4.1

What?	Notes
Formula :	relative_angle_difference ~ resistor + (1|Fish_number)
Experiment Round	Round 1
Complement to :	Post-Detection Reorientation
Assumption : Normality	Satisfied (see panels "Normality of residuals" from Figure 64)
Assumption : Homoskedasticity	Satisfied (see panels "Homogeneity of Variance" from Figure 64)
Variance of RE : Fish number	Doesn't account for any variance (see Figure 63)
Dispersion test :	Satisfied (see Figure 63)

Table 12. Summary of LMM 4.1.

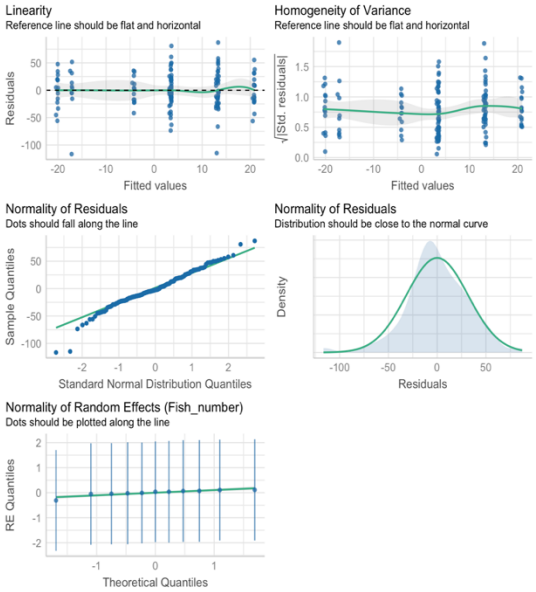

Figure 64. Diagnostic figure for LMM 4.1.

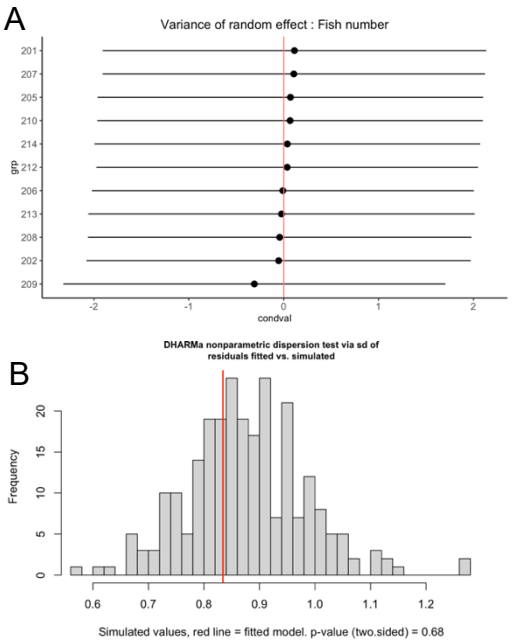

Figure 63. Variance of RE and dispersion test of LMM 4.1. *Panel A shows the variance of the random effect "Fish number" for LMM 4.1. Panel B shows the dispersion test figure for LMM 4.1.*

LMM 4.2

What?	Notes
Formula :	relative_angle_difference ~ resistor + (1|Fish_number)
Experiment Round	Round 2
Complement to :	Post-Detection Reorientation
Assumption : Normality	Satisfied (see panels "Normality of residuals" from Figure 65)
Assumption : Homoskedasticity	Satisfied (see panels "Homogeneity of Variance" from Figure 65)
Variance of RE : Fish number	Doesn't account for any variance (see Figure 66)
Dispersion test :	Satisfied (see Figure 66)

Table 13. Summary of LMM 4.2.

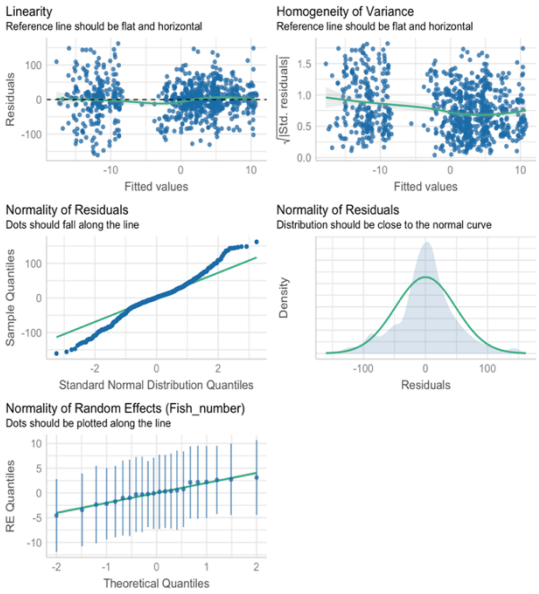

Figure 65. Diagnostic figure for LMM 4.2.

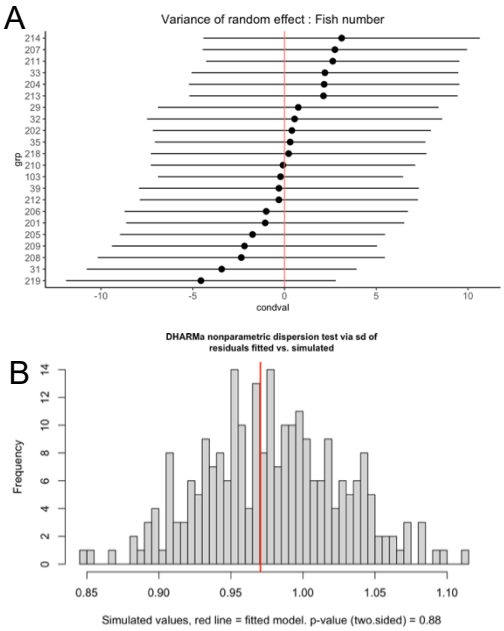

Figure 66. Variance of RE and dispersion test of LMM 4.2. *Panel A shows the variance of the random effect "Fish number" for LMM 4.2. Panel B shows the dispersion test figure for LMM 4.2.*

LMM 5

This linear mixed model is an additional analysis that was not used due to overdispersion of the data (see Figure 67). In other words, the variance is higher than even the value of the mean, which is not good in this scenario where we are talking about time (only positive values, Poisson family). If it wasn't for that, both effects of initial closest proportion and initial distance on threshold crossing time would have been statistically significant (p=0.003 and p<0.001 respectively).

What?	Notes
Formula :	TC_time ~ prop_t0 + dist_t0 + (1|Fish_number) + (1|sample)
Experiment Round	Round 2
Complement to :	Post Detection Repositioning and Threshold Crossing
Assumption : Normality	Satisfied (see panel "Normality of residuals" from Figure 68)
Assumption : Homoskedasticity	Satisfied (see panels "Homogeneity of Variance" from Figure 68)
Variance of RE : Fish number	Accounts for some variance (see Figure 69)
Variance of RE : Sample number	Accounts for some variance (see Figure 69)
Dispersion test :	Not satisfied (see Figure 67)

Table 14. Summary of LMM 5.

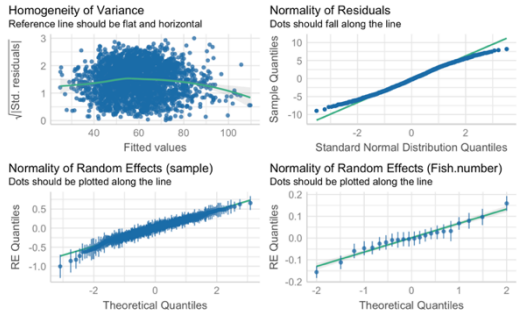

Figure 68. Diagnostic figure for LMM 5.

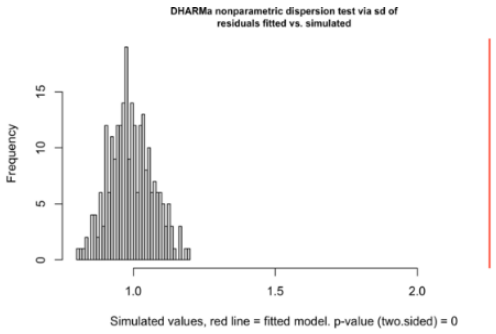

Figure 67. Dispersion test figure for LMM 5.

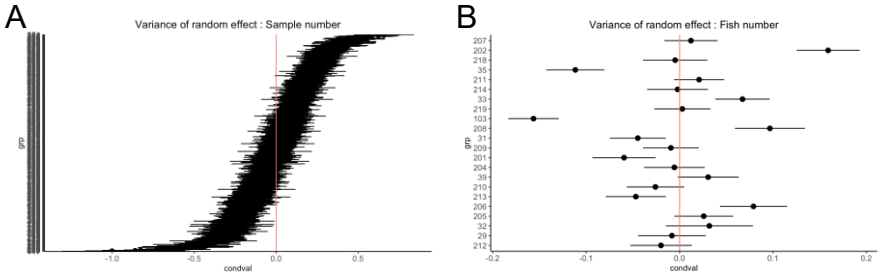

Figure 69. Variance of random effects for LMM 5.

Kolmogorov-Smirnov Test

A Kolmogorov-Smirnov test was conducted on the data from the histograms of Figure 9. The data selected was the proportions between 5% and 95% of the body length of the fish to remove the peaks at both ends. The data was tested against a uniform distribution and yielded significant differences between them and that uniform distribution. Complement to Stimulus Origin Distribution.